New Jersey Institute of Technology
Digital Commons @ NJIT

Dissertations | Electronic Theses and Dissertations

Summer 8-31-2019

Modelling in vitro dissolution and release of sumatriptan succinate from polyvinylpyrrolidone-based microneedles aided by iontophoresis

James Paul Ronnander
New Jersey Institute of Technology

Follow this and additional works at: https://digitalcommons.njit.edu/dissertations

 Part of the Biomedical Engineering and Bioengineering Commons, Chemical Engineering Commons, and the Pharmacy and Pharmaceutical Sciences Commons

Recommended Citation

Ronnander, James Paul, "Modelling in vitro dissolution and release of sumatriptan succinate from polyvinylpyrrolidone-based microneedles aided by iontophoresis" (2019). *Dissertations*. 1426.
https://digitalcommons.njit.edu/dissertations/1426

This Dissertation is brought to you for free and open access by the Electronic Theses and Dissertations at Digital Commons @ NJIT. It has been accepted for inclusion in Dissertations by an authorized administrator of Digital Commons @ NJIT. For more information, please contact digitalcommons@njit.edu.

Copyright Warning & Restrictions

The copyright law of the United States (Title 17, United States Code) governs the making of photocopies or other reproductions of copyrighted material.

Under certain conditions specified in the law, libraries and archives are authorized to furnish a photocopy or other reproduction. One of these specified conditions is that the photocopy or reproduction is not to be "used for any purpose other than private study, scholarship, or research." If a, user makes a request for, or later uses, a photocopy or reproduction for purposes in excess of "fair use" that user may be liable for copyright infringement,

This institution reserves the right to refuse to accept a copying order if, in its judgment, fulfillment of the order would involve violation of copyright law.

Please Note: The author retains the copyright while the New Jersey Institute of Technology reserves the right to distribute this thesis or dissertation

Printing note: If you do not wish to print this page, then select "Pages from: first page # to: last page #" on the print dialog screen

NJIT New Jersey's Science & Technology University

The Van Houten library has removed some of the personal information and all signatures from the approval page and biographical sketches of theses and dissertations in order to protect the identity of NJIT graduates and faculty.

ABSTRACT

MODELLING IN VITRO DISSOLUTION AND RELEASE OF SUMATRIPTAN SUCCINATE FROM POLYVINYLPYRROLIDONE-BASED MICRONEEDLES AIDED BY IONTOPHORESIS

by
James Paul Ronnander

A novel dissolving microneedle array system is developed to investigate permeation of a sumatriptan succinate formulations through the skin aided by iontophoresis. Three formulations consisting of hydrophilic, positively charged drug molecules encapsulated in a water-soluble biologically suitable polymer, polyvinylpyrrolidone (PVP), have been accepted by the U.S. Food and Drug Administration (FDA). The microneedle systems are fabricated with 600 pyramid-shaped needles, each 500 μm tall, on a 0.785-cm^2 circular array. *In vitro* transdermal studies with minipig skin and vertical Franz diffusion cells show > 68% permeation of sumatriptan over a 24-hour period. A combination of microneedle and electrical current density ranging from 100 to 500 $\mu A/cm^2$ using Ag / AgCl electrodes displays increased flux with current density. At 500 $\mu A/cm^2$, a dissolving array loaded with 4.3 mg sumatriptan leads to a steady-state delivery rate of 490 $\mu g/cm^2h$ with negligible lag time. In theory, a 9.58-cm2 microneedle-array patch loaded with 47.30 mg of sumatriptan succinate could provide the required plasma concentration, 72 ng/ml, for nearly six hours.

In parallel, a mathematical model based on first principles is developed to predict the amount of drug delivered into the skin using software (e.g., Mathematica). A system of mass balance equations are derived to simulate the dissolution, diffusion, electromigration and transport of the active ingredient through the epidermis. The analytical approach allows for the evaluation and estimation of the effects of key parameters (i.e., loading dose,

polymer concentration, needle height, needle pitch width and current density) on the release profile. The skin layer concentration increases significantly with either increased loading dose or elongated height of the microneedle. The percentage of sumatriptan permeating through skin increased favorably with increased electrical current applied to microneedle patch. An inverse correlation was observed between the pitch width (center to center distance of adjacent needles) and the cumulative amount of sumatriptan permeated into the dermis. Predicted cumulative release data from mathematical model simulations of each of the three formulations were successfully validated with *in vitro* permeation data administered with Franz cells and minipig skin.

MODELLING IN VITRO DISSOLUTION AND RELEASE OF SUMATRIPTAN SUCCINATE FROM POLYVINYLPYRROLIDONE-BASED MICRONEEDLES AIDED BY IONTOPHORESIS

by
James Paul Ronnander

A Dissertation
Submitted to the Faculty of
New Jersey Institute of Technology
in Partial Fulfillment of the Requirements for the Degree of
Doctor of Philosophy in Chemical Engineering

Otto H. York Department of
Chemical and Materials Engineering

August 2019

Copyright © 2019 by James Paul Ronnander

ALL RIGHTS RESERVED

APPROVAL PAGE

MODELLING IN VITRO DISSOLUTION AND RELEASE OF SUMATRIPTAN SUCCINATE FROM POLYVINYLPYRROLIDONE-BASED MICRONEEDLES AIDED BY IONTOPHORESIS

James Paul Ronnander

Dr. Laurent Simon, Dissertation Advisor — Date
Associate Professor of Chemical and Materials Engineering, NJIT

Dr. Piero Armenante, Committee Member — Date
Distinguished Professor of Chemical and Materials Engineering, NJIT

Dr. Ecevit Bilgili, Committee Member — Date
Associate Professor of Chemical and Materials Engineering, NJIT

Dr. Xiaoyang Xu, Committee Member — Date
Assistant Professor of Chemical and Materials Engineering, NJIT

Dr. Rick Chan, Committee Member — Date
Executive Scientific Officer, Lohmann Therapy Systems Corp.

BIOGRAPHICAL SKETCH

Author: James Paul Ronnander

Degree: Doctor of Philosophy

Date: August 2019

Undergraduate and Graduate Education:

- Doctor of Philosophy in Chemical Engineering,
  New Jersey Institute of Technology, Newark, NJ, 2019

- Master of Science in Chemical Engineering,
  Polytechnic Institute of New York University, Brooklyn, NY, 2013

- Bachelor of Science in Chemical Engineering,
  Northwestern University, Chicago, IL, 2001

Major: Chemical Engineering

Publications:

Ronnander, P., et al. "Dissolving polyvinylpyrrolidone-based microneedle systems for in-vitro delivery of sumatriptan succinate." European Journal of Pharmaceutical Sciences 114 (2018): 84-92.

Ronnander, P., et al. "Modelling the in-vitro dissolution and release of sumatriptan succinate from polyvinylpyrrolidone-based microneedles." European Journal of Pharmaceutical Sciences 125 (2018): 54-63.

Ronnander, P., et al. "Transdermal delivery of sumatriptan succinate using iontophoresis and dissolving microneedles." Journal of Pharmaceutical Sciences (Accepted).

Patent Submitted:

Ronnander, P., Simon, L., LTS Lohmann Therapie-Systeme AG, & New Jersey Institute of Technology 2019, *Iontophoretic Microneedle Device*, WO2019053051.

My Lord and Savior Jesus Christ
Gives me strength in all my endeavors

And

For my beautiful wife Bobbette,
Her love and support inspires me to accomplish great things

And

For my amazing son Jonathan,
His smile and laughter brings joy to my heart

And

For my parents, James and Judy Ronnander, my brother, Chris Ronnander
Who taught me to dream big and finish what you start

ACKNOWLEDGEMENT

First and foremost, I would like to sincerely thank Dr. Laurent Simon who has advised me during my entire tenure at NJIT. Thank you for giving me this opportunity and technical background to complete this dissertation. I would also like to thank my committee members for their support and guidance with my research: Dr. Piero Armenante, Dr. Ecevit Bilgili, Dr. Xiaoyang Xu, Dr. Heiko Spilgies, and Dr. Rick Chan.

A special thanks to the Innovative Injection Systems (IIS) group at LTS Lohmann Therapie-Systeme AG headed by Dr. Stefan Henke, including Dr. Heiko Spilgies and Sebastian Scherr's collaboration on microneedle design.

Many thanks to the Research and Development group at LTS Lohmann Therapie-Systeme AG headed by Dr. Hanshermann Franke. In particular, Dr. Andreas Koch and his colleagues in the analytical development group for support with analytical and in vitro work.

Finally, my sincere appreciation to the leadership at LTS Lohmann Therapie-Systeme AG and LTS Lohmann Therapy Systems Corp; including Dr. Tim Schlange, Thomas Maichle, Dr. Joachim Franke, Dr. Hanshermann Franke, Dr. Stefan Henke, Dr. Michael Komenda; for providing financial support and allowing use of laboratories and resources.

TABLE OF CONTENTS

Chapter		Page
1	INTRODUCTION ……	1
	1.1 Objective…..……..……...	1
	1.2 Motivations…….…….……..	2
	1.3 Research Significance and Impact..……..	10
2	MATERIALS AND METHODS ……..…….	12
	2.1 Chemicals and Reagents……...	12
	2.2 Preparation of Sumatriptan Microneedle Arrays……..	12
	2.3 Characterization of Microneedles with Light Microscope…..…….	14
	2.4 Tensile Strength……	15
	2.5 Mass, Drug Content and Density of Microneedle Systems…..……..	16
	2.6 Simulated Biological Fluid Preparation……	17
	2.7 Polyvinylpyrrolidone Solubility……	17
	2.8 Minipig Skin Preparation……..	18
	2.9 Optical Coherence Tomography Imaging……	19
	2.10 Transepidermal Water Loss (TEWL).…….	19
	2.11 *In vitro* Permeation Studies……	20
	2.11 Analytical Methods……	24
	2.12 Statistical Methods…….	25
3	DEVELOPMENT OF SOLUBLE MICRONEEDLE SYSTEM FOR DELIVERY OF SUMATRIPTAN SUCCINATE ……..……	26
	3.1 Formulation of Sumatriptan Dissolving Microneedle Array.…….....	26

TABLE OF CONTENTS
(Continued)

Chapter **Page**

3.2 Characterization of Sumatriptan Dissolving Microneedle Array…….. 32

3.3 *In vitro* Diffusion of Sumatriptan Microneedles Using Minipig Skin Model… 48

3.4 *In vitro* Delivery of Sumatriptan From Dissolving Microneedle Arrays Aided by Iontophoresis…….…. 57

3.5 Transdermal Microneedle Devices for Drug Delivery of Sumatriptan Succinate With and Without Iontophoresis……..... 70

3.5.1 Sumatriptan Dissolving Microneedle Device Design…… 71

3.5.2 Sumatriptan Dissolving Microneedle Iontophoretic Device Design….. 72

4 MATHEMATICAL MODELLING FOR THE *IN VITRO* RELEASE OF SUMATRIPTAN SUCCIANTE FROM DISSOLVING MICRONEEDLE SYSTEMS..…… 73

4.1 Development of Mathematical Model for the *In vitro* Dissolution and Release of Sumatriptan From Dissolving Microneedle Arrays...…….. 73

4.1.1 Derivation of Dissolution Governing Equation for Microneedle Height…… 82

4.1.2 Derivation of Dissolution Governing Equation for Skin Layer Drug Concentration…… 84

4.1.3 Derivation of the Dissolution Equation for Drug Release From the Microneedle Base-plate……. 85

4.2 *In vitro* Release Studies for Validation of Sumatriptan Microneedle Dissolution Mathematical Model…… 87

4.2.1 Comparison of Simulated and Experimental *In vitro* Minipig Results…… 87

4.2.2 Simulation Studies……..... 91

4.3 Development of Mathematical Model for *In vitro* Dissolution, Diffusion and Release of Drug Substance From Dissolving Microneedle Array……..…… 94

TABLE OF CONTENTS
(Continued)

Chapter	Page
4.4 *In vitro* Release Studies for Validation of Sumatriptan Microneedle Dissolution and Diffusion Mathematical Model…….…..	98
4.4.1 Simulation Experiments……	98
4.4.2 Comparison of Simulated and Experimental *In vitro* Minipig Results…	103
4.5 Development of Mathematical Model for *In vitro* Dissolution, Diffusion, and Release of Sumatriptan From Dissolving Microneedle Array Aided by Iontophoresis..…… ……...…….	109
4.5.1 Derivation of Electrophoretic Transport Governing Equations for Skin Layer Concentration……	112
4.6 Simulation Studies to Evaluate Sumatriptan Microneedle Dissolution, Diffusion, and Electro-migration Mathematical Model…..……...	113
5 CONCLUSIONS ……..……..	115
REFERENCES ……...	118

LIST OF TABLES

Table		Page
2.1	Microneedle Array Wet Composition (%, w/w)……..	13
3.1	Microneedle Dimensions and Physical Properties……..……..	37
3.2	TEWL Values of Minipig Skin Pre- and Post- Microneedle Treatment or Tape-Striping Technique (15x); Average Values ± SD……	47
3.3	Franz Cell *In vitro* Permeation Data for Sumatriptan Succinate Through Minipig Skin After 32-h; Average Values ± SD……..	52
3.4	TEWL Values of Minipig Skin Pre- and Post- Microneedle Treatment or Microneedle Treatment Aided by Iontophoresis; Average Values ± SD……..	61
3.5	Franz Cell *In vitro* Permeation Data for Sumatriptan Succinate Through Minipig Skin After Six Hours Aided by Iontophoresis; Average Values ± SD……..	64
4.1	Definition of Governing Equation Parameters……...	81
4.2	Estimated Sumatriptan Microneedle Formulation Parameters for Dissolution Model……..	88
4.3	Estimated Sumatriptan Microneedle Formulation Parameters for Dissolution and Diffusion Model……..…….	105

LIST OF FIGURES

Figure		Page
1.1	Transdermal matrix-controlled system ……..	4
1.2	Schematic representation of dissolvable microneedles for rapid release of encapsulated drug……	8
1.3	Iontophoretic transdermal microneedle patch…….	8
2.1	Photographs of P1 formulated dissolving microneedle arrays; A) circle array containing 600 pyramid-shaped needles; B) square array containing 196 pyramid-shaped needles…..……...……..	14
2.2	Set-up of three-point bend apparatus for testing mechanical strength of microneedle array…….……...	16
2.3	Viscosity – concentration curve for PVP in simulated biological fluid……..	18
2.4	Non-woven pad attached to minipig skin sample……...	22
2.5	Two-chamber franz cell system with electrical current……..……	23
2.6	Two-chamber franz cell system with silver-silver chloride electrodes…….……..	24
3.1	Photographs of polyvinylpyrrolidone microneedle arrays; (A) microneedle containing only PVP (20 %, w/w) are glassy, brittle, non-uniform and contain bubbles; (B-C) microneedles containing PVP (20 %, w/w) , glycerol (1 %, w/w) and polysorbate 80 (1 %, w/w) are uniform and uniform, flexible and without bubbling effect; (D-E) P1 formulated microneedles with sumatriptan are uniform, flexible and without bubbling…….. .	29
3.2	Photographs of laboratory set-up; (A) silicone mold filled with P1 solution; (B) stand to transfer filled microneedle molds into pressure vessel; (C) pressure vessel; (D) dried P1 microneedle in silicone mold…….	31
3.3	Optical microscope image P1 circle microneedle; (A) top-down view; (B) side view……..……..	33
3.4	Optical microscope image P2 circle microneedle; (A) top-down view; (B) side view……	34

LIST OF FIGURES
(Continued)

Figure **Page**

3.5 Optical microscope image P3 circle microneedle; (A) top-down view; (B) side view…… 34

3.6 Optical microscope image P4 circle microneedle; (A) top-down view; (B) side view…… 35

3.7 Optical microscope image P1 square microneedle; (A) top-down view; (B) side view…… 35

3.8 Mechanical test (3-pt bend) of P1 microneedles (circle); average values (n = 3)…… 40

3.9 Mechanical test (3-pt bend) of P2 microneedles (circle); average values (n = 3)…… 40

3.10 Mechanical test (3-pt bend) of P3 microneedles (circle); average values (n = 3)…… 41

3.11 Mechanical test (3-pt bend) of P4 microneedles (circle); average values (n = 3)…… 41

3.12 Mechanical test (3-pt bend) of P1 microneedles (square); average values (n = 3)…… 42

3.13 Optimal microscope images; (A) blank minipig tissue (10 x mag); (B) minipig tissue post-treatment with P1 microneedle (10 x mag); (C) minipig tissue post-treatment with P1 microneedle (50 x mag)…… 43

3.14 Photographic images of minipig tissue stained with nitrazine yellow dye; (A) blank minipig tissue with no dye; (B) P1 circle array treated minipig tissue; (C) P2 circle array treated minipig tissue; (D) P3 circle array treated minipig tissue; (E) P1 square array treated minipig tissue…… 44

3.15 Optical coherence tomographic image of P1 circle microneedle dissolving in minipig tissue over time; dissolution of microneedle at (A) 1 min; (B) 2 min; (C) 4 min; (D) 10 min…… 46

3.16 *In vitro* cumulative release of sumatriptan drug from dissolving microneedle preparations P1 (■), P2 (♦), P3 (●); average values ± SD, n = 3…… 53

LIST OF FIGURES
(Continued)

Figure **Page**

3.17 *In vitro* cumulative release profile of sumatriptan succinate over 32 hour period from circle array dissolving microneedle preparations P1 microneedle (♦), P1 control (microneedle inverted on minipig tissue) (■), P1 microneedle + tape-stripping (15x) (●) and reference solution (×); average values ± SD (n = 3). 54

3.18 *In vitro* cumulative release profile of sumatriptan succinate over 32 hour period from circle array dissolving microneedle preparations P2 microneedle (♦), P2 control (microneedle inverted on minipig tissue) (■), P2 microneedle + tape-stripping (15x) (●) and reference solution (×); average values ± SD (n = 3). 55

3.19 *In vitro* cumulative release profile of sumatriptan succinate over 32 hour period from circle array dissolving microneedle preparations P3 microneedle (♦), and reference solution (×); average values ± SD (n = 3)…… 56

3.20 Photographic images of minipig tissue stained with nitrazine yellow dye; (A) blank minipig tissue; (B) P1 circle array treated minipig; (C) P2 circle array treated minipig tissue; (D) P3 circle array treated minipig tissue; (E) P1 square array treated minipig tissue …… 59

3.21 *In vitro* cumulative release profile of sumatriptan succinate over six hour period from circle dissolving microneedle aided by iontophoresis; P1 microneedle + 500 μA/cm^2 (■); P2 microneedle + 500 μA/cm^2 (♦); P3 microneedle + 500 μA/cm^2 (●); average values ± SD (n = 3)…..……. 65

3.22 *In vitro* cumulative release profile of sumatriptan succinate over six hour period from circle dissolving microneedle aided by iontophoresis; P1 microneedle (♦); P1 control (microneedle inverted on minipig tissue) (■); P1 microneedle + 100 μA/cm^2 (x); P1 microneedle + 300 μA/cm^2 (+); P1 microneedle + 500 μA/cm^2 (●); average values ± SD (n = 3)…… 66

3.23 *In vitro* cumulative release profile of sumatriptan succinate over six hour period from circle dissolving microneedle aided by iontophoresis; P2 microneedle (♦); P2 control (microneedle inverted on minipig tissue) (■); P2 microneedle + 500 μA/cm^2 (●); average values ± SD (n = 3)…… 67

3.24 *In vitro* cumulative release profile of sumatriptan succinate over six hour period from circle dissolving microneedle aided by iontophoresis; P3 microneedle (♦); P3 control (microneedle inverted on minipig tissue) (■); P3 microneedle + 500 μA/cm^2 (●); average values ± SD (n = 3)…… 68

LIST OF FIGURES
(Continued)

Figure		Page
3.25	*In vitro* cumulative release profile of sumatriptan succinate over six hour period from square dissolving microneedle aided by iontophoresis; P1 square microneedle (♦); P1 square control (microneedle inverted on minipig tissue) (■); P1 square microneedle + 500 μA/cm^2 (●); average values ± SD (n = 3)…..……	69
4.1	Drug release from dissolving pyramid-shaped microneedle with base-plate…….	76
4.2	Schematic of pyramid-shaped needle; (A) cross-section view; (B) half angle view……	77
4.3	Plots comparing minipig *in vitro* cumulative percent release of P1 microneedles (solid dots) to predicted profiles (solid lines)…….	88
4.4	Plots comparing minipig *in vitro* cumulative percent release of P2 microneedles (solid dots) to predicted profiles (solid lines)…….	89
4.5	Plots comparing minipig *in vitro* cumulative percent release of P3 microneedles (solid dots) to predicted profiles (solid lines)…….	89
4.6	*In vitro* percent release sumatriptan succinate from dissolving microneedle after 6 hours from formulation P1 (●), P2 (■) and P3(♦); average values (n = 3)…….	90
4.7	Modelling effect of needle height on sumatriptan succinate release using P1 formulation parameters; needle height, h [h=0.06cm (– •), h=0.1 (—), h=0.1(--)].	93
4.8	Modelling effects of pitch width on sumatriptan succinate release using P1 formulation parameters; pitch width, pw, of microneedle [pw=0.035cm (--), pw =0.0525cm (—), pw =0.07cm (– •)]…….……	93
4.9	Modelling effects of drug loading on sumatriptan succinate release using P1 formulation parameters; mass fraction (β) sumatriptan succinate in microneedle [β=0.1% (– •), β=0.2% (—), β=0.3% (--)]…….	94
4.10	Contour plot of sumatriptan drug release from P1 microneedle after 4 hours [h=0.05 cm, β = 21.42%, pw =0.035 cm]……...	100
4.11	Contour plot of sumatriptan drug release from P1 microneedle after 4 hours with reduced mass fraction API [h=0.05cm, β = 17.14%, pw =0.035cm]……..	101

LIST OF FIGURES
(Continued)

Figure **Page**

4.12 Contour plot of sumatriptan drug release from P1 microneedle after 4 hours with reduced pitch width [h=0.05cm, β = 21.42%, pw =0.028cm]…… 102

4.13 Contour plot of sumatriptan drug release from P1 microneedle after 4 hours with reduced microneedle height [h=0.04cm, β = 21.42%, pw =0.035 cm]…….. 103

4.14 Plots comparing minipig in-vitro cumulative percent release of P1 microneedles (solid dots) to predicted profiles (solid lines)……. 105

4.15 Plots comparing minipig in-vitro cumulative percent release of P2 microneedles (solid dots) to predicted profiles (solid lines)……..… 106

4.16 Plots comparing minipig in-vitro cumulative percent release of P3 microneedles (solid dots) to predicted profiles (solid lines)……. 106

4.17 Contour plot of sumatriptan drug release from P1 microneedle after 4 hours…… 107

4.18 Contour plot of sumatriptan drug release from P2 microneedle after 4 hours…… 108

4.19 Contour plot of sumatriptan drug release from P3 microneedle after 4 hours…… 109

4.20 Predicted effect of the iontophoretic parameter, γ, on *in vitro* cumulative percent sumatriptan released from P1 microneedles over an 8 hour period; γ = 0 (solid); γ = 0.8 (dashed); and γ = 1.6 (dot-dash)……. 114

CHAPTER 1

INTRODUCTION

1.1 Objective

The goal of this dissertation is to help provide improved clinical results for large molecule pharmaceutical products and biological drugs using minimally invasive transdermal delivery systems. More specifically, this research focuses on the development of a theoretical model based on transport phenomena principles to assess and predict drug delivery of encapsulated sumatriptan succinate active pharmaceutical ingredients in soluble microneedle systems alone and soluble microneedles aided by iontophoresis. The theory-based approach has the potential for validating preliminary laboratory studies and enhancing properties of the microneedle systems. Methods based on laboratory experiments and mechanistic modeling will make the clinical research less risky, less empirical and more reliable than trial-and-error experimental procedures.

In Chapter 2, materials and methods for development, the evaluation and *in vitro* testing of the microneedle array systems are described. The micro array formulations are analyzed to determine the best properties with respect to uniformity, strength, and flexibility, and the ability to penetrate minipig skin. This step is critical because dissolving microneedle arrays need to preserve uniformity in terms of needle array pattern, pitch (space between needles), height and width. Test methods include: optical microscopy, mechanical testing, and transepidermal water loss (TEWL). *In vitro* experiments with vertical Franz diffusion cells measure the transdermal permeation of the active pharmaceutical ingredient (API) across Göttingen minipig skin. Permeation experiments

are conducted with dissolving microneedles alone and aided by iontophoresis to enhance penetration of drug molecules through the skin.

In Chapter 3, dissolving microneedle array systems are investigated as a suitable alternative delivery method of sumatriptan for the relief of migraine. The formulations consist of a positively-charged, encapsulated pharmaceutical ingredient (sumatriptan succinate) and a hydrophilic, bio-compatible polymer (polyvinylpyrrolidone) approved by the U.S. Food and Drug Administration (FDA). *In vitro* diffusion studies with Göttingen minipig skins demonstrate an increase in drug release as compared to previously developed sumatriptan transdermal patch systems. Further enhancement with electrical current densities of 100, 300 and 500 $\mu A/cm^2$ shows an increase in the steady-state flux of drug with current density.

Finally, in Chapter 4, a mathematical model is developed to predict the *in vitro* permeation of sumatriptan succinate molecules across the skin. Mass balance equations are derived to detail the dissolution, diffusion, electromigration and transport of encapsulated drug substance across the epidermis. A mathematical software (Mathematica®) is used to solve the equations and derive relationships to predict the effects of critical parameters on drug release. The computed (e.g., theoretical) release profiles were then validated with *in vitro* diffusion studies using female minipig skin. The model successfully describes the *in vitro* permeation of three distinct microneedle formulations containing sumatriptan.

1.2 Motivations

The oral administration of biological and pharmaceutical drug products is limited by poor drug absorption and/or first pass effect metabolism in gastrointestinal (GI) tract or liver [1-3]. The most common alternative is drug administration through subcutaneous/

intramuscular injections or intravenous infusion. However, the use of hypodermic needles have several drawbacks, including the pain associated with injection. In addition, they are difficult to administer, cost more and must be sterile. Another disadvantage is that these drug delivery routes (except for intravenous infusion) lead to fluctuations in concentration of drug in the blood plasma, a situation which can lead to toxic effects or ineffective treatment [4].

This is the case with the drug sumatriptan succinate prescribed for the treatment of acute migraines and cluster headaches. A triptan compound acts to bind serotonin (5-hydroxytriptamine) receptors in the brain and induce vasoconstriction of arteries to reduce neurogenic inflammation. Sumatriptan was the first available triptan compound and is recognized as the leading standard in prescription migraine therapy [5-7]. Migraines affect over 1 in 10 people globally, 31.8 % of patients experience three or more headaches per month, and 53.7 % of migraine's require bedrest due to severity [8, 9]. Migraine symptoms typically include throbbing or pulsing pain, aura, sensitivity (light and sound), nausea and vomiting [10-12]. There are several treatment options including various dosage forms (intranasal spray, oral tablet, subcutaneous injection) but each method has limitations which reduce patient compliance. For example, the oral and intranasal delivery routes demonstrate lower therapeutic response (bioavailability 14% and 16%, respectively) and may cause side effects (nausea and vomiting) [13, 14]. On the other hand, subcutaneous injection is difficult for an individual to administer and may cause pain around the injection site [15].

An attractive minimally invasive alternative is the use of transdermal systems which can be self-administered and deliver a controlled amount of medication through the

skin over an extended period of time (up to 7 days). These systems provide effective, pain-free delivery of active ingredients into the bloodstream (avoiding first-pass metabolism effects) with minimal side effects. A typical model of a transdermal therapeutic system (TTS) is the matrix-controlled patch shown in Figure 1.1. The patch is comprised of an occlusive backing layer, a drug-containing adhesive and a release liner. After removing the release liner, the patch is applied to the skin for controlled release of the medication. The drug must diffuse through the stratum corneum (10-20 μm thick) and the viable epidermis (50-100 μm thick) to enter the capillary-rich dermis for systemic absorption. The primary barrier is the stratum corneum comprised of "bricks" of corneocyte cells surrounded by a "mortar" of intercellular lipid matrix of lipid bilayers. Typically, successful transdermal drugs are low molecular weight compounds (< 500 Da), lipophilic (log P ~ 1 - 3), and effective at low doses (few milligrams per day) [16-19]. Chemical permeation enhancers can be added to formulations as excipients to reversibly disrupt the intracellular lipid structures located in the stratum corneum and increase the permeation of large molecules. The challenge is that the chemicals increase skin irritation and can damage deeper living cells in dermal layers. Only a limited subset of chemical enhancers have been used to successfully increase small molecule diffusion without skin irritation [20, 21].

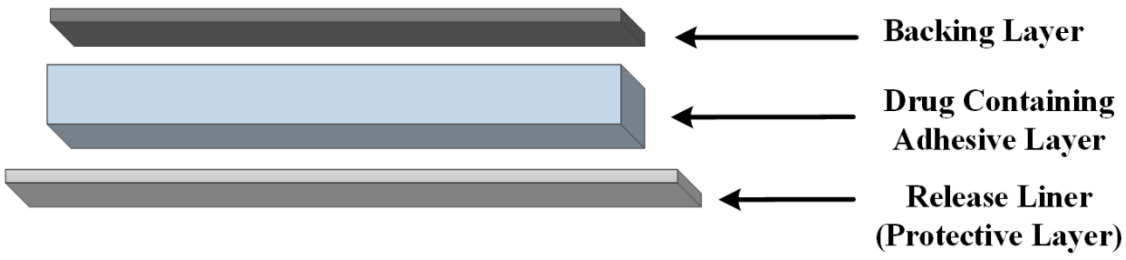

Figure 1.1 Transdermal matrix-controlled system.

Sumatriptan Succinate ($C_{18}H_{27}N_3O_6S$) has a molecular weight of 413.5 g/mol, is freely soluble in water, hydrophilic (Log $P_{pH\ 7.4}$ = -1.5), and has melting point of 165°C making it ideal for aqueous formulations [22, 23]. However, previous *in vitro* studies by Balaguer-Fernandez et al. demonstrate that standard transdermal methods, including enhancers, are not suitable for the delivery of sumatriptan. A patch system comprised of drug solution, methyl cellulose polymer and Azone® (enhancer) required a lag time of 15.21 h and surface area of 293 cm^2 to achieve the target C_{max} value of 72 ng/ml [24, 25].

Modern transdermal applications incorporate microneedle (MN) technology, or an array of micron-sized needles in a small patch, designed to deliver macromolecules and hydrophilic compounds through the skin. These microneedles effectively bypass the stratum corneum and epidermis to achieve systemic drug uptake into the dermis. They are designed with a pattern of micron-sized needles for perforation of the epidermis with micron-sized 'holes', which create channels for drug delivery into dermal capillaries and entry into the blood circulatory system. The individual microneedles are designed with height in the range of 150 to 1,500 μm and a surface density less than 2000 needles/cm^2. These dimensions allow them to puncture the dermis without causing pain as they do not penetrate into deeper skin layers to sever nerves and blood vessels. Several types of microneedles (solid, coated, hollow and dissolving polymeric microneedles) have been developed and investigated for different drug delivery applications. Solid microneedles are used to enhance permeation of drugs through the skin by pre-treating an area of the skin with microneedles prior to application of a transdermal formulation (i.e., 'poke and patch' method). Coated microneedles are coated with drug solution and inserted into the skin (i.e., 'coat and poke' method). Hollow microneedles contain arrays of solid, hollow micron-

sized needles filled with drug solution that is deposited directly into the dermis by diffusion or pressure-driven flow (i.e., 'poke and flow' method). Dissolving microneedles are fabricated with biodegradable polymers containing encapsulated active drug ingredients which solubilize and are released into the skin [26-28].

Microneedle technology has been shown to greatly enhance *in vitro* and *in vivo* transport of sumatriptan succinate drug across the skin. The 'poke and patch' method was successfully utilized by Nalluri et al. (2015) for transdermal delivery of sumatriptan through pig ear skin following pretreatment with Dermaroller® microneedle roller or AdminPatch® solid microneedle patch. *In vitro* permeation results indicated that acceptable therapeutic dose was possible with a 2.5 cm^2 transdermal patch following pre-treatment with an AdminPatch®, fitted with 1.5 mm length needles [29]. However, these solid, stainless steel AdminPatch® microneedle systems are not disposable and considered biohazardous sharps waste [30, 31]. Separately, two research groups developed dissolving microneedles from polysaccharide polymers (sodium hyaluronate or dextran) for *in vivo* delivery of sumatriptan succinate. *In vivo* studies for both polysaccharide microneedle systems showed promising bioavailability (> 90%) compared to subcutaneous 6-mg Imitrex® (sumatriptan) injection [32, 33]. Finally, a polyvinylpyrrolidone-based microneedle device, ZP-Zolmitriptan, was developed by Kellerman et al. to deliver zolmitriptan. Clinical phase I results showed ZP-Zolmitriptan achieved maximum blood serum levels, and a Cmax value equal or greater than 2.5-mg oral dose of Zolmitriptan [34].

The combination of iontophoresis and microneedle technologies has been shown to have synergistic effects and increase uptake of macromolecules through the skin while

modulating the drug delivery rate. Iontophoresis applies a low-density electric current (< 500 $\mu A/cm^2$) to the skin to propel charged drug molecules through the low-resistance tunnels created by the needles. For a positively charged drug, molecules are repelled by the positive electrode (anode) and attracted to the negatively charged electrode (cathode) [16, 35-38]. Several *in vivo* and *in vitro* studies have demonstrated increased delivery of macromolecules (oligonucleotides, dextrans, proteins) through porcine skin with microneedle pre-treatment and iontophoresis as compared to iontophoresis alone [20]. However, research on the combination of dissolving microneedle and iontophoresis technologies for drug administration is limited and neither method has influenced greatly the transdermal drug delivery market.

The experimental portion of this research focused on i) developing dissolving microneedles for the release of sumatriptan and ii) combining microneedle arrays with iontophoresis to optimize delivery (Figure 1.2 and 1.3). Dissolving microneedles are formulated from water-soluble biodegradable polymers that encapsulate the API within the matrix. The dissolvable microneedles are inserted into the epidermis where they dissolve in minutes, releasing the API into the dermis for rapid release into the systemic circulation. Microneedles dissolve leaving no sharp medical waste for disposal after use and studies show that skin punctures left by microneedles are painless and heal within 3 days [39-41]. There are several factors that affect drug delivery with microneedles, including microneedle height, microneedle density, number of microneedles, drug concentration, and size of encapsulated drug molecule [28, 39]. This research considered several sumatriptan preparations to evaluate the formulations with respect to its strength, flexibility, uniformity, and ease of insertion into the skin. These preparations were then combined with a range of

current densities (100 – 500 µA/cm^2) to determine the effect of the system on lag time, steady-state diffusion flux and cumulative drug release. *In vitro* studies were conducted with vertical Franz cells to determine sumatriptan release, from microneedle alone and microneedle combined with iontophoresis, through Göttingen minipig skin [42].

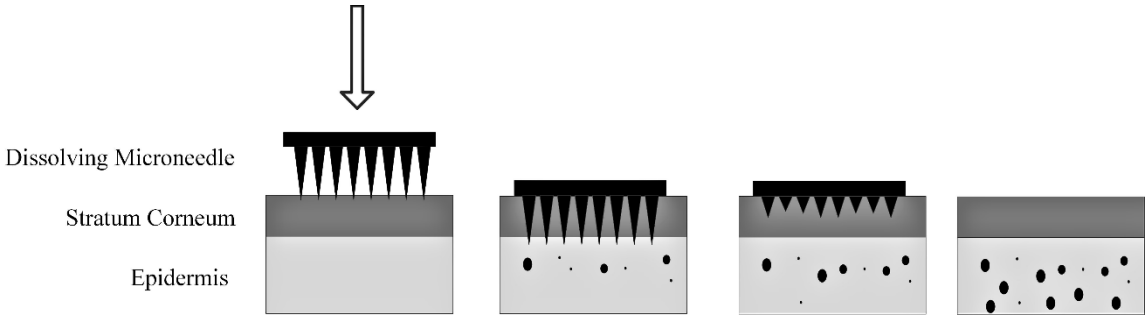

Figure 1.2 Schematic representation of dissolvable microneedles for rapid release of encapsulated drug.

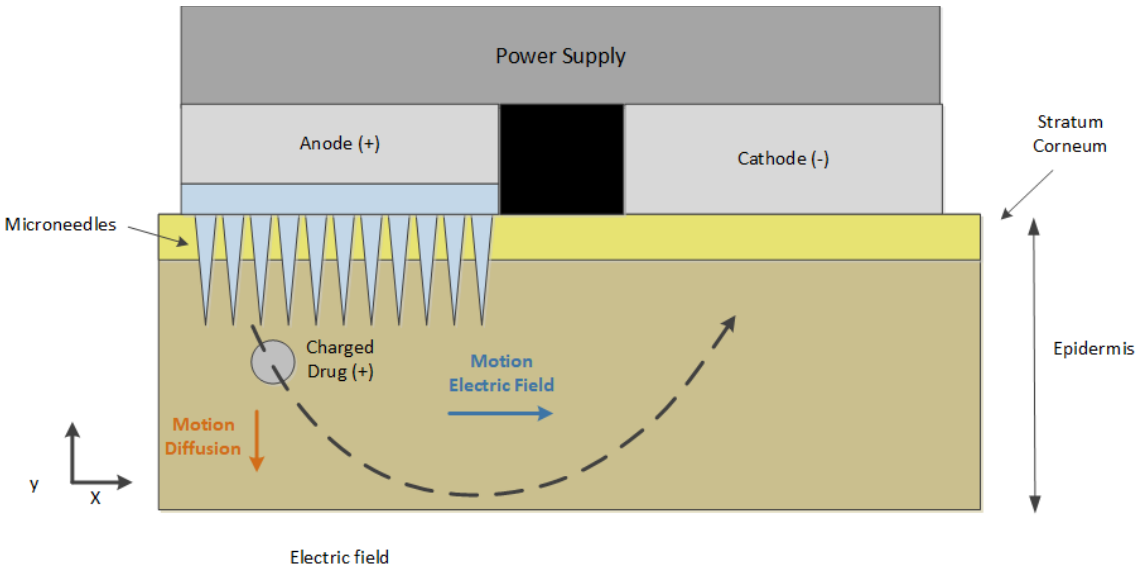

Figure 1.3 Iontophoretic transdermal microneedle patch.

Design optimization of the essential parameters of the microneedle systems is paramount to improving drug delivery through the skin. The dissolving microneedle systems must be able to properly insert into the skin without fracturing individual needles in the array. Several physical properties effect microneedle insertion, including microneedle geometry (shape of array), surface area, needle height, pitch width (center-to-center distance of adjacent needles), and polymer matrix type. In 2004, a study by Davis et al. demonstrated that the needle height and pitch-width were important properties with long, densely packed arrays required for greater needle penetration into the skin [28, 43]. In 2008, Al-Qallaf et al. working with hollow or solid squared-shaped microneedle arrays, developed a mathematical algorithm for determining the best parameters for the transport of drug macromolecules across the skin. The study showed that the pitch width had a greater impact on drug delivery than the needle radius [44]. In a separate study, Al-Qallaf and Davidson et al. developed a mathematical model, based on Fick's first law of diffusion, to predict delivery of macromolecules from coated solid microneedles which confirmed that needle height and pitch-width were crucial for increasing drug diffusion [45]. These models are based on solid and hollow microneedle systems and cannot be applied to drug delivery from dissolving microneedle arrays which involve dissolution and diffusion processes.

In 2015, Kim et al. designed a system of dimensionless governing equations for describing dissolution of an individual conical shaped microneedle and release of encapsulated drug into a control volume. Several simulations were conducted with sucrose microneedle containing encapsulated fentanyl citrate active substance that indicated i) a decreased pitch led to an increased permeation and ii) the dissolution rate was independent

of the elimination rate constant [46]. This research builds on previous studies by deriving several mathematical models based on Nernst-Brunner equation, Fick's 2nd law and Coulomb's law to describe: 1) dissolution of dissolving microneedles, 2) diffusion of drug through the skin and 3) impact of iontophoresis on microneedle dissolution and drug diffusion. Simulation experiments for each model allowed for a thorough analysis of the impact of model parameters (e.g., drug load, needle height, needle pitch width and polymer concentration) on the device performance. The predictions were then evaluated in the lab with *in vitro* permeation experiments using Franz cells, excised Göttingen minipig skin samples, and iontophoresis. Soluble microneedles with different formulations consisting of PVP polymer and sumatriptan succinate API were tested to confirm the models.

1.3 Research Significance and Impact

This research focused on the development of theoretical models based on transport phenomena principles to assess and predict drug delivery of encapsulated sumatriptan succinate in soluble microneedle systems alone and soluble microneedles aided by iontophoresis. The models were then used to identify critical attributes of the microneedle system (i.e., microneedle height, base width, pitch width), formulation factors (i.e., concentration, solubility and density) and process parameters (i.e., current density). The work was validated using *in vivo* permeation experiments with vertical Franz diffusion cells and skin excised from female Göttingen minipigs.

The developed platform can help explain new experimental results, aid in product design and the development of manufacturing processes. The contribution can be used to evaluate the delivery of protein and peptide macromolecules, as well as, poorly soluble drug molecules. The framework will potentially reduce R&D expenses, increase the quality

of results and make the clinical research less risky, less empirical and more reliable than trial-and-error experimental procedures.

The advantages of this research will be i) development of optimal transdermal drug systems for the delivery of macromolecules to the systemic circulation, ii) more precise prediction of drug delivery into the body, iii) reduction of therapeutic ‘lag time’ effect, and iv) increased therapeutic effects of drug molecules.

The application and benefits of combining dissolved microneedles and iontophoresis merit further analysis to unlock the full potential of this burgeoning technology. A detailed assessment of the synergistic effects of the two methods promises to result in a deeper understanding of design criteria pertinent to the transdermal delivery of macromolecules. For example, many medical diseases and conditions require treatment over a long period, e.g., from 24 hours to 7 days. For these cases, a slow and constant supply of a macromolecule can be achieved by designing an iontophoretic transdermal system with a slow dissolution of the microneedles. The current density is easily increased to provide a faster release for patients requiring an immediate pain relief. It is possible to adjust the device to design appropriate treatment regimens for specific patient groups and drug molecules.

CHAPTER 2

MATERIALS AND METHODS

2.1 Chemicals and Reagents

Microneedle formulations consisted of the active pharmaceutical ingredient (API) sumatriptan succinate [3-[2-(dimethylamino) ethyl]-N-methyl-indole-5-methane-sulfonamide succinate (1:1)] purchased from Meohs Fine Chemicals (Iberica SL), polyvinyl pyrrolidone (Kollidon K30) acquired from BASF (Ludwigshafen, Germany), polysorbate 80 procured from Croda (New Castle, DE), and glycerine obtained from P&G chemicals (Cincinnati, OH). All other chemicals and reagents were analytical grade.

2.2 Preparation of Sumatriptan Microneedle Arrays

The sumatriptan succinate microneedle systems were fabricated using methods previously described by the author [42]. A total of four PVP-based sumatriptan microneedle formulations were developed for characterization studies and their compositions are listed in Table 2.1.

Table 2.1 Microneedle Array Wet Composition (%, w/w)

Excipients	P1	P2	P3	P4
Sumatriptan	10	5	5	15
Polyvinylpyrrolidone	30	30	20	30
Water	58	63	73	53
Glycerine	1	1	1	1
Polysorbate 80	1	1	1	1

An aqueous pre-solution was prepared by slowly dissolving PVP, polysorbate 80 and glycerine in purified water, and degass by sitting on benchtop. The active solution was formulated by adding an aliquot of this pre-solution (e.g., 2 – 5 ml) to a small beaker, adding the sumatriptan succinate API, stirring until fully dissolved, and degas by sitting un-stirred on the bench-top. Approximately 100 mg of active solution was pipetted into each negative mold of platinum-cured silicone microneedle arrays (i.e., negative molds) and pressed into microneedle chambers by pressure using methods described by other research groups [47, 48]. The molds were dried at room temperature under ambient conditions overnight on the lab bench. The dried microneedle arrays were carefully removed from the PDMS molds and sealed in water-resistant containers. The PVP-sumatriptan microarrays were stored in the sealed containers at room temperature for up to 6 weeks and retained their pyramid needle shape, as examined under microscope.

These fabrication techniques were used to prepare circle microneedle arrays from each preparation (P1 – P4) and square arrays from P1 formulation (Figure 2.1).

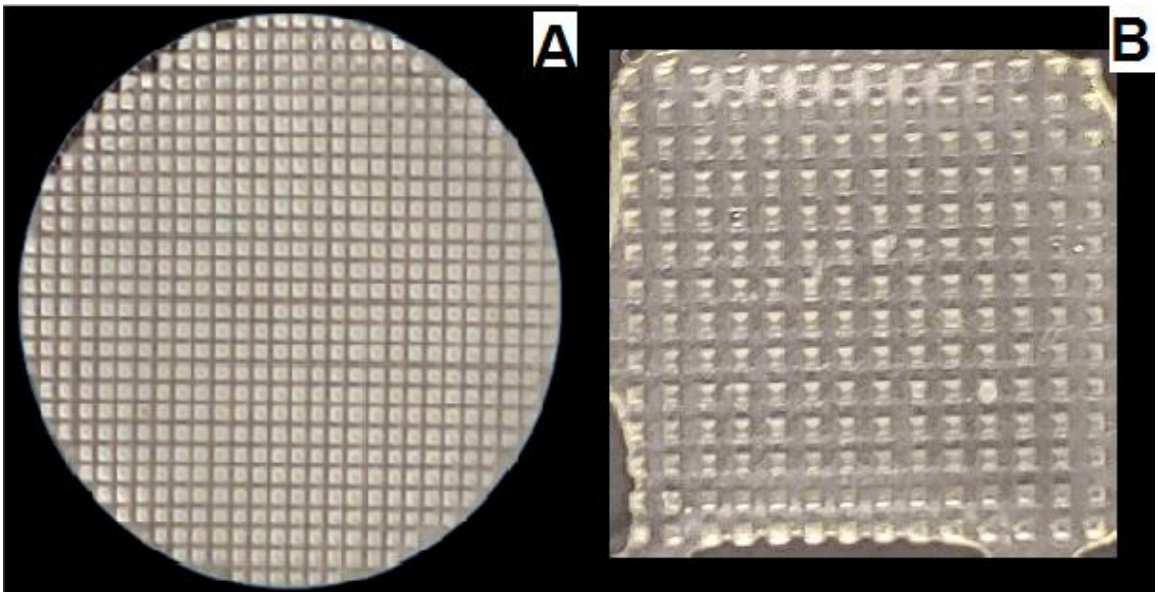

Figure 2.1 Photographs of P1 formulated dissolving microneedle arrays; A) circle array containing 600 pyramid-shaped needles; B) square array containing 196 pyramid-shaped needles.

2.3 Characterization of Microneedles with Light Microscope

The microneedle systems were visually examined using light microscope (Nikon Optishot-2, Nikon, Japan), digital sight (Nikon D5-Fi1, Nikon, Japan) and imaging software (NIS-Elements, Nikon, Japan) [42]. Circle microneedle arrays from each preparation (P1 – P4) and square arrays from P1 formulation were inspected to ensure they maintained consistent appearance, shape and dimensions. Circle arrays from each formulation were inspected to ensure they contained 600 uniform pyramid-shaped needles with consistent height of 500 µm, base width of 300 µm and pitch width (i.e., center-to-center distance between needles) of 300 µm (Figures 3.4 – 3.7). Also, square-shaped arrays (P1 formulation) were examined

to confirm each contained 196 individual pyramid-shaped needles with consistent height of 500 µm, base width of 385 µm and pitch width of 700 µm.

A different optimal microscope (Swift-Duo, Vision Engineering, Woking, UK) and imaging software (M3 Metrology, Vision Engineering, Woking, UK) were used to examine minipig tissue samples following *in vitro* permeation trials. The minipig samples were inspected for patterns of small holes corresponding to the circle and square microneedle array patterns.

2.4 Tensile Strength

The microneedle systems mechanical strength was evaluated using a texture analyzer (TA.XTPlus, Stable Microsystems Ltd, Godalming, UK), as described previously [42]. The mechanical failure force of individual arrays was measured using the instrument in compression mode equipped with a 3-point bend fixture (HPD/3 PB, Stable Microsystems Ltd, Godalming, UK). Prior to performing the tests, the PVP-sumatriptan microneedles were stored for 24 hours at 25 °C and 45% relative humidity for 24 hours. For each test, a single microarray is loaded onto the 3-point bend fixture (Figure 2.1), a sensor probe applied an axial load to the microneedle at 0.1 mm/s. The test was terminated when a maximum displacement (5 mm) was attained or force decreased below a threshold (< 0.1 N). For each test, a force (N) versus displacement (mm) curve (similar to stress versus strain curve), based on average force values (n=3), was generated.

Figure 2.2 Set-up of three-point bend apparatus for testing mechanical strength of microneedle array.

2.5 Mass, Drug Content and Density of Microneedle Systems

Laboratory experiments were conducted to determine the mass, drug content and density of the microneedle systems. Ten microneedles, from each formulation, were prepared per the methods described in Section 2.2. During preparation, the wet weight of drug solution dispensed into each mold, m_{wet}, and the dry weight of fabricated microneedles, m_{dry}, were measured on an analytical balance. The mass of the microneedle was calculated as the average dry weight of the ten microneedles. The average drug content (i.e., mass fraction

of sumatriptan API, β), in each microneedle was calculated using Eq. 3.1l; where $\%\ Drug_{MN,wet}$ is the percent (%, w/w) of sumatriptan in the microneedle solution.

$$\beta = \frac{\left(\%\ Drug_{MN,wet}\right)\left(m_{wet}\right)}{\left(m_{dry}\right)} \tag{2.1}$$

The density of the microneedle systems was measured by standard water displacement technique described in [49]. A 5 ml aliquot of purified water was dispensed into a 10 ml volumetric flask. The ten microneedles were inserted into the flask and submerged beneath the surface of the water. The total volume of water was measured and used to calculate the average density of the dissolving microneedles from each formulation.

2.6 Simulated Biological Fluid Preparation

A simulated biological solution was prepared, as previously described [49], as a surrogate for interstitial fluid located in the skin. A one liter parenteral simulated body fluid, developed by Marquis et. al. [50], was blended in the lab. The solution was determined to be a suitable substitute for determining the solubility of the microneedle matrix polymer (i.e., polyvinylpyrrolidone) in tissue fluid. The fluid was originally designed as a dissolution medium for conducting experiments on parenteral dosage forms including subcutaneous, intravenous, and intramuscular injections or implants.

2.7 Polyvinylpyrrolidone Solubility

The solubility of the matrix polymer (PVP) was measured in a simulated biological fluid (solvent), as previously described by the author [49]. One hundred milliliter of simulated biological solution was dispensed into a 250 ml glass beaker and stirred with a stand mixer

(Eurostar, IKA, Staufen, Germany). PVP polymer was added to solution in increments of 10 g and allowed to dissolve into solution. The visual appearance was recorded and solution viscosity was measured using a handheld Brookfield viscometer (Viscotester 2-plus, Haake, Karlsruhe, Germany). The biological solution was determined to reach saturation at 1.0 g/ml when the fluid viscosity exceeded that of lubricant oil (approximately 10 dPas). It is presumed that the interstitial fluid viscosity would not exceed that of lubricant oil and that this described a realistic solubility value. A plot of the viscosity (dPas) versus concentration (g/ml) is shown in Figure 2.2.

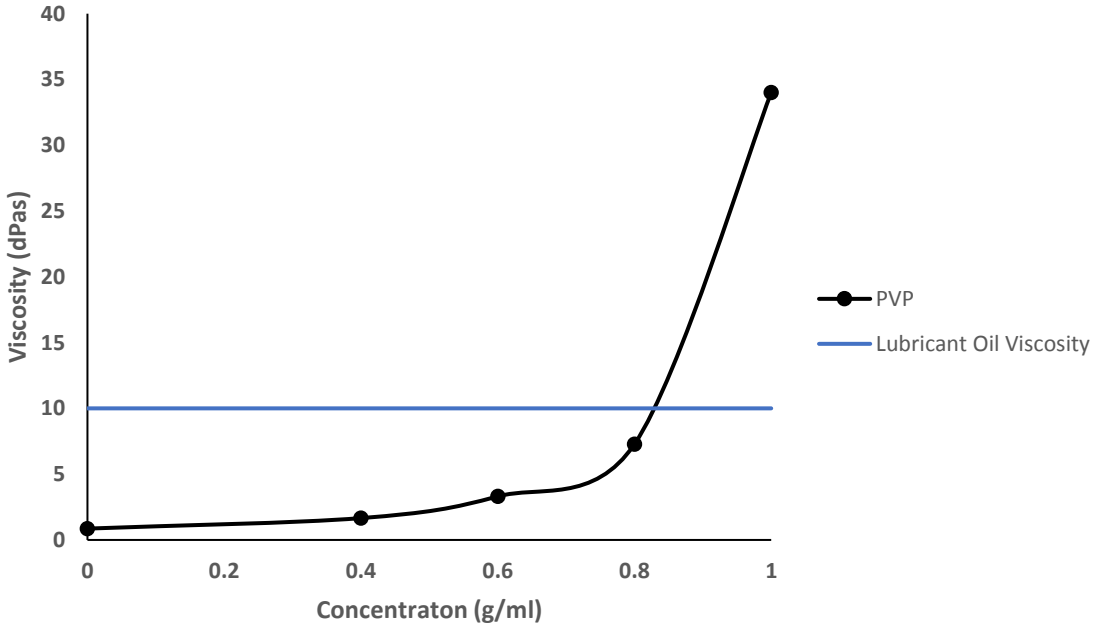

Figure 2.3 Viscosity – concentration curve for PVP in simulated biological fluid.

2.8 Minipig Skin Preparation

Whole female Göttingen minipig skin tissue samples (Ellegaard Göttingen Minipigs Agricultural Service, Denmark) were purchased and prepared as described in [42]. Frozen

full minipig skin samples were thawed at room temperature, rinsed with water, shaved to remove hair and dermatomed to thickness of 800 µm (Acculan 3TI; Aesculap AG). The prepared skin samples were punched into samples (25 mm diameter), frozen and stored for use within a 9-month period. Göttingen minipig tissue was selected for the *in vitro* permeation studies as an excellent model for human skin. The minipig skin is histologically similar to human skin and exhibits lower inter- and intra-variation due to breeding standardization [51, 52].

2.9 Optical Coherence Tomography Imaging

Optical coherence tomography (OCT) imaging equipment was used to generate high-resolution, cross-sectional tomographic images of the Göttingen tissue structures in real-time during microneedle treatment. OCT imaging creates a set of 2-dimensional images representing back-reflected light from a series of cross-sectional planes through the sample [53]. In the lab, imaging was performed with an optical coherence tomography device (VivoSight TP1302, Michelson Diagnostics Ltd., Kent, UK) and imaging software (VivoSight 4.5 software, Michelson Diagnostics Ltd., Kent, UK). *In vitro* studies of microneedle systems dissolving within the minipig tissue samples were imaged in real-time until needles were fully dissolved.

2.10 Transepidermal Water Loss (TEWL)

Transepidermal water loss (TEWL) was used to characterize the barrier function of the minipig skin using a TEWL device (Biox AquaFlux, AF200, London, UK). The TEWL, or skin surface vapor loss, is good indicator of the barrier function of the stratum corneum with damaged skin (e.g., dry skin) displaying high TEWL values compared to normal skin

[54-56]. Tests were conducted on mini-pig skin samples before and after insertion of dissolving microarrays into the skin. Individual 10 mm diameter microneedles were applied to a 25 mm diameter mini-pig skin samples. The microneedles were inserted using a custom device which applied uniform tangential force across the skin (approximately 150 N/cm^2). After insertion, the microneedle was held in-place on the skin for a period of 15 seconds to ensure good penetration into the skin surface. For comparison, TEWL was measured before and after tape-stripping minipig skin 15x to remove the stratum corneum. Tape-stripping skin 15x has been shown to remove horny corneocyte layers (stratum corneum) from the epidermis [57]. The tape-stripping method involved applying a standard pressure-sensitive adhesive tape (e.g., Scotch-tape®) to the skin surface, pressing firmly for over 5 seconds and slowly remove tape.

2.11 *In vitro* Permeation Studies

In vitro diffusion experiments, as described previously [42], were performed in vertical Franz diffusion cells (Glastechnik, Gräfenroda, Germany) with a diffusion area of 1.595 cm^2. Frozen tissue samples (25 mm diameter) were thawed and placed with skin surface (stratum corneum side) facing up on benchtop. To imitate realistic conditions, the tissue samples were not pre-wetted. Sumatriptan microneedle arrays were placed gently onto the skins and inserted into the skin using a custom applicator device designed to apply a uniform impulse force (150 N/cm^2) during insertion. The microneedle-skin samples were covered with a PET liner and immediately placed into the Franz cells with the microneedles facing the donor compartment. The occlusive PET liner was placed over the microneedle-skin samples to facilitate diffusion into the skin. The receptor chamber was filled with 10-mL phosphate buffer solution (pH 7.4) (PBS) containing sodium azide (0.1%, w/w), stirred,

and controlled at 32 °C. At prearranged time intervals, the receiver cell solution was withdrawn completely and replaced with fresh PBS (10 ml) to maintain sink conditions. The diffusion studies were used to acquire data, including microneedle drug load (µg/cm^2); percentage drug released after 24 hours (%); cumulative amount of drug released after 24 hours, Q_{24h} (µg/cm^2); sumatriptan steady-state flux, Jss (µg/cm^2/h); sumatriptan retained in skin (µg/cm^2) and lag time (h).

For comparison, passive diffusion (control) studies were conducted with inverted microneedle samples from preparations P1 and P2. The control samples were prepared by gently placing inverted microneedles (i.e., needles faced upward) onto minipig skin samples, covered with occlusive PET liners and inserted into vertical Franz cell device. Additional passive diffusion studies were performed with P1 and P2 microneedles on skin samples after removing the skin's stratum corneum. The stratum corneum was carefully removed from the minipig skin samples using the tape-stripping method (15x) described in Section 2.10. Following removal of the stratum corneum, inverted microneedles were gently placed onto skins and covered with PET liners for placement in Franz cell. Finally, *in vitro* permeation of a sumatriptan reference donor solution was measured. Reference solution samples were prepared by applying 100 µl aliquot of 5 mg/ml sumatriptan succinate in PBS (pH 7.4) solution to the non-woven pad (SA = 1.188 cm^2) applied to the skins (Figure 2.3), cover with PET liner and inserted into Franz cell.

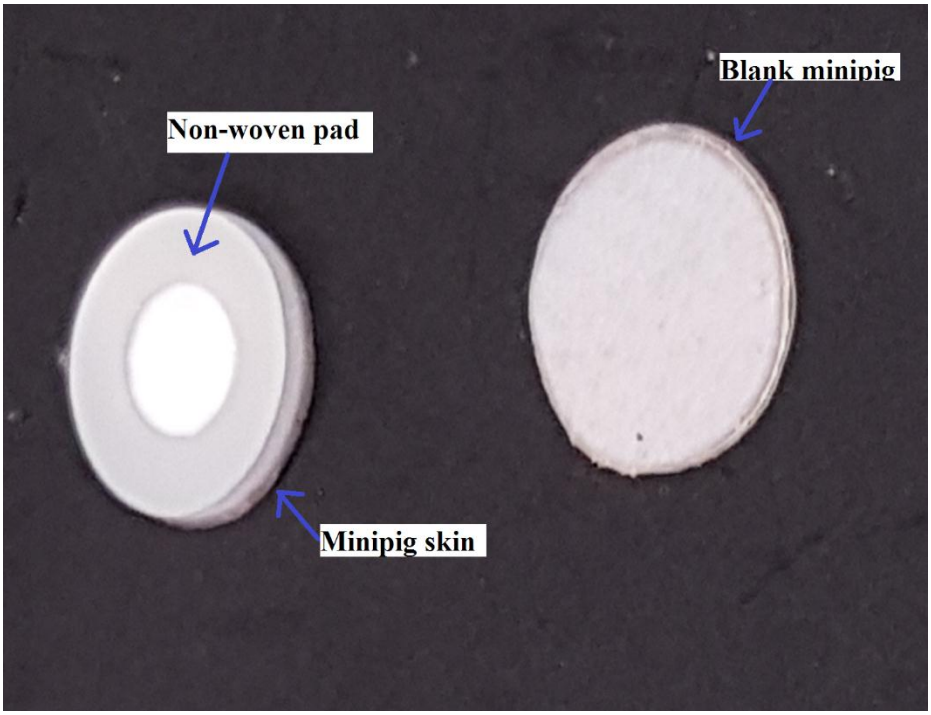

Figure 2.4 Non-woven pad on minipig skin containing sumatriptan reference solution.

For iontophoresis, *in vitro* permeation studies were set-up in a two chamber Franz cell configuration with silver/ silver chloride electrode couples connected by a silver wires (Figures 2.4 - 2.5). Sumatriptan succinate is positively (+) charged at pH 7.4, the anode electrodes were placed in the donor compartment directly on-top of the microneedle-skin samples [58]. A constant physiologically acceptable electric current, between 100 to 500 $\mu A/cm^2$, was applied to microneedle-skin samples using a power supply (Hameg HM 7042-5, Mainhausen, Germany) [37, 59, 60]. The iontophoretic diffusion studies were used to acquire data including: microneedle drug load ($\mu g/cm^2$); percent drug permeated in 6 hours (%); cumulative amount after 6 h, Q_{6h} ($\mu g/cm^2$); sumatriptan steady-state flux, Jss ($\mu g/cm^2/h$); and lag time (h).

Figure 2.5 Two-chamber franz cell system with electrical current.

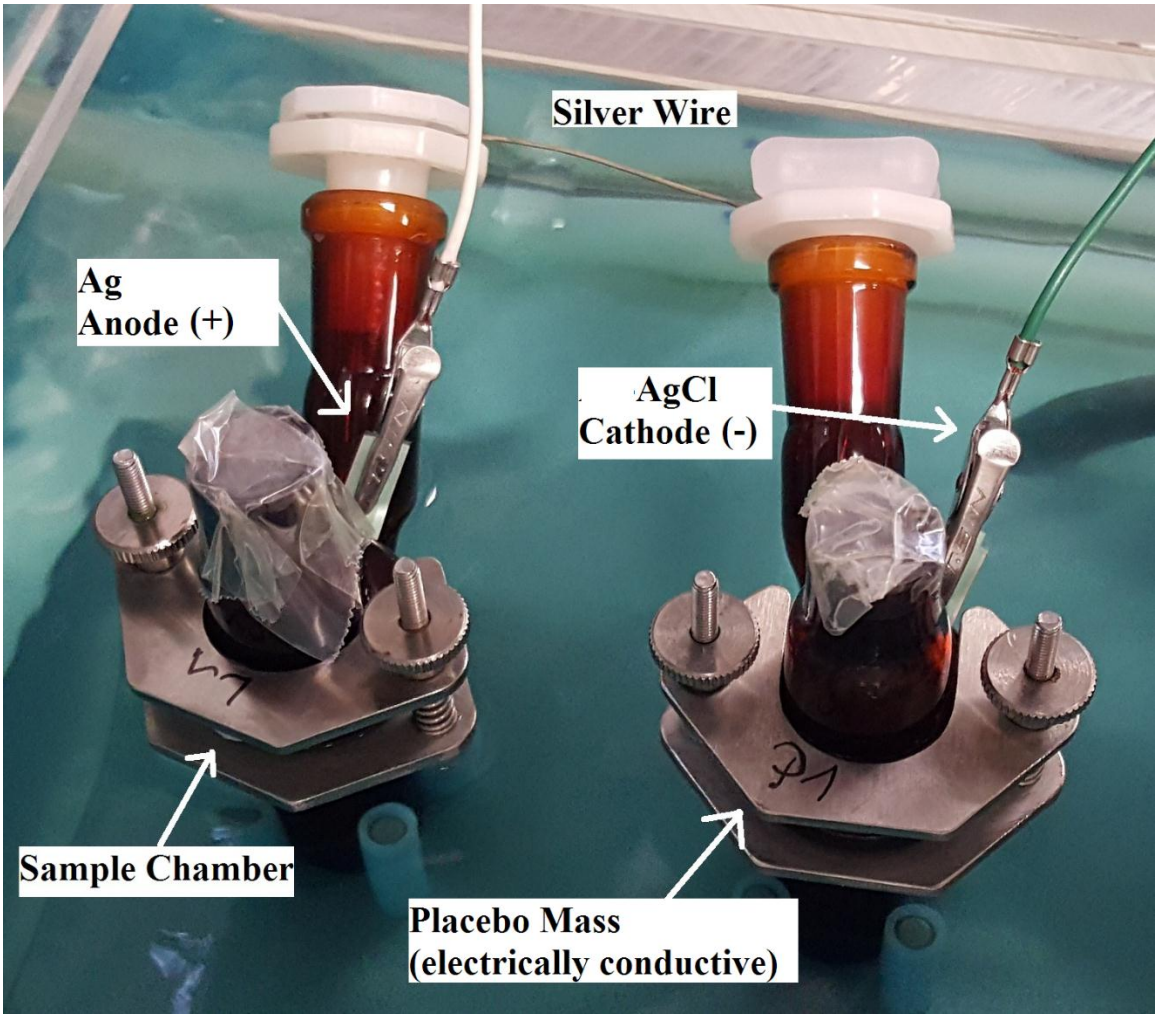

Figure 2.6 Two-chamber franz cell system with silver-silver chloride electrodes.

2.11 Analytical Methods

Analytical sample aliquots, collected from the receiver cell, were analyzed with a High-Performance Liquid Chromatography (HPLC) system (Jasco LC-2000Plus Series, Tokyo, Japan) [42]. The HPLC was equipped with a C18 column (Kromasil, 250 x 4.6 mm, 5 µm, VDS Optilab, Berlin, Germany) and a UV Detector (Jasco 2077). The mobile phase contained a mixture of sodium dihydrogen phosphate solution and acetonitrile (pH 3.2) (90:10, v/v); flow rate of 1.5 ml/min. The UV detection set at 227 nm and the injection

volume was 20 µL. The sumatriptan drug retained in the tissue samples after *in vitro* diffusion were extracted by shaking samples in 5 ml methanol for 24 hours.

2.12 Statistical Methods

Statistical analysis was performed with Matlab software (Mathworks, Natick, Massachusetts, US). An unpaired students t-test was applied to evaluate multiple data sets using a one-way analysis of variance (ANOVA). The ANOVA comparison results were considered statistically significant if $p < 0.05$.

CHAPTER 3

DEVELOPMENT OF SOLUBLE MICRONEEDLE SYSTEM FOR DELIVERY OF SUMATRIPTAN SUCCINATE

3.1 Formulation of Sumatriptan Dissolving Microneedle Array

For this research, a dissolving microneedle system was developed to meet several integral design criteria including:

- Microneedle is comprised of biocompatible polymer.
- Microneedle is soluble in water.
- Microneedle system has sufficient mechanical strength to penetrate skin.
- Microneedle formulation is stable over long term storage at room temperature.
- Active pharmaceutical ingredient is positively (+) charged at physiologic pH 7.4 for iontophoretic delivery.
- Microneedle fabrication process is scalable for commercial manufacturing.
- Microneedle device will meet regulatory compliance requirements.

These criteria were considered when selecting active and inactive pharmaceutical excipients for the microneedle formulation.

A medium viscosity polyvinylpyrrolidone (Kollidon K30) polymer was chosen as a binder due to its favorable properties that include readily soluble in water, inert, low toxicity, biodegradeable, and biologically compatible [61]. Polyvinylpyrrolidone (PVP) has been used in numerous oral tablet formulations as a binding agent and in ophthalmic solutions as a lubricant. The polymer was approved by the FDA for use as an inactive ingredient in pharmaceutical formulations [62]. Laboratory experiments confirmed PVP (k30) readily dissolves in water at concentrations equal or less than 30% (w/w) and

mixtures quickly degassed with slow mixing or standing still on lab bench. In contrast, exploratory experiments with water-soluble carboxymethylcellulose (CMC) yielded aerated, highly viscous solutions at low concentrations (< 5%, w/w) which could not be degassed with a vacuum pump. For these reasons, PVP (k30) was selected as matrix polymer for microneedle systems.

The active ingredient sumatriptan succinate (C18H27N3O6S) was selected as an ideal active pharmaceutical ingredient for assessment of microneedle formulations. Imitrex® (sumatriptan) is approved by the FDA for use in oral, subcutaneous, intranasal and iontophoretic prescriptions [14, 25, 63, 64]. Sumatriptan has a molecular weight of 413.5 Da, an octanol/water partition coefficient of -1.5 (pH 7.4), a solubility in water of 101 mg/ml (20 °C), a low melting point of 165°C, and is positively charged. Thus, it is not suitable for passive transdermal diffusion which requires small molecules with low molecular weight (< 500 Da) and a high lipophilicity (Log P ~2-3) [18, 19]. However, a well-designed microneedle device should be able to deliver large hydrophilic macromolecules, such as sumatriptan, through the skin [28, 39]. Furthermore, iontophoresis, or the application of a mild electric current (< 500 $\mu A/cm^2$), has been shown to significantly increase *in vitro* and *in vivo* transdermal delivery of sumatriptan succinate [65, 66]. Thus, the sumatriptan succinate API will be used to evaluate microneedle formulations for enhanced transdermal delivery with and without iontophoresis.

The excipient glycerin (i.e., glycerol) was added to the formulation as a lubricant to provide smoothness to the microneedle systems. Preliminary formulations containing PVP, sumatriptan and water resulted in microarrays that were difficult to remove from silicone molds and often deformed during the de-molding process. Addition of 1% (w/w)

glycerin to the formulations yielded smooth microneedle arrays that remained intact during the demolding process (Figure 3.1b-e). The glycerin additive is frequently used in pharmaceutical products with low risk of toxicity and accepted by the FDA as 'generally recognized as safe' (GRAS).

The hydrophilic nonionic compound polysorbate 80 (PS 80) was incorporated as a surfactant in the aqueous formulation. The PS 80 helped facilitate proper wetting of drug solution onto the negative silicone molds by reducing surface beading effects. Additionally, PS 80 increased the flexibility of the dried microneedle systems. Initial PVP, sumatriptan and water formulated arrays yielded non-uniform, brittle microneedles with small air bubbles (Figure 3.1a). Formulations with 1% (w/w) PS 80 provided uniform, flexible microneedle systems that were bubble-free (Figure 3.1b-e). The PS 80 has been approved by FDA for use in pharmaceutical and cosmetic industry in lotions, vaccines and intravenous medications.

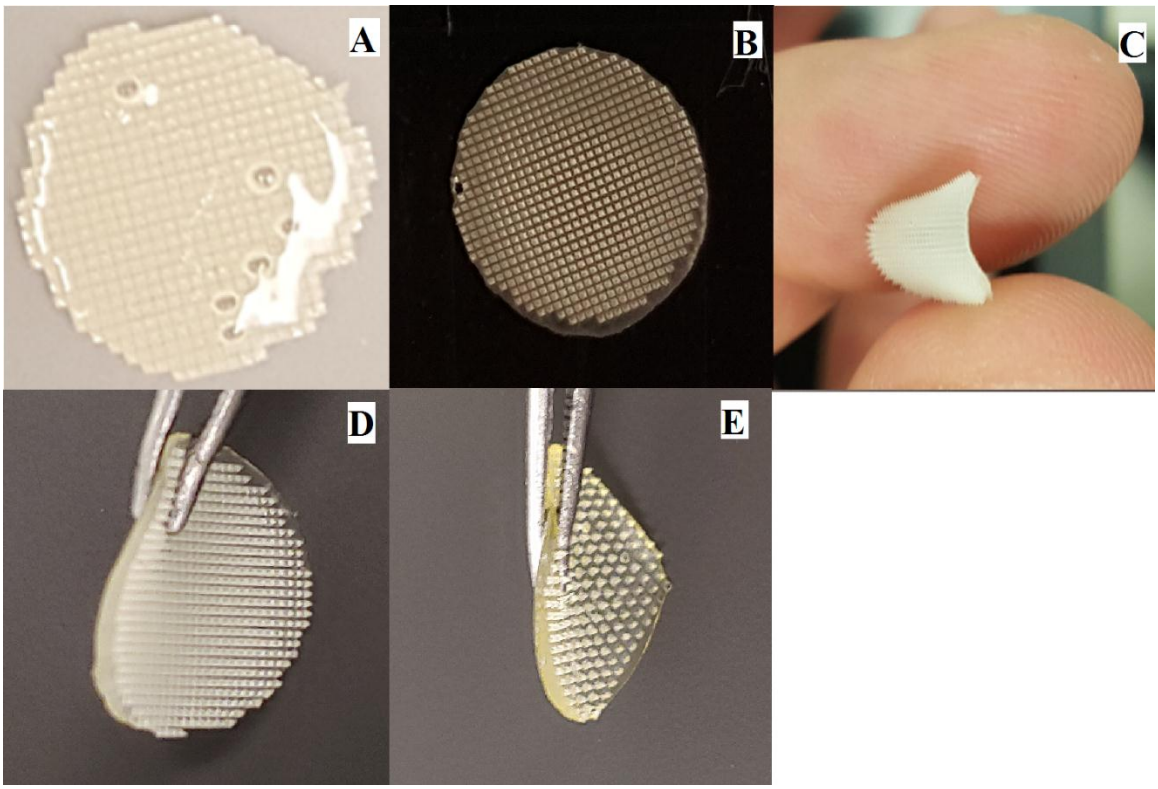

Figure 3.1 Photographs of polyvinylpyrrolidone microneedle arrays; (A) microneedles, containing only PVP (20%, w/w), are glassy, brittle, non-uniform and contain bubbles; (B-C) microneedles, containing PVP (20%, w/w) , glycerol (1%, w/w) and polysorbate 80 (1%, w/w), are uniform, flexible and produce no bubbles; (D-E) P1 formulated microneedles with sumatriptan are uniform, flexible and do show any bubble.

The formulations were made in the laboratory using standard mixing equipment. Four different systems, with compositions described in Table 2.1, were prepared with purified water, 5 – 15% (w/w) sumatriptan succinate, 10 – 20% (w/w) PVP, small amounts of glycerin and polysorbate 80. A 50 ml pre-solution was prepared from inactive ingredients in a beaker using a powered stand mixer. The pre-solution was easily degassed with slow mixing or by standing still on the lab benchtop. A 2 – 5 ml active solution was prepared by manually mixing sumatriptan powder with the pre-solution in a small beaker using a metal spatula. The active solutions were degassed by allowing them to sit on a benchtop. The sumatriptan API did not dissolve into solution at the higher 15% (w/w)

concentration (P4 formulation) and tiny particulates were observed in the solution. However, P4 microneedles were fabricated to assess the effects of increased drug load on the physical properties of the microneedles, including needle geometry and mechanical strength.

The circle and square-shaped microneedle arrays (Figure 2.1) were prepared from the active solution using silicone molds (negative) and a small pressure vessel. The drug solution was carefully pipetted into silicone molds which were then placed onto a custom microneedle stand (Figure 3.2.b) for transfer into the pressure vessel (Figure 3.2.c). The drug solution was filled into the needle cavities in the molds by applying 2 – 6 bar pressure over the molds for approximately 15 minutes, similar to procedure described by Ripolin et al. [47].

The molds were removed from the pressure vessel and dried overnight under ambient conditions of 25 °C and 65% relative humidity (Figure 3.2.d). Following drying, the microneedles were carefully peeled from the silicone molds and sealed in moisture resistant containers. The microneedles were stored up to 6 weeks at room temperature and individual needles retained their pyramid-shape, as verified by inspection under a microscope.

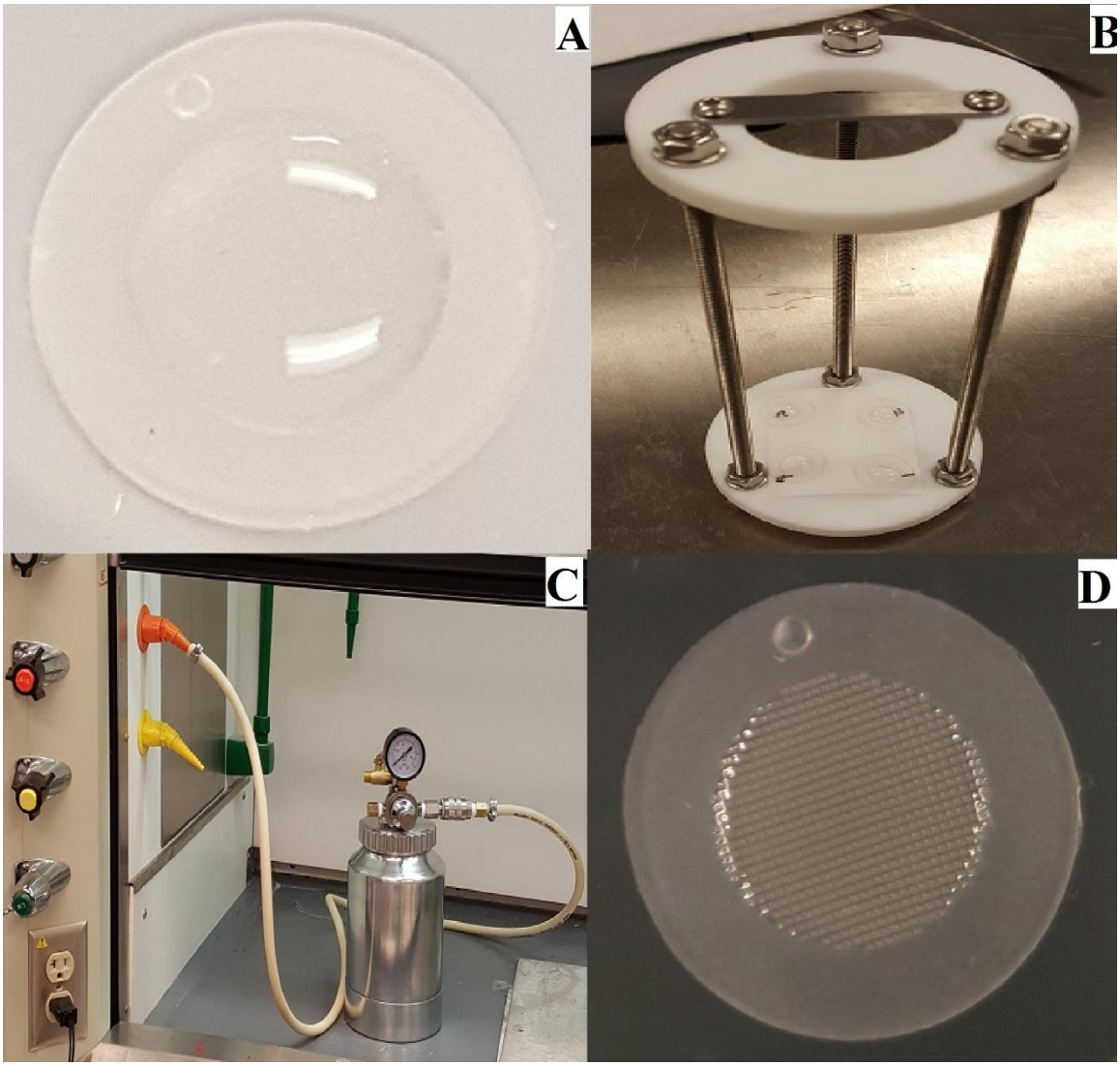

Figure 3.2 Photographs of the laboratory setup; (A) silicone mold filled with P1 solution; (B) stand to transfer filled microneedle molds into the pressure vessel; (C) pressure vessel; (D) dried P1 microneedles in the silicone mold.

For commercial applications, regulatory agencies will probably require that the microneedle devices be sterile and produced under aseptic conditions to prevent infection during treatment. The previously described manufacturing process should be amended to

sterile filter (0.22 μm) the active solution. The casting, drying and packaging operations should be performed under aseptic conditions [67].

3.2 Characterization of Sumatriptan Dissolving Microneedle Array

The PVP-Sumatriptan dissolving microneedles were evaluated to determine the optimal formulation (P1 – P4) in relation to a number of physical characteristics including:

- Microneedle array uniformity.
- Microneedle Drug Load, β
- Microneedle Density, ρ
- Solubility of PVP polymer in body fluid, c_S
- Microneedle mechanical strength
- Microneedles ability to penetrate minipig skin
- Transepidermal water loss (TEWL)

The microneedle formulations (P1 – P4) were evaluated with respect to uniformity, strength, flexibility and ability to penetrate minipig tissues [42]. The microneedle systems must maintain structural integrity with respect to needle array pattern, height, width, and pitch width pre- and post- insertion for proper drug delivery. For example, an array with non-uniform needle heights may lead to difficulty inserting the array into skin and/or failure of some needles to penetrate the skin. Dissolving microneedle systems from each formulation (P1 – P4) were visually inspected with a light microscope (Figures 3.3 – 3.7). For each formulation, circular microneedle systems had a surface area of 0.785 cm^2 and contained a total of 600 needles with a height of 500 μm, width of 300 μm and pitch width

of 350 µm. Square microneedle array systems were molded from P1 solution to form square array patterns with a 0.884 cm^2 surface area consisting of 196 needles with needle height of 500 µm, needle width of 385 µm and pitch width of 700 µm. Table 3.1 contains a summary of the geometric dimensions for each microneedle formulation, including the microneedle surface area (SA), base width (w), height (h), needle pitch width (p_w) and base-plate thickness (d_{bp}). All microneedle formulations (P1 – P4) produced uniform microneedle systems in terms of needle spacing, height, width and pitch width.

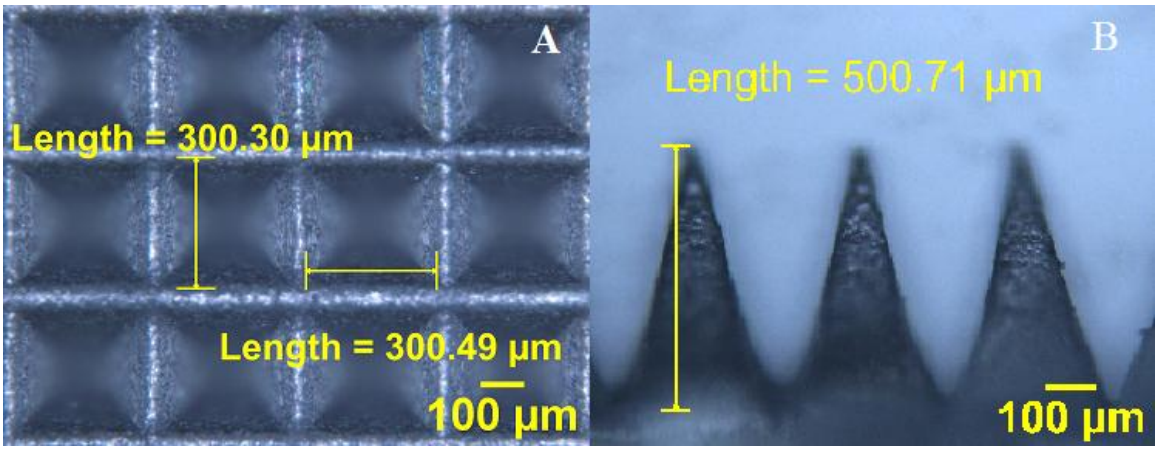

Figure 3.3 Optical microscope image P1 circle microneedle; (A) top-down view; (B) side view.

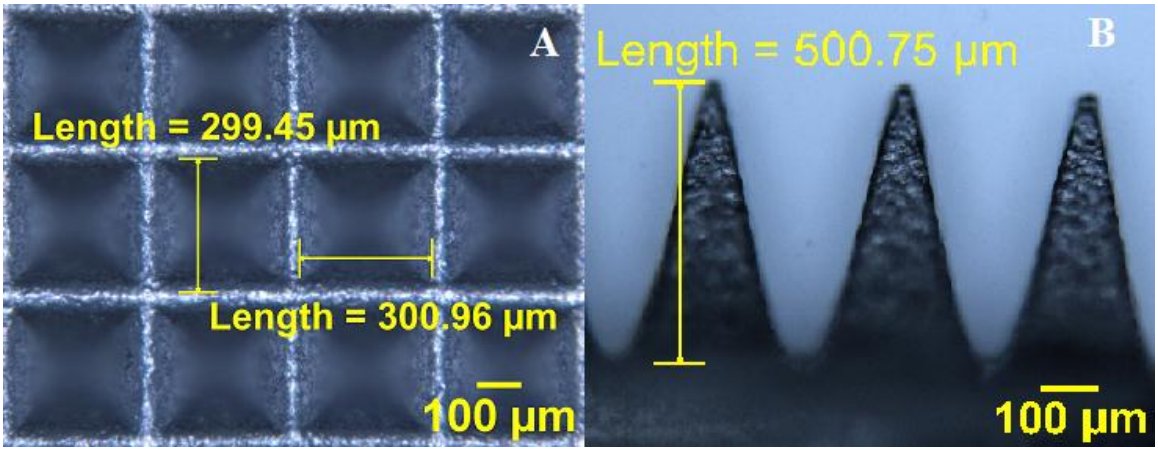

Figure 3.4 Optical microscope image P2 circle microneedle; (A) top-down view; (B) side view.

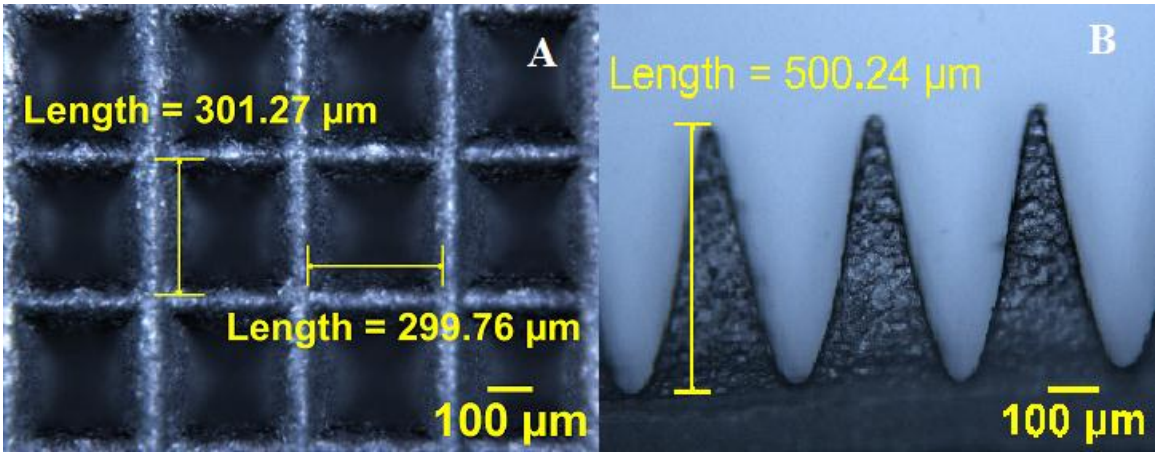

Figure 3.5 Optical microscope image P3 circle microneedle; (A) top-down view; (B) side view.

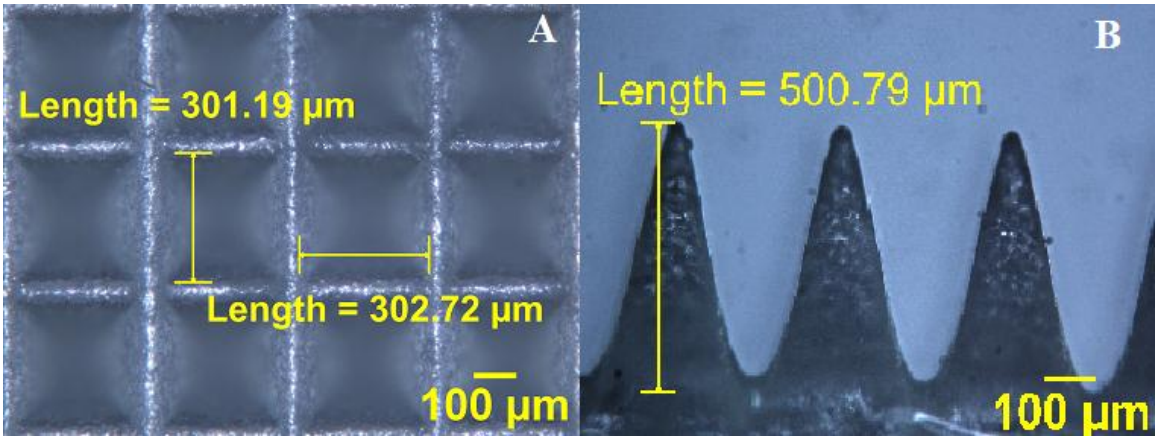

Figure 3.6 Optical microscope image P4 circle microneedle; (A) top-down view; (B) side view.

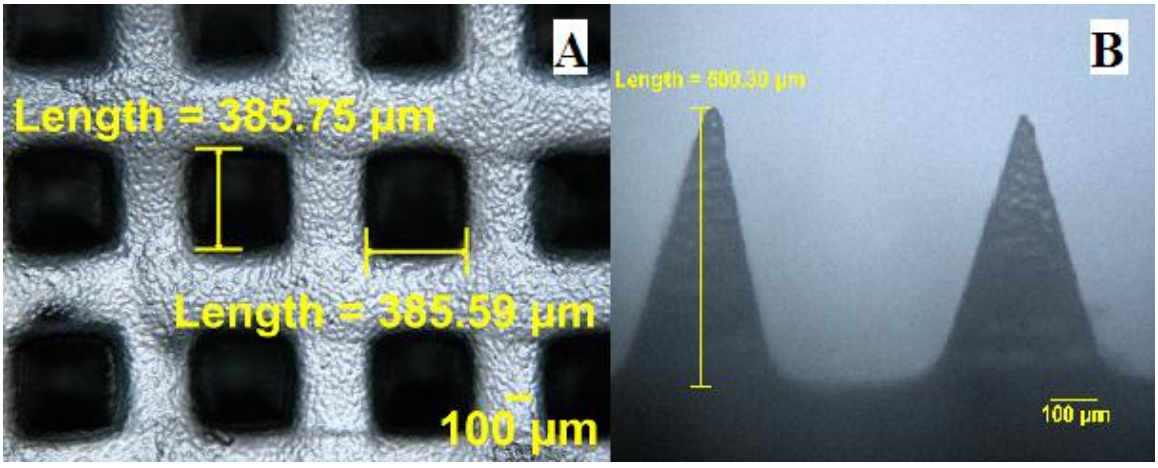

Figure 3.7 Optical microscope image P1 square microneedle; (A) top-down view; (B) side view.

Laboratory experiments were performed to determine the physical properties of the different microneedle formulations, including the microneedle dried mass (m_{dry}), microneedle drug load (β), microneedle density (ρ), and solubility of PVP in body fluid (c_S) (Table 3.1). The microneedle systems mass, drug content and density were calculated using the methods described in Section 2.5, except for the P4 microneedles. The drug

content and density of P4 microneedles were not measured due to the insolubility of sumatriptan in the formulation. The arrays contained increasing drug content (β) in the order of P2 < P3 < P1; with P1 micro arrays containing the most mass and drug content, as expected, due to the higher PVP content and drug loading. The P1 square arrays had a slightly higher drug content than circle arrays, which was attributed to a lower moisture retention due to increased surface area. The most dense microneedle system was P3 with array density decreasing in the order of P3 > P2 > P1. The determination of the solubility of polyvinylpyrrolidone polymer matrix in simulated body fluid is described in Section 2.7. The United States Pharmacopeia (USP) suggests the simulated biological fluid as a dissolution medium for testing *in vitro* release rate of parenteral dosage forms including subcutaneous, intravenous, and intramuscular injections [50].

Table 3.1 Microneedle Dimensions and Physical Properties

	Geometric Dimensions						Formulation Properties			
			Needle							
	Needles	**SA (cm^2)**	**w (µm)**	**h (µm)**	**p_w (µm)**	**d_{bp}* (µm)**	**m_{dry} (mg)**	**β (%)**	**ρ (g/cm^3)**	**c_S (g/cm^3)**
Circle Arrays										
P1	n = 600	0.785	0.03	0.05	0.035	0.038 ± 0.005	40.2	0.2142	1.150	1.0
P2	n = 600	0.785	0.03	0.05	0.035	0.032 ± 0.002	36.3	0.1234	1.210	1.0
P3	n = 600	0.785	0.03	0.05	0.035	0.019 ± 0.005	25.8	0.1784	1.291	1.0
P4	n = 600	0.785	0.03	0.05	0.035	NT	46.4	N/A	NT	1.0
Square Array										
P1	n = 196	0.884	0.0385	0.05	0.07	NT	66.6	0.2256	1.480	1.0

NT – not tested; N/A – not applicable; * Average values ± SD (n = 3)

The mechanical strength of the dissolving microneedle formulations was measured using a texture analyzer device. A 3-pt bend test was performed using the set-up depicted in Figure 2.3. The 3-pt test was selected as means to evaluate both the strength and flexibility of microneedle base-plate and individual needles. The microneedle base-plate and needles require a certain degree of flexibility to prevent cracking during removal of systems from the negative silicone molds. On the other hand, both the base-plate and individual needles require strength to penetrate the skin's surface during insertion without deforming or breaking. The mechanical strength for each microneedle formulation was measured and plotted in Force (N) – Displacement (mm) curves (comparable to stress-strain curves) displayed in Figures 3.8 – 3.11. The Force-Displacement curves represent the average mechanical strength (n = 3) of microneedles from each formulation (P1 – P4). The overall force for all formulations (P1 – P4) started to decline after being displaced approximately 1.1 mm due to bending of the microneedle base-plate. Following mechanical testing, each microneedle system was inspected under an optical microscope for system failures, including cracks in the base-plate, deformed needles and/or broken needles. For all formulations (P1 – P4), no cracks were observed in the base-plate and the individual needles maintained a pyramid-shape with no observed deformations or broken needles. The mechanical tests showed that increasing polymer concentration led to much stronger microneedles and increasing drug content reduced microneedle strength. The results met expectations as increasing polymer content increases the polymer lattice strength and increasing the amount of API molecules in the formulation decreases the stability of the polymer lattice. For example, the P2 microneedles were prepared with the highest concentration of polyvinylpyrrolidone polymer (30%, w/w) and lowest amount of

sumatriptan succinate (5%, w/w) and exhibited the greatest maximum strength of 4.97 N. Decreasing PVP concentration to 20% in P3 microneedles resulted in a drastic 42-fold reduction in microneedle strength from 4.97 N to 0.12 N ($p < 0.01$). However, increasing the microneedle sumatriptan load from 5 to 15% (w/w) with P4 microneedles yielded a smaller 5-fold reduction in strength from 4.97 N to 0.90 N ($p < 0.01$).

The mechanical strength of square microneedles prepared from P1 solution were tested and an average Force (N) – Displacement (mm) curve is plotted in Figure 3.12. Following mechanical testing, the microneedle arrays were inspected under an optical microscope and no cracks were observed in the base-plate and all needles maintained a pyramid-shape with no deformations or cracks. The larger square microneedle showed similar decline in peak force after being displaced approximately 1.1 mm. The square arrays maximum peak force of 2.24 N was higher than the P1 circle array maximum force of 1.63 N. The greater strength was attributed to the higher density (1.480 g/cm^3) in the square array as compared to the circle arrays (1.150 g/cm^3).

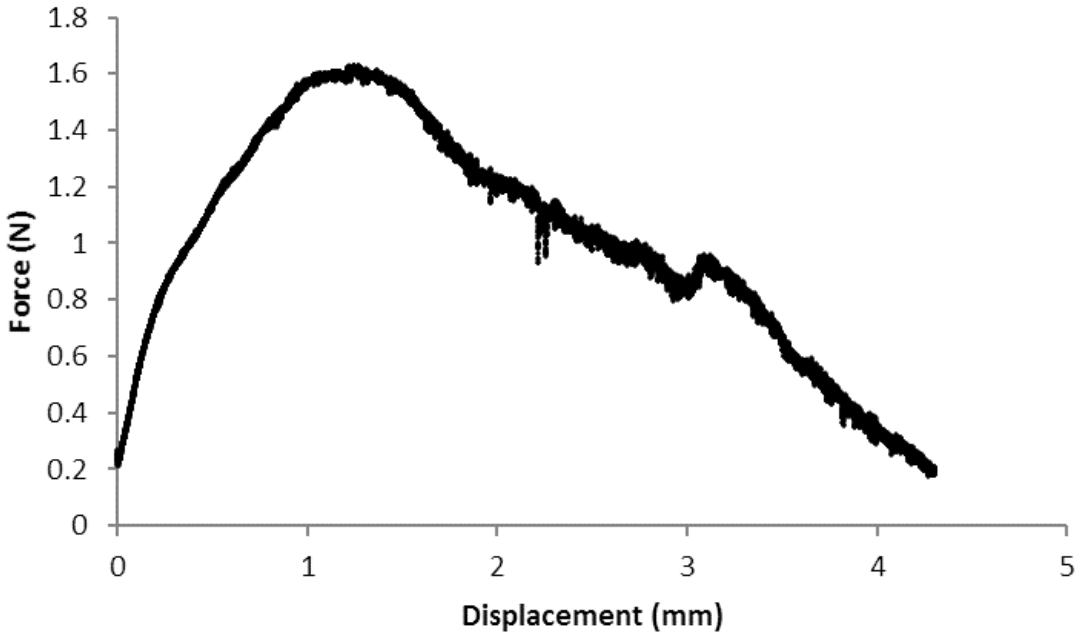

Figure 3.8 Mechanical test (3-pt bend) of P1 microneedles (circle); average values (n = 3).

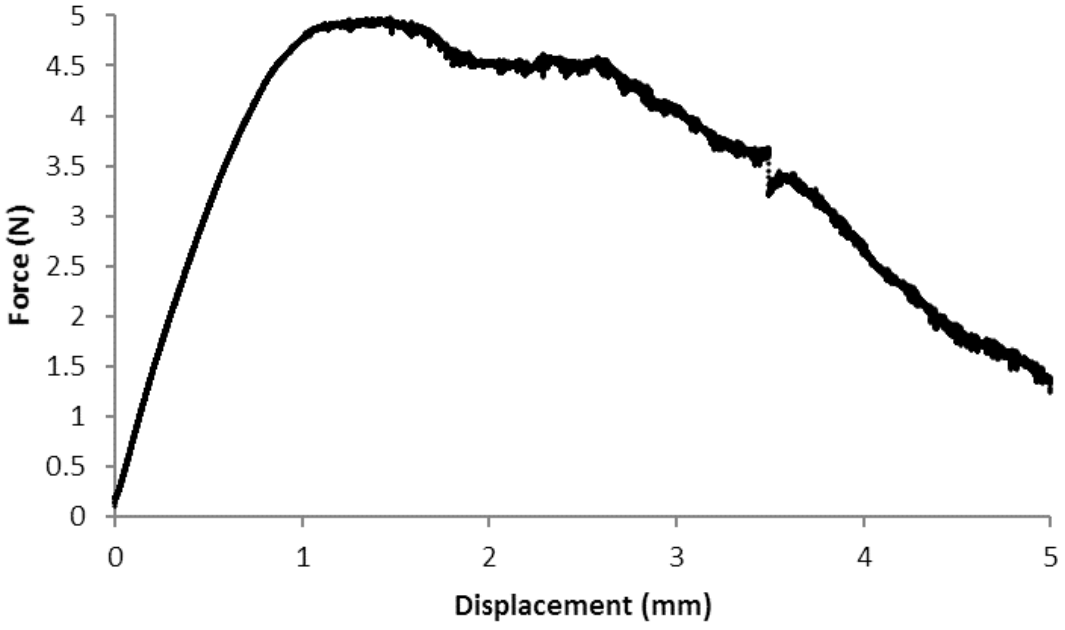

Figure 3.9 Mechanical test (3-pt bend) of P2 microneedles (circle); average values (n = 3).

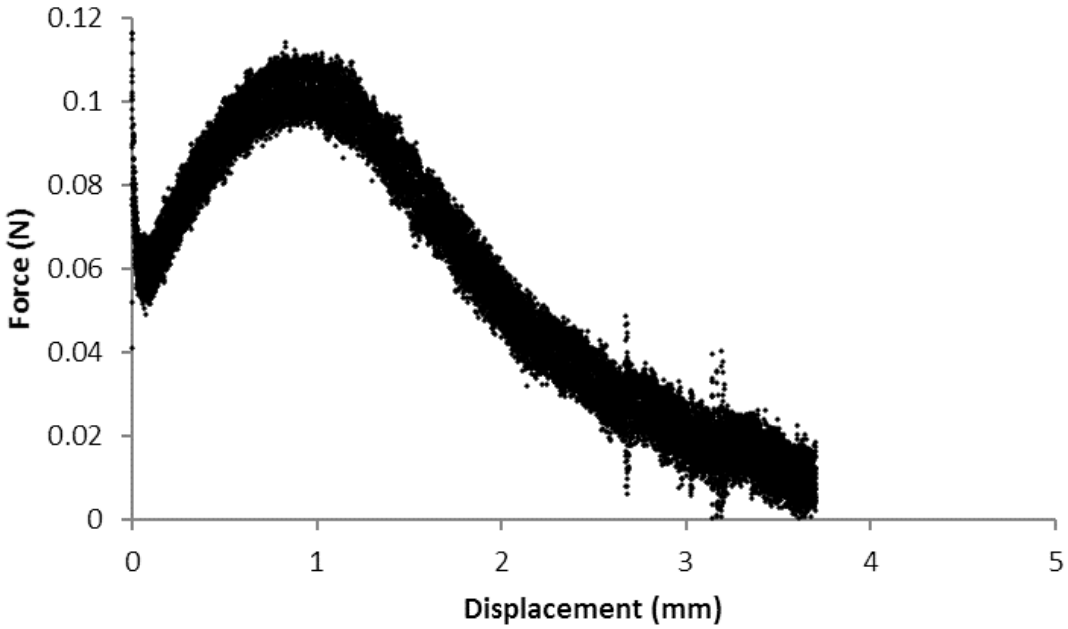

Figure 3.10 Mechanical test (3-pt bend) of P3 microneedles (circle); average values (n = 3).

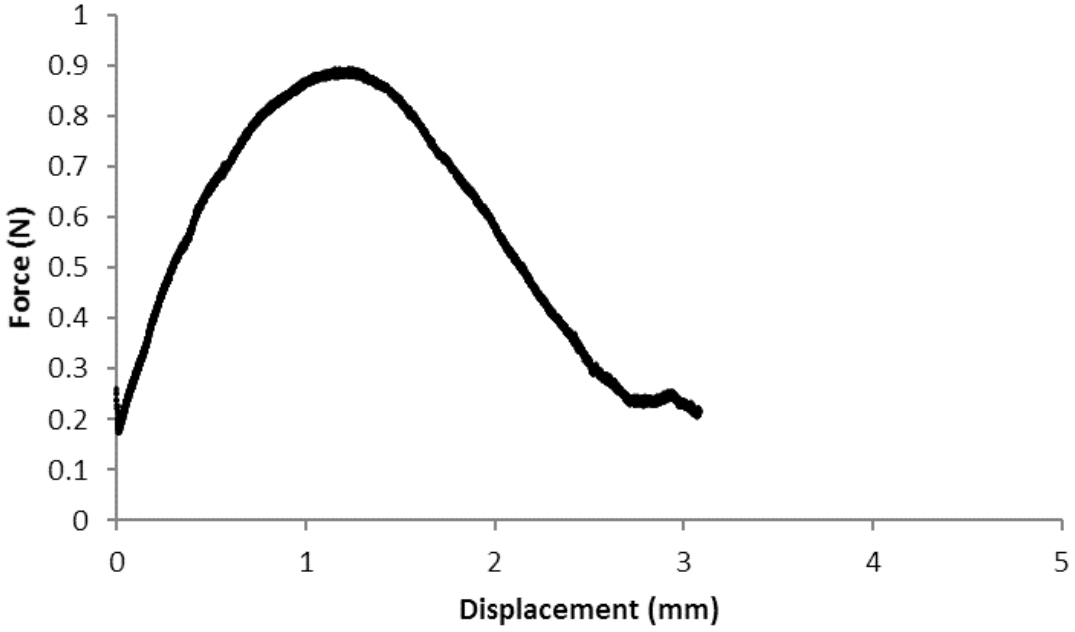

Figure 3.11 Mechanical test (3-pt bend) of P4 microneedles (circle); average values (n = 3).

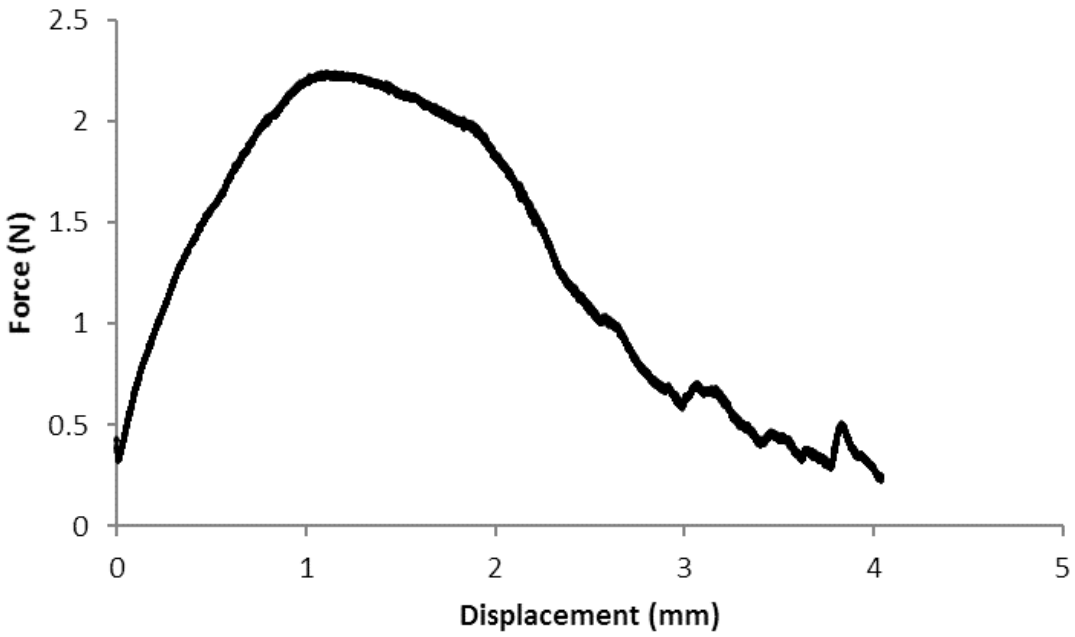

Figure 3.12 Mechanical test (3-pt bend) of P1 microneedles (square); average values (n = 3).

During *in-vitro* trials the minipig skin samples were examined to assess the microneedles ability to puncture and penetrate the skins surface. Microscopic images of the skin samples post-treatment were taken and visually confirmed the needles successfully punctured the skin (Figure 3.13). In addition, an indicator solution (nitrazine yellow dye) was applied to minipig skin following treatment to increase visibility of the skin punctures. The dye turned the minipig skin blue allowing for quick visual inspection of minipig skins un-aided by the microscope. An inspection of minipig skin confirmed successful penetration of circle arrays (P1 – P3) and square arrays (P1) (Figure 3.14).

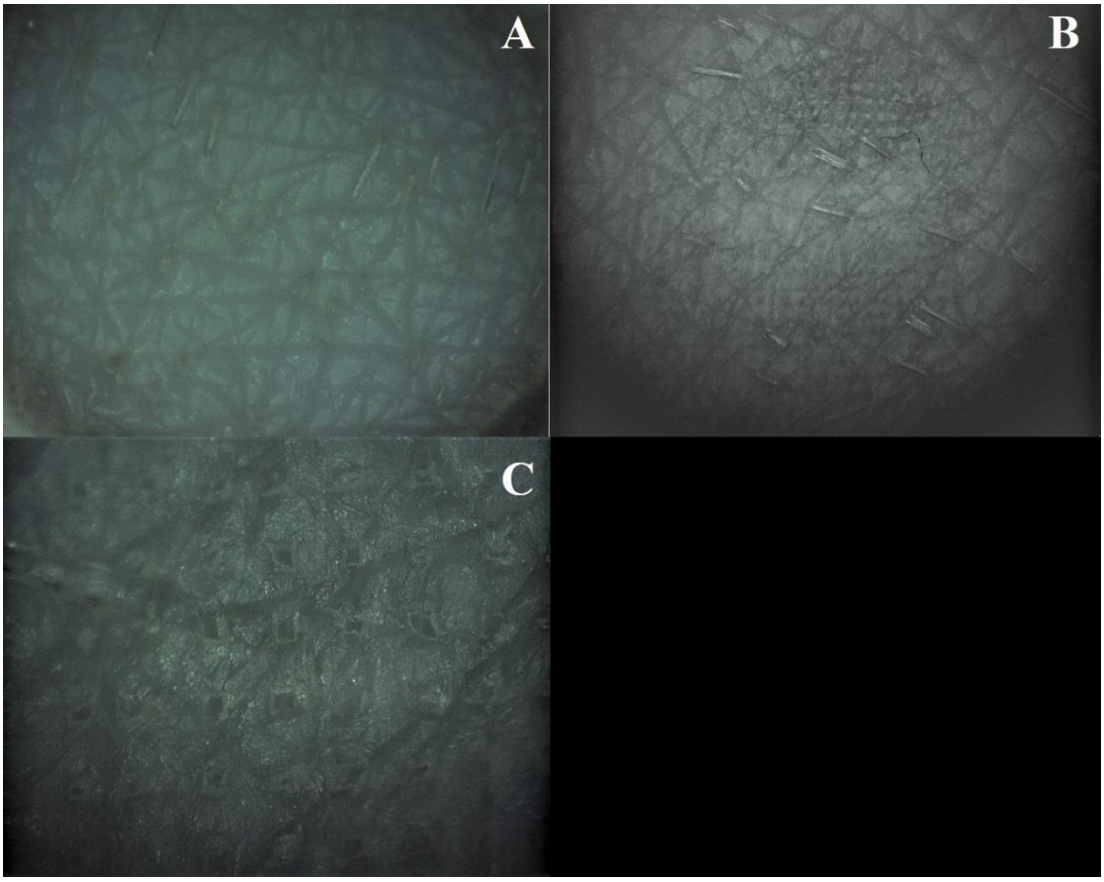

Figure 3.13 Optimal microscope images; (A) blank minipig tissue (10x mag); (B) minipig tissue post-treatment with P1 microneedle (10x mag); (C) minipig tissue post-treatment with P1 microneedle (50x mag).

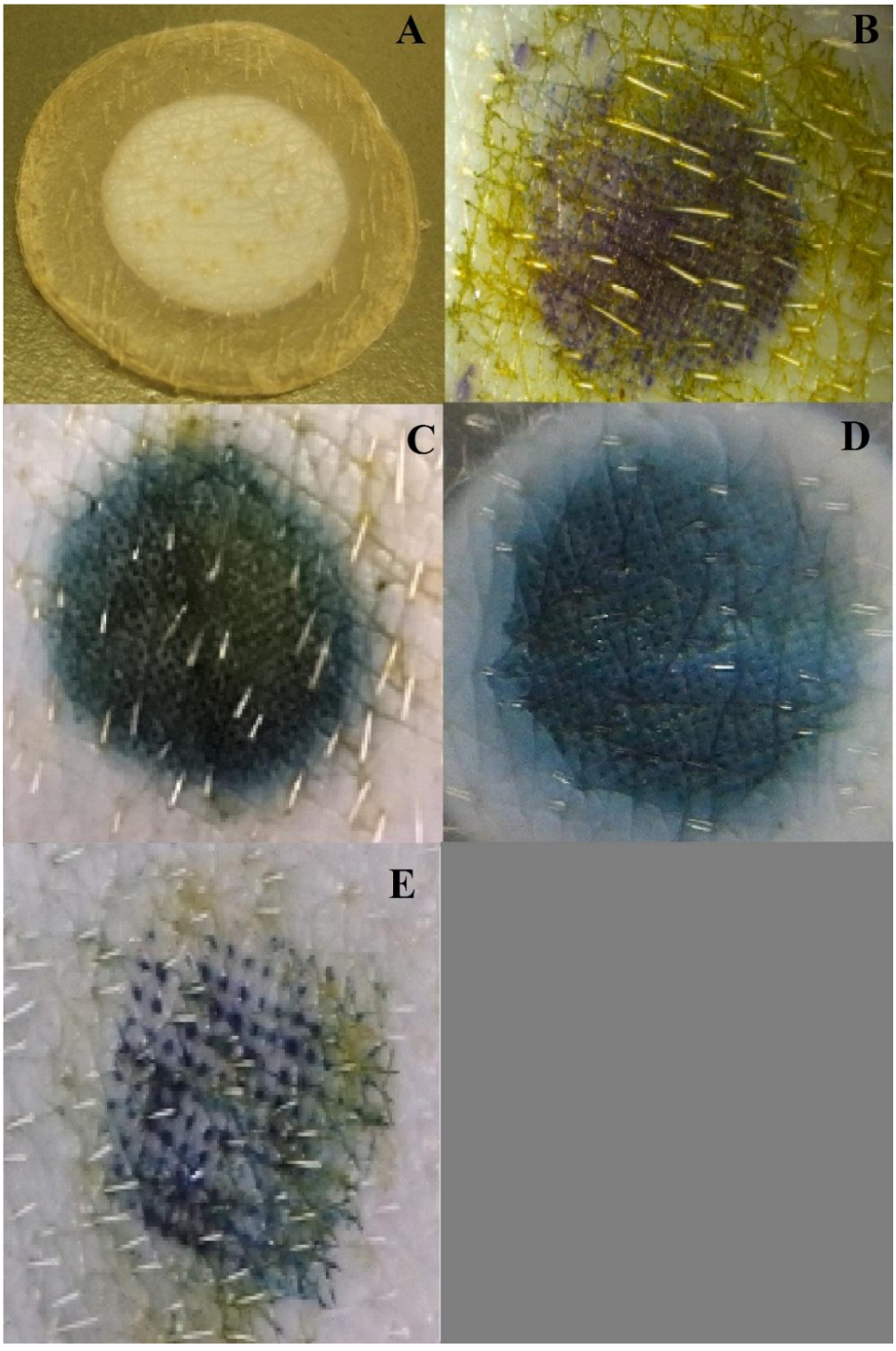

Figure 3.14 Photographic images of minipig tissue stained with nitrazine yellow dye; (A) blank minipig tissue; (B) P1 circle array treated minipig tissue; (C) P2 circle array treated minipig tissue; (D) P3 circle array treated minipig tissue; (E) P1 square array treated minipig tissue.

In vitro optical coherence tomography (OCT) study was used to observe and evaluate the microneedle systems solubilize and dissolve within the skin. The OCT imaging system was capable of generating micron-scale, high resolution 2-D cross-sectional images of the needles within the tissue samples [68, 69]. Figure 3.15 displays images of P1 formulated microneedles dissolving in dermatome (800 μm) female Göttingen minipig skin over a ten minute period. The images confirm the PVP-based needles rapidly dissolve immediately following insertion into the moist skin. Following 10 minutes, the individual needles were completely solubilized and the microneedle base-plate had begun to dissolve.

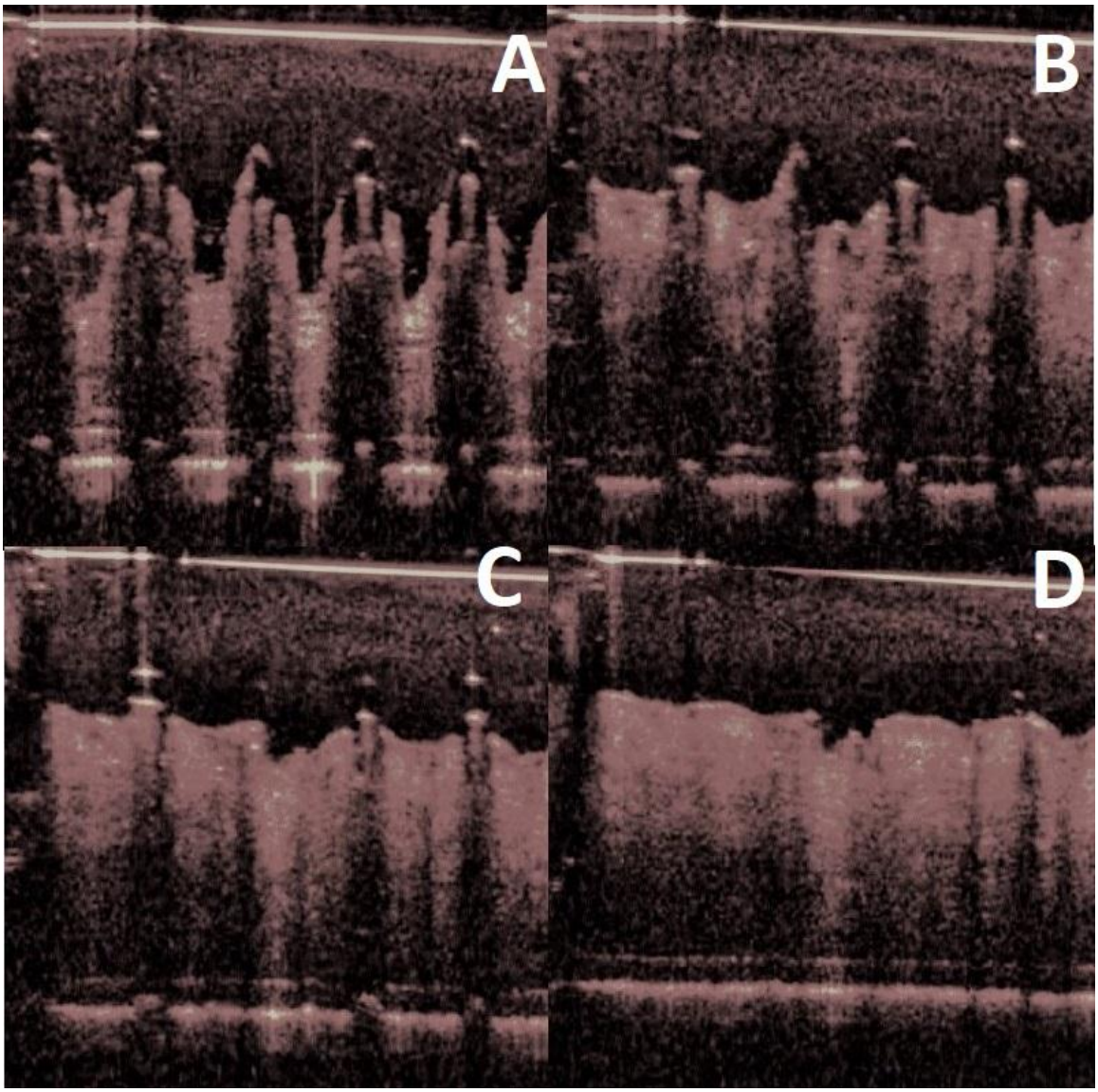

Figure 3.15 Optical coherence tomographic images of P1 circle microneedle dissolving in minipig tissue over time; dissolution of microneedle at (A) 1 min; (B) 2 min; (C) 4 min; (D) 10 min.

The skin barrier function was characterized by measuring transepidermal water loss (TEWL) of minipig skin pre-and post- treatment with dissolving microneedles. TEWL, or measurement of skin surface vapor loss, is an effective tool for determining the integrity of the stratum corneum (i.e., skin barrier). Damaged skin (i.e., dry skin) is unable to retain moisture and will result in higher TEWL values [54, 55, 70]. TEWL measurements were

taken before and after application of microneedles (circle) into the skin for 15 seconds (Table 3.2). Following treatment of skin with the P1 microneedle arrays, the minipig skin surface average water loss increased 4.9-fold ($p < 0.001$). The increased evaporation is explained by the array of micron-scale tunnels present in the skin after microneedle treatment which create low resistance pathways for transport of water through the skin. A similar 4.6-fold increase in average TEWL was realized after removing the stratum corneum from the skin utilizing the tape-stripping technique (15x) ($p < 0.001$). A comparison of the TEWL values for skin treated with P1 circle microneedles versus skin treated by tape-stripping method showed no significant differences ($p > 0.05$). These results indicate the circle microneedle arrays effectively bypass the stratum corneum.

Table 3.2 TEWL Values of Minipig Skin Pre- and Post- Microneedle Treatment or Tape-Striping Technique (15x); Average Values ± SD

Sample	Minipig Lot	Sample Size	Insertion Time (sec)	TEWL ($g/m^2/h$)	Difference ($g/m^2/h$)
Circle Microneedle					
Control (no microneedle)	325975	n = 3	15	15.18 ± 2.92	N/A
P1 Microneedle	325975	n = 3	15	73.86 ± 0.36	58.68 ± 2.70
Tape-Stripping					
Control (no tape-strip)	325975	n = 3	15	15.36 ± 1.21	N/A
Tape-strip (15x)	325975	n = 3	15	70.41 ± 3.56	55.05 ± 2.38

An overall comparison of the physical characteristics of the four formulations (P1 – P4) and array types (circle & square) indicates the optimal dissolving microneedle system is a P1 formulated circle microneedle. The P1 formulation contains optimal sumatriptan API drug loading (10%, w/w), highest possible PVP-polymer content (20%, w/w), good

mechanical properties and inserts well into minipig tissue. The other three formulations were sub-optimal for various reasons: P4 formulation contained undissolved sumatriptan API, P2 and P3 formulations contained lower drug load. The circle and square arrays both penetrated the minipig skin, but the circle array is preferred as it contains a denser array pattern with over three times the number of individual needles in a smaller surface area.

3.3 *In vitro* Diffusion of Sumatriptan Microneedles Using Minipig Skin Model

In vitro permeation studies to determine drug release of sumatriptan succinate through minipig skin were executed with circle microneedle arrays from three of the formulations (P1 – P3) [42]. Permeation trials were carried out using vertical Franz diffusion cells with female Göttingen minipig tissue as a suitable and preferred model for *in vitro* diffusion through human skin. The minipig skin has been shown to exhibit lower intra-donor variation compared to human skin due to variations in the human skin age of donors and lifestyles [51, 71]. Each of the minipig skin samples was shaved to remove hair on skin, dermatomed to 800 µm thickness and skin surface was gently dried. A tissue sample thickness of 800 µm was selected to ensure the 500 µm needles in the microneedle systems did not pierce through skin releasing drug directly into the receiver compartment. The top-layer skin surface was carefully dried and not pre-wetted to mimic realistic conditions for microneedle treatment. A detailed description of the minipig skin preparation is described in Section 2.8. The permeation trials were carried out over 32 hour period with samples collected at 1, 2, 6, 8, 24, and 32 hours. During each interval the receiver cell solution was completely emptied and replaced with phosphate buffer solution to maintain sink conditions. The *in vitro* minipig permeation trial lab set-up and test condition specifics are outlined in Section 2.11.

The permeation trials included transdermal diffusion experiments with dissolving microneedles, passive diffusion (control) experiments, passive diffusion experiments following removal of stratum corneum and a sumatriptan succinate reference solution (Figures 3.16 – 3.19). The dissolving microneedle experiments were performed with microarrays inserted into minipig skins and placed into Franz cells with the needles facing the donor compartment. Passive diffusion (control) tests were conducted with P1 and P2 arrays by inverting the microneedles on the skin samples (i.e., needles facing up) to mimic application of a traditional transdermal patch. Additional passive diffusion experiments were carried out with inverted P1 and P2 microneedles on minipig skin after removal of the stratum corneum using the tape-stripping technique (15x). Finally, the permeation of a sumatriptan succinate reference solution was evaluated which comprised 5 mg/ml sumatriptan API in phosphate buffer solution (pH 7.4). At the completion of each trial, skin samples were visually inspected with blue dye solution (nitrazine blue dye) to ensure microneedles fully dissolved and the full array penetrated the skin.

Results, included microneedle drug load (μg/cm^2); percentage drug released after 24 hours (%); cumulative amount of drug released after 24 hours, Q_{24} (μg/cm^2); sumatriptan steady-state flux, J_{SS} (μg/cm^2/h); lag time (h), and sumatriptan API retained in skin (μg/cm^2). The steady-state flux was determined by calculating the slope of the steady-state part of the cumulative flux curves. The steady-state flux was reached between 2 – 8 hours for microneedle systems, between 24 – 32 hours for control samples, between 2 – 8 hours for tape-stripped control samples, and 24 – 32 hours for reference samples. All *in vitro* results are summarized in Table 3.3 and cumulative flux curves are contained in Figures 3.16 – 3.19.

Circle microneedle arrays from each of the three formulations P1, P2 and P3 successfully released over 26% sumatriptan API after eight hours (average, n = 3), over 68% sumatriptan API after twenty-four hours (average, n = 3) and over 82% after thirty-two hours (average, n = 3). A linear relationship was observed between loading of sumatriptan succinate in microneedles versus cumulative drug release at 24 hour and steady-state flux. For example, a 2-fold increase in drug load from 5 – 10% (w/w) related to 2-fold increase in the cumulative drug release and steady-state flux. This is observed when comparing the P1 circular microneedles (10% w/w sumatriptan, Q_{24h} = 7598 µg/cm^2; J_{ss} = 395 µg/cm^2/h); with either the P2 circular microneedles (5% w/w sumatriptan, Q_{24h} = 4059 µg/cm^2; J_{ss} = 192 µg/cm^2/h; $p < 0.001$) or P3 circular microneedles (5% w/w sumatriptan, Q_{24h} = 4291 µg/cm^2; J_{ss} = 268 µg/cm^2 h; $p < 0.001$). Increasing the polyvinylpyrrolidone polymer content from 10 to 20% (w/w) in P2 circle arrays versus P3 circle arrays had no effect on drug release ($p > 0.05$) and a slight decrease in steady-state flux ($p < 0.05$). Circle microneedle arrays from each of the formulations exhibited quick release with lag times < 40 minutes. For all three formulations, over 85% sumatriptan succinate API was accounted for in the receiver cell aliquots and retained in minipig skin post-testing.

Control experiments were performed with circle-shaped microneedles (P1 and P2) as a means to evaluate the effectiveness of dissolving microneedle systems. The P1 and P2 control samples exhibited a higher degree of variability between samples (SD > 70%) and significantly lower drug release at 24 hour ($p < 0.05$) and steady-state flux ($p < 0.001$), as compared to the microneedle samples. Furthermore, the release was extremely slow with lag times of 6 hours and 9. 4 hours for P1 and P2 control samples, respectively. This data

demonstrates the circle-shaped dissolving microneedle arrays are a very effective active transdermal system for transporting sumatriptan through the epidermis.

The circular microneedles ability to completely bypass the skin's stratum corneum (i.e., primary barrier) was tested by placing inverted microneedles (similar to control test) on tissue samples after the stratum corneum was removed tape-stripping (15x). The inverted microneedles (P1 and P2) on tape-stripped skin released over 24% sumatriptan API after eight hours (average, n = 3), over 54% sumatriptan API after twenty-four hours (average, n = 3) and over 64% after thirty-two hours (average, n =3). For P1 and P2 microneedles, no significant differences were observed between drug release at 24 hours ($p > 0.5$) and steady-state flux ($p > 0.5$), as compared to the inverted microneedles on tape-stripped skin. These results prove the microneedles effectively bypass the stratum corneum for drug delivery directly into the dermal layers of the skin. The arrays have needles with length of 500 µm which penetrates through the stratum corneum (approximately 50 µm) and deep into the epidermal layers of the skin. This creates deep channels for solubilized sumatriptan drug to transport through the skin.

Review of the *in vitro* microneedle data from the three formulations (P1 – P3) indicates the optimal microneedle system is a P1 formulated circle microneedle array. The P1 formulation contains the maximum amount of sumatriptan API (10%, w/w) which related to the highest drug release. However, results show that the PVP concentration should be reduced to (20%, w/w) which would lead to increased steady-state flux of sumatriptan.

Table 3.3 Franz cell *in vitro* permeation data for sumatriptan succinate through minipig skin after 32-h; average values ± SD

Sample	Sample Size	Drug Load ($\mu g/cm^2$)	Cumulative Drug Released, Q_{24} ($\mu g/cm^2$)	Percentage Drug Released after 24 h (%)	Steady-state Flux, J_{SS} ($\mu g/cm^2/h$)	Drug Retained in Skin ($\mu g/cm^2$)	Lag Time (h)
Reference Solution							
Sumatriptan Solution (5mg/mL)	n = 6	421 ± 3.4*	15 ± 22	2.4 ± 3.5	1.3 ± 2.0	56 ± 39	13.5 ± 3.1
P1 Microneedles							
Control	n = 3	10684 ± 192	1491 ± 1066	13.9 ± 9.9	78 ± 52	419 ± 250	6.0 ± 2.4
Inverted + Tape Strip (15x)	n = 3	10820 ± 130	5904 ± 2379	54.7 ± 22.5	458 ± 325	NT	1.5 ± 0.22
Dissolving Microneedle	n = 3	11070 ± 84	7598 ± 223	68.6 ± 2.5	395 ± 31	367 ± 35	0.65 ± 0.19
P2 Microneedles							
Control	n = 3	5499 ± 184	443 ± 388	8.0 ± 6.9	30 ± 24	419 ± 250	9.4 ± 1.6
Inverted + Tape Strip (15x)	n = 3	5361 ± 89	3585 ± 681	67.0 ± 13.5	193 ± 86	NT	1.5 ± 0.16
Dissolving Microneedle	n = 3	5522 ± 111	4059 ± 179	73.5 ± 3.8	192 ± 19	188 ± 42	< 0.1
P3 Microneedles							
Dissolving Microneedle	n = 3	5433 ± 161	4291 ± 367	78.9 ± 4.5	268 ± 62	136 ± 120	< 0.1

NT – Not Tested

*100 µL pipette accuracy is ≤ 0.8%

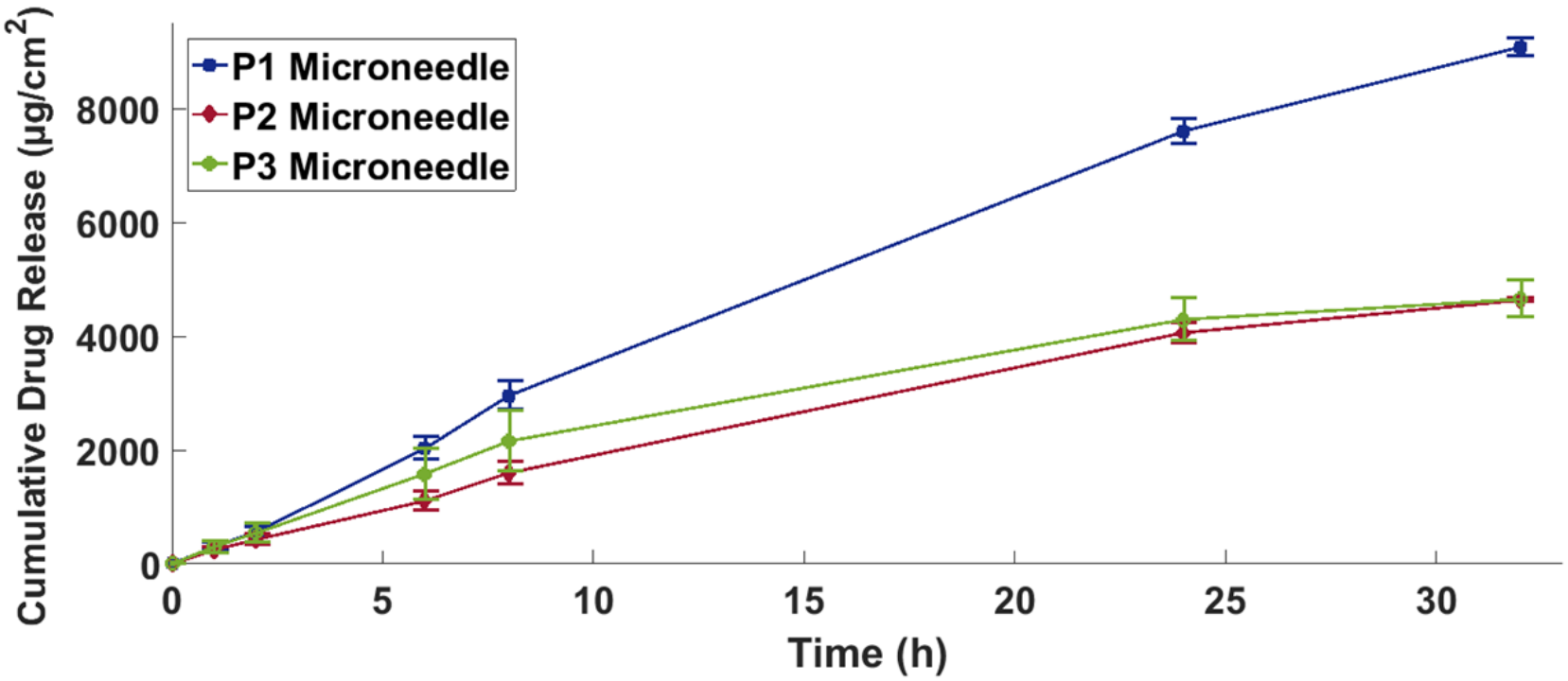

Figure 3.16 *In vitro* cumulative release of sumatriptan drug from dissolving microneedle preparations P1 (■), P2 (♦), P3 (●); average values ± SD (n = 3).

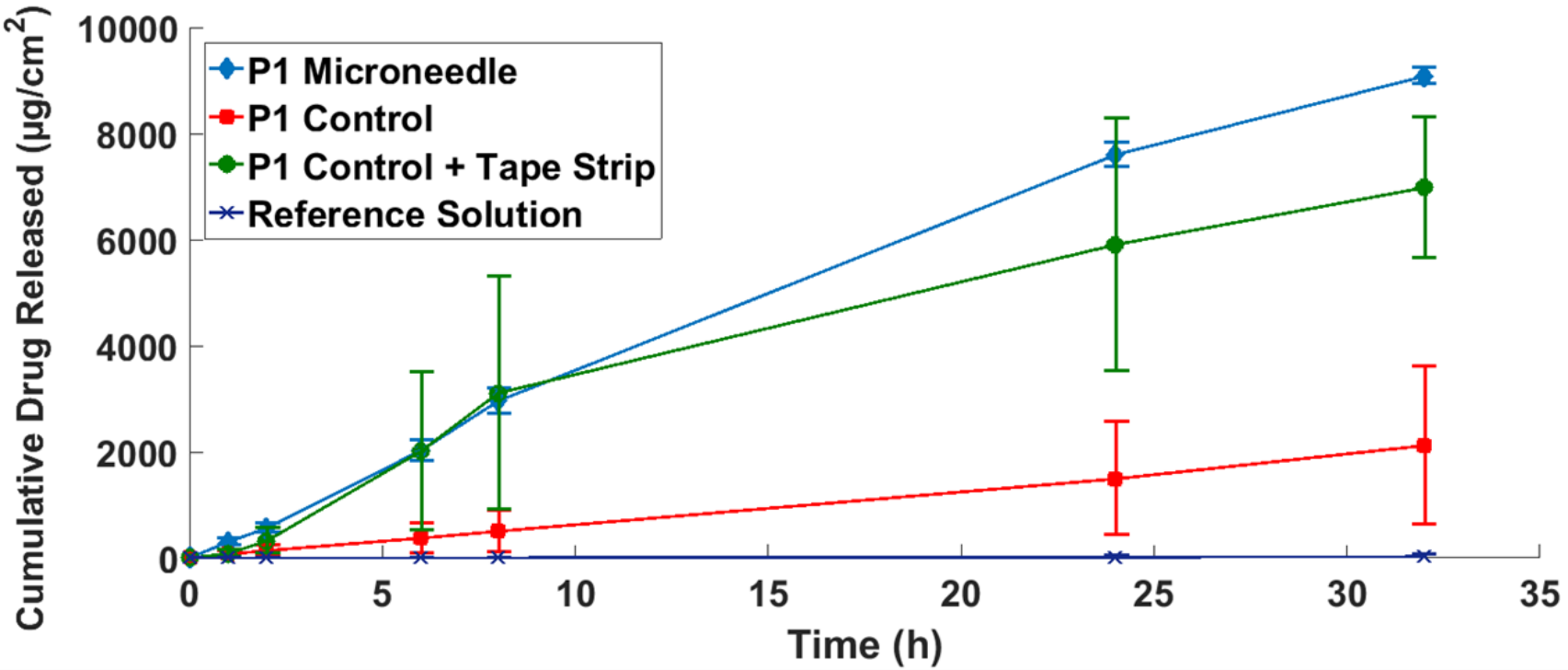

Figure 3.17 *In vitro* cumulative release profile of sumatriptan succinate over 32 hour period from circle array dissolving microneedle preparations P1 microneedle (♦), P1 control (microneedle inverted on minipig tissue) (■), P1 microneedle + tape-stripping (15x) (●) and reference solution (×); average values ± SD (n = 3).

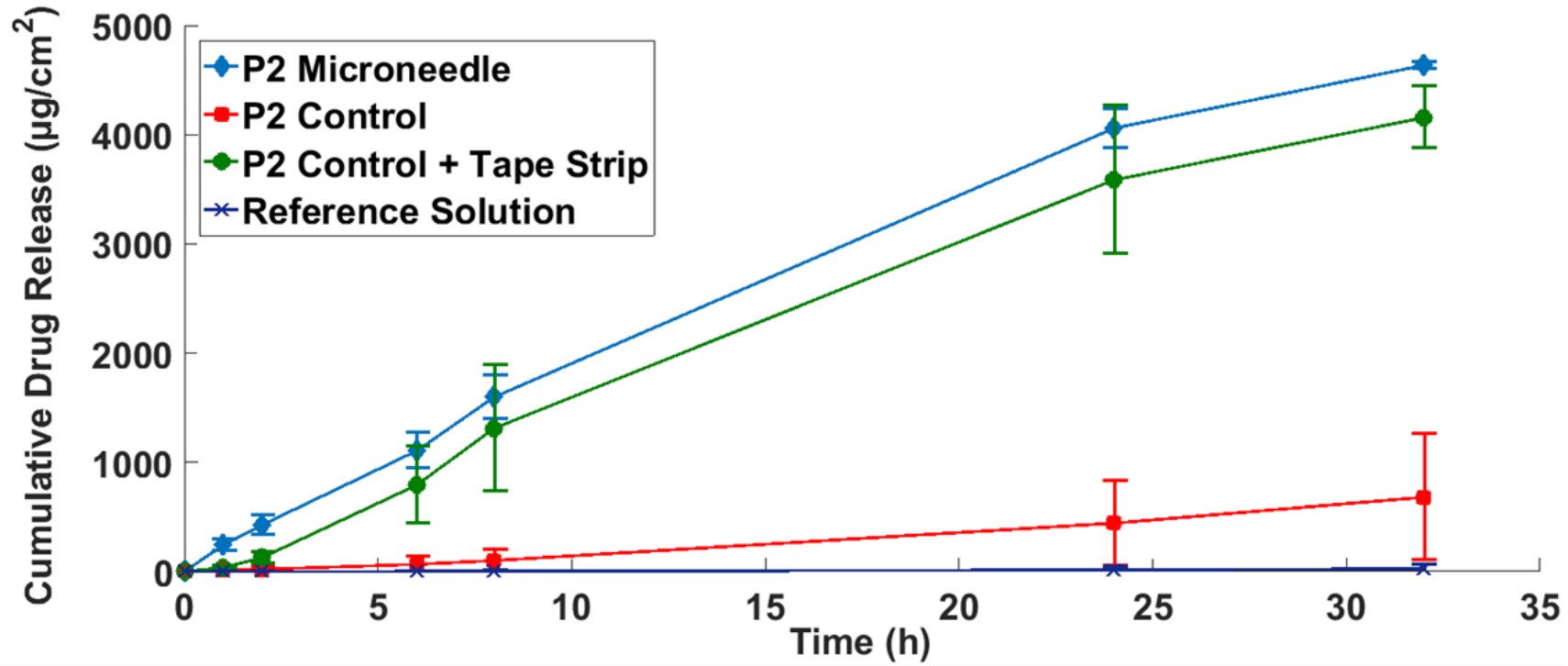

Figure 3.18 *In vitro* cumulative release profile of sumatriptan succinate over 32 hour period from circle array dissolving microneedle preparations P2 microneedle (♦), P2 control (microneedle inverted on minipig tissue) (■), P2 microneedle + tape-stripping (15x) (●) and reference solution (×); average values ± SD (n = 3).

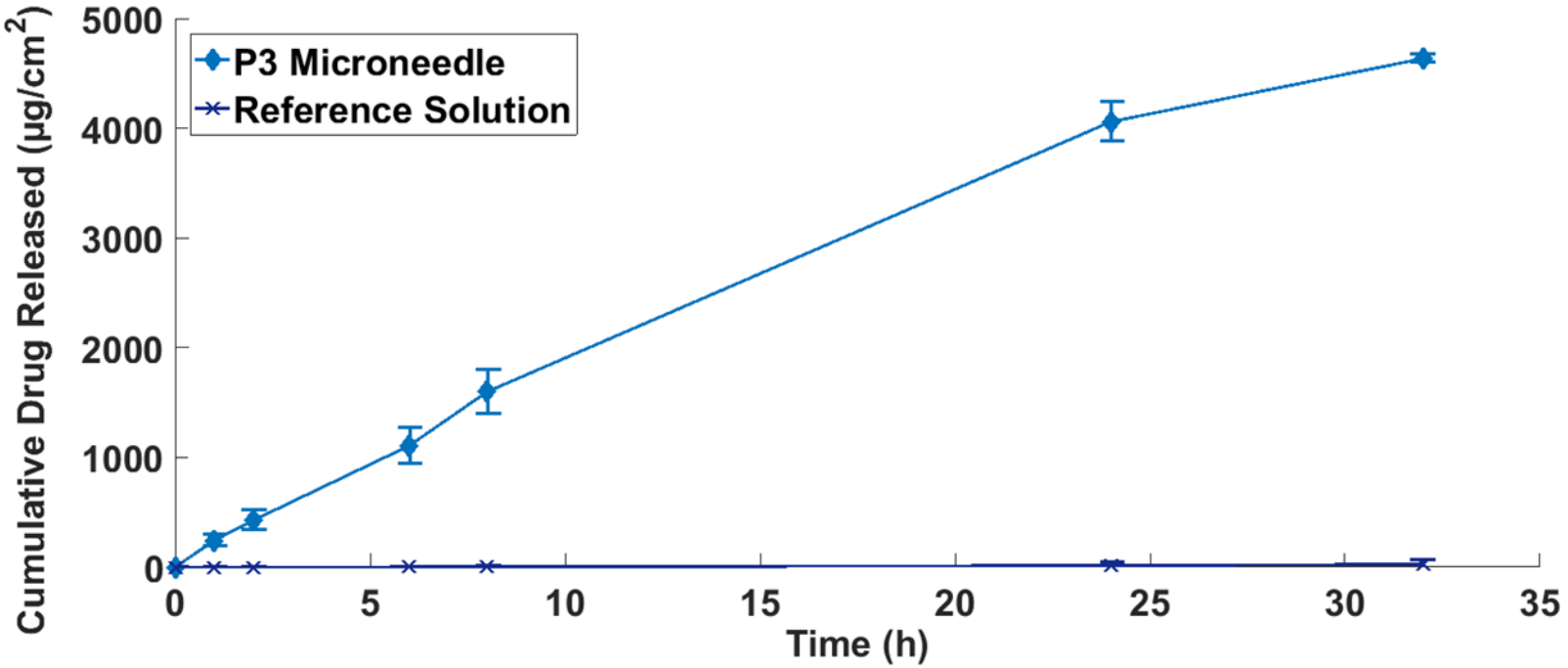

Figure 3.19 *In vitro* cumulative release profile of sumatriptan succinate over 32 hour period from circle array dissolving microneedle preparations P3 microneedle (♦), and reference solution (×); average values ± SD (n = 3).

3.4 *In vitro* Delivery of Sumatriptan From Dissolving Microneedle Arrays Aided by Iontophoresis

Iontophoresis *in vitro* studies were carried out to enhance the transdermal delivery of the positively-charged sumatriptan succinate molecules through the skin. *In vitro* tests included:

- Visual examination of microneedle and iontophoresis treated minipig skin.
- Transepidermal water loss (TEWL) of microneedle and iontophoresis treated minipig skin.
- *In vitro* Franz cell permeation studies with iontophoresis.

The *in vitro* experiments involved insertion of microneedle arrays into Göttingen minipig skin and applying a mild, constant electrical current, 100 to 500 $\mu A/cm^2$, across the samples during diffusion. Tests included circle-shaped microneedle arrays formulated from P1, P2 and P3 solulation, as well as, square-shaped microneedle arrays formulated from P1 solution. Permeation trials were implemented over a six-hour period with samples extracted at 1, 2, 3, 4, and 6 hours. Sink conditions were maintained by completely emptying and refilling the Franz receiver cell following each interval. The six-hour treatment time was selected as comparable to the Zecuity® iontophoretic device approved by the FDA for transdermal delivery of sumatriptan succinate over four hours [35, 72]. The *in vitro* iontophoretic diffusion trial lab set-up and test conditions are described in detail in Section 2.11.

In vitro studies included experiments with dissolving microneedles aided by iontophoresis, dissolving microneedles un-aided by iontophoresis, and passive diffusion (control) experiments. Tests involving dissolving microneedles were conducted with

individual circle or square microarrays inserted into minipig skins and placed into Franz cells with the microneedles facing the donor compartment.. The passive diffusion (control) tests were conducted by inverting microneedle arrays on top of the minipig skin (i.e., needles facing up) to simulate passive transdermal delivery from these systems.

At the completion of each trial, skin samples were visually inspected with blue dye solution (nitrazine yellow) to verify microneedles pierced the skin and were fully dissolved. For circle arrays (P1 – P3) and square arrays (P1), a recognizable circle or square pattern was visible in the skin samples. Applying increasing electrical current made the patterns darker and more distinct with the higher current density (500 $\mu A/cm^2$) being the most pronounced. This is observed in Figure 3.20 which contains photographs of the blue dyed tissue samples following in vitro testing with and without iontophoresis.

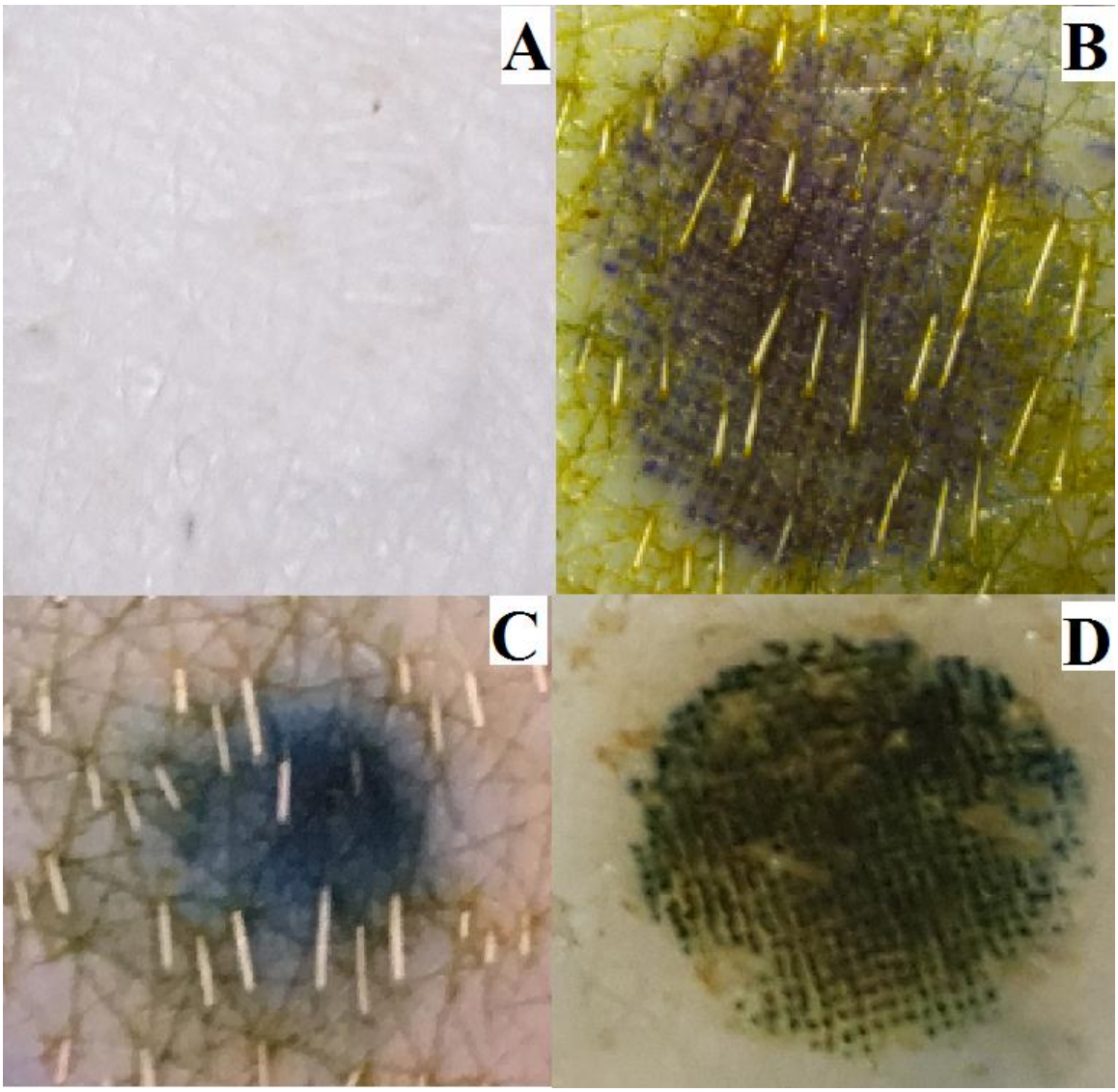

Figure 3.20 Photographic images of minipig tissue dyed with nitrazine yellow dye; (A) blank minipig tissue; (B) P1 circle microneedle; (C) P1 circle microneedle with 100 µA/cm^2; (D) P1 circle microneedle with 500 µA/cm^2.

TEWL values were used to assess iontophoretic microneedle treatments effect on skin barrier functionality for both circle and square microneedle arrays. TEWL measurements were taken before and after six-hour *in vitro* permeation trials with control samples, dissolving microneedle samples and dissolving microneedle samples with electrical current (Table 3.4). For circle microneedle arrays without iontophoresis, the

average TEWL measurements increased 2.6-fold for minipig samples treated\using P1 circle micro arrays ($p < 0.001$), 3.1-fold for P2 micro arrays ($p < 0.001$), and 3.1-fold for P3 micro arrays ($p < 0.001$). The addition of a high electric current (500 $\mu A/cm^2$) across samples during the six-hour diffusion period correlated to minor increases in TEWL values. For minipig skin treated with P1, P2 and P3 circle microneedles and iontophoresis, the average TEWL increased 2.7-fold ($p < 0.001$), 3.1-fold ($p < 0.001$) and 3.3-fold ($p < 0.001$), respectively. For P1 and P2 microneedles, no significant difference was observed between microneedles with or without iontophoresis ($p > 0.5$). However, for P3 microneedles a significant difference was observed ($p < 0.01$). The results indicate that iontophoresis has an increased effect on microneedle arrays containing less polymer. The square microneedles formulated from P1 solution resulted in a 2.6-fold increase in average TEWL values ($p < 0.001$). Testing with a high electrical current (500 $\mu A/cm^2$) electric current resulted in slightly larger average TEWL values exhibiting a 3.2-fold increase which were not significantly different from non-iontophoresis results ($p > 0.05$).

Table 3.4 TEWL Values of Minipig Skin Pre- and Post- Microneedle Treatment or Microneedle Treatment Aided by Iontophoresis; Average Values ± SD

Sample	Minipig Lot	Sample Size	Insertion Time (h)	TEWL ($g/m^2/h$)	Difference ($g/m^2/h$)
P1 Circle Array					
Control (no microneedle)	228932	n = 3	0	25.46 ± 4.69	N/A
Microneedle	228932	n = 3	6	65.24 ± 3.49	39.78 ± 5.00
Microneedle + 500 $\mu A/cm^2$	228932	n = 3	6	69.52 ± 5.69	44.07 ± 4.26
P2 Circle Microneedle					
Control (no microneedle)	229025	n = 3	0	21.82 ± 2.22	N/A
Microneedle	229025	n = 3	6	67.59 ± 3.57	45.76 ± 4.53
Microneedle + 500 $\mu A/cm^2$	229025	n = 3	6	68.28 ± 2.66	46.46 ± 4.51
P3 Circle Microneedle					
Control (no microneedle)	229025	n = 3	0	21.00 ± 3.20	N/A
Microneedle	229025	n = 3	6	64.94 ± 1.06	43.94 ± 3.97
Microneedle + 500 $\mu A/cm^2$	229025	n = 3	6	68.60 ± 0.40	47.60 ± 2.89
P1 Square Microneedle					
Control (no microneedle)	231545	n = 3	0	20.57 ± 1.48	N/A
Microneedle	231545	n = 3	6	54.21 ± 4.88	33.64 ± 4.88
Microneedle + 500 $\mu A/cm^2$	231545	n = 3	6	65.59 ± 4.11	45.48 ± 3.12

In vitro permeation data, including microneedle drug loading ($\mu g/cm^2$); percentage drug released at six-hours (%); cumulative amount drug released at six-hours, Q_6 ($\mu g/cm^2$); steady-state flux, J_{SS} ($\mu g/cm^2/h$); and lag time (h). The steady-state flux and lag time were determined from the slope of the steady-state portion of the cumulative flux curves between 2 – 6 h. For control samples, the steady-state flux and lag time were not calculated as the steady-state portion of the cumulative flux curves occurred between 24 – 32 h, see

Section 3.4. All *in vitro* results are summarized in Table 3.5 and cumulative flux curves are contained in Figures 3.21 – 3.25.

The circle dissolving arrays from the three formulations (P1 – P3) each successfully released over 953 μg/cm^2 after six hours (average, n = 3). The lag time for microneedles to reach steady-state flux varied from 30 – 60 minutes for all microneedle samples. A relationship was not observed between increased drug loading and either cumulative drug release or steady-state flux. For example, increasing drug load 2-fold from 5 to 10% (w/w) and keeping PVP concentration constant at 30% (w/w) led to negligible increases in the cumulative drug release and steady-state flux. This is observed in comparing P2 circular microneedles (Q_{6h} = 953 μg/cm^2; J_{ss} = 184 μg/cm^2/h) to P1 circular microneedles (Q_{6h} = 1133 μg/cm^2; J_{ss} = 206 μg/cm^2/h); $p > 0.05$). Doubling the drug load and increasing polymer concentration from P3 (Q_{6h} = 1050 μg/cm^2; J_{ss} = 226 μg/cm^2/h) to P1 ($p > 0.5$) led to insignificant changes in cumulative drug release and steady-state flux. And a 10% (w/w) higher concentration in PVP polymer between P3 and P2 did not have a significant impact on drug release or steady-state flux ($p > 0.5$). That said, the cumulative drug release of sumatriptan from control samples at six hours was 23 – 51% lower than their dissolving microneedle counterparts. This confirms the effectiveness of the microneedle arrays in circumventing the stratum corneum to deliver drug within the dermis versus passive transdermal diffusion.

Addition of an electrical current of 500 μA/cm^2 resulted in 149% increase in drug release at six hours for P3 microneedles, 95.2% increase for P1 microneedles and 50.6% increase for P2 microneedles. The P3 formulated microneedle aided by iontophoresis demonstrated no lag time, but the P1 and P2 had lag times between 36 and 54 minutes.

Increasing the polymer matrix concentration from 20 – 30% (w/w) while maintaining constant drug load resulted in approximate 2-fold increase drug release and steady-state flux values. This was demonstrated between the P2 microneedles (Q_{6h} = 1437 µg/cm^2; J_{ss} = 266 µg/cm^2/h) with under 500 µA/cm^2 electrical current in comparison to P3 microneedles (Q_{6h} = 2888 µg/cm^2; J_{ss} = 490 µg/cm^2/h, $p < 0.01$). Doubling the sumatriptan succinate load between P2 and P1 (Q_{6h} = 2262 µg/cm^2; J_{ss} = 433 µg/cm^2/h, $p < 0.05$) increased drug release and steady-state diffusion by > 57%.

Square microneedle arrays formulated from P1 solution and loaded with 17.04 mg/cm^2 sumatriptan demonstrated a cumulative release of 258 µg/cm^2 and steady-state diffusion of 49 µg/cm^2/h after six hours. The results were disappointing as drug release was 22.8% lower than a P1 formulated circle array loaded with less sumatriptan succinate (10.8 mg/cm^2). Combining the P1 square microneedles (Q_{6h} = 258 µg/cm^2; J_{ss} = 49 µg/cm^2/h) with 500 µA/cm^2 electrical current significantly increased drug release 327% and steady-state diffusion 279% (Q_{6h} = 1102 µg/cm^2; J_{ss} = 186 µg/cm^2/h, $p > 0.01$). The higher electrical current was able to increase flux of charged molecules and compensate for the square microarrays reduced ability to bypass stratum corneum.

The results of *in vitro* microneedle testing with iontophoresis for the three formulations (P1 – P3) demonstrate the most suitable microneedle device as a P3 formulated circle microneedle array. The P3 formulation contained minimal sumatriptan succinate (5%, w/w) but released 27% more drug than P1 microneedle with double the amount of API when combined with 500 µA/cm^2 electrical current. The higher drug load is attributed to reduced polymer matrix in formulation P3 which allows for faster diffusion of charged molecules into epidermis by iontophoresis and no lag time. These results

indicate an optimal iontophoretic microneedle device would contain 10% (w/w) sumatriptan succinate and 20% (w/w/) polyvinylpyrrolidone which should lead to even greater drug release and higher steady-state flux values.

Table 3.5 Franz Cell *In vitro* Permeation Data for Sumatriptan Succinate Through Minipig Skin After Six Hours Aided by Iontophoresis; Average Values ± SD

Sample	Sample Size	Drug Load ($\mu g/cm^2$)	Cumulative Drug Released, Q_{6h} ($\mu g/cm^2$)	Percentage Drug Released, Q_{24h} (%)	Steady-state Flux, J_{SS} ($\mu g/cm^2/h$)	Lag Time (h)
Circle Arrays						
P1 (Control)	n = 3	10679 ± 206	579 ± 396	5.5 ± 3.8	N/A	N/A
P1 MN	n = 3	10773 ± 285	1133 ± 259	10.5 ± 2.5	206 ± 49	0.5 ± 0.7
P1 MN + 100 $\mu A/cm^2$	n = 3	10887 ± 128	1362 ± 311	12.5 ± 2.9	267 ± 63	1.0 ± 0.1
P1 MN + 300 $\mu A/cm^2$	n = 3	10913 ± 159	1132 ± 193	10.4 ± 1.7	208 ± 43	0.6 ± 0.1
P1 MN + 500 $\mu A/cm^2$	n = 3	11062 ± 110	2262 ± 437	20.5 ± 4.0	433 ± 74	0.9 ± 0.1
P2 (Control)	n = 3	5380 ± 162	223 ± 237	4.2 ± 4.5	N/A	N/A
P2 MN	n = 3	5361 ± 87	953 ± 233	17.8 ± 4.1	184 ± 42	0.9 ± 0.2
P2 MN + 500 $\mu A/cm^2$	n = 3	5369 ± 121	1437 ± 163	26.8 ± 2.9	266 ± 23	0.6 ± 0.3
P3 (Control)	n = 3	5416 ± 135	243 ± 124	4.5 ± 2.4	N/A	N/A
P3 MN	n = 3	5367 ± 131	1050 ± 332	21.4 ± 6.2	226 ± 62	1.0 ± 0.2
p3 MN + 500 $\mu A/cm^2$	n = 3	5437 ± 89	2888 ± 350	53.2 ± 7.3	490 ± 17	0.0 ± 0.7
Square Arrays						
P1 (Control)	n = 3	17048 ± 346	64 ± 62	0.4 ± 0.4	N/A	N/A
P1 MN	n = 3	17040 ± 458	258 ± 89	1.5 ± 0.5	49 ± 28	0.3 ± 1.3
p1 MN + 500 $\mu A/cm^2$	n = 3	17131 ± 173	1102 ± 668	6.5 ± 4.0	186 ± 110	0.1 ± 0.1

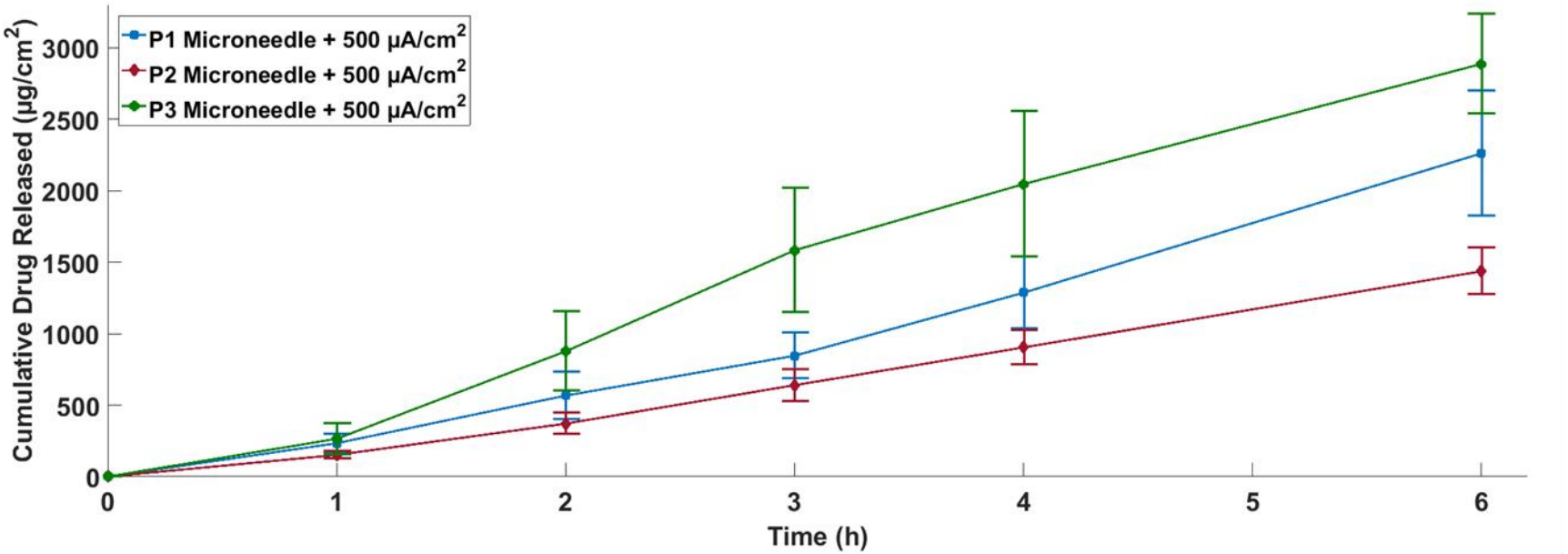

Figure 3.21 *In-vitro* cumulative release profile of sumatriptan succinate over six hour period from circle dissolving microneedle aided by iontophoresis; P1 microneedle + 500 µA/cm^2 (■); P2 microneedle + 500 µA/cm^2 (♦); P3 microneedle + 500 µA/cm^2 (●); average values ± SD (n = 3).

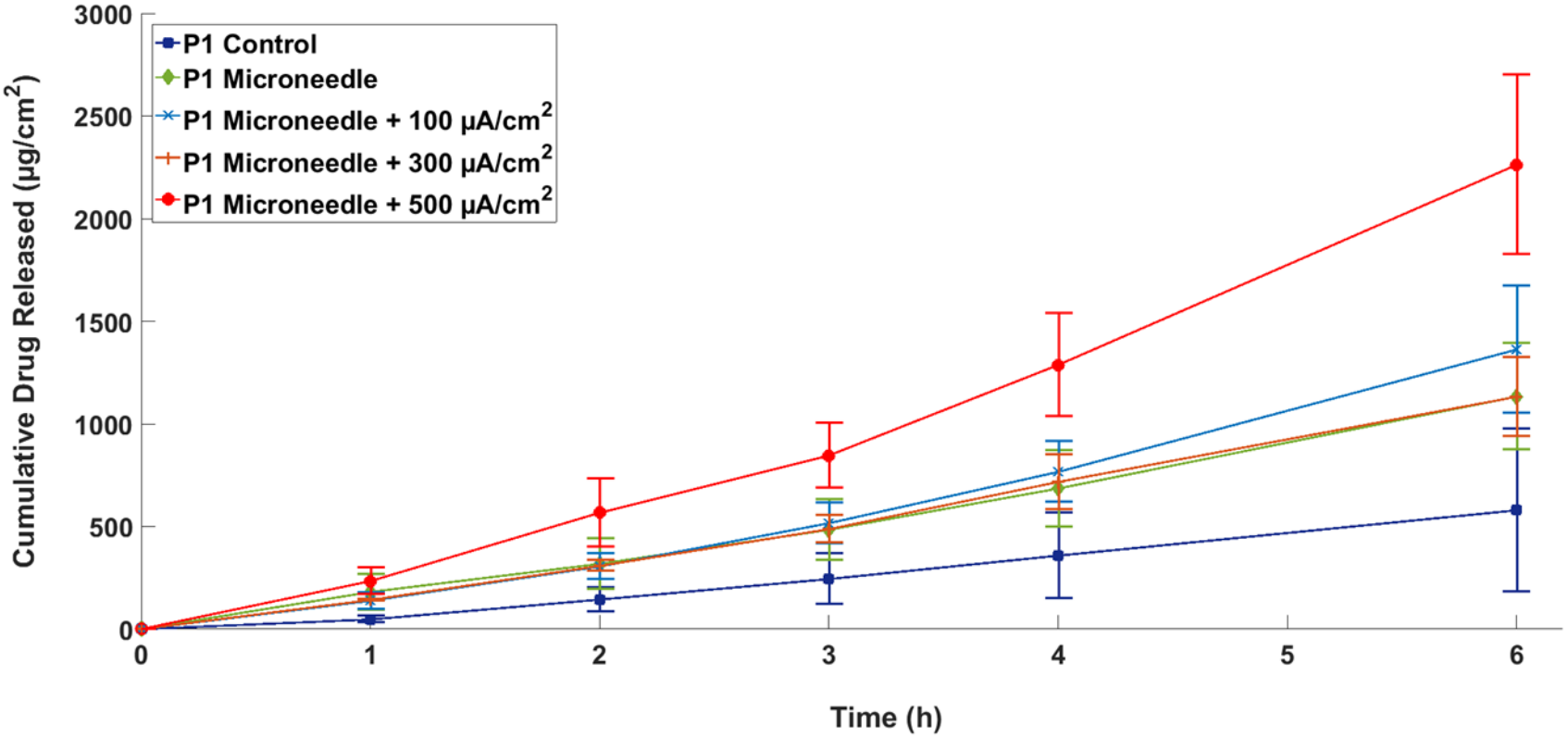

Figure 3.22 *In-vitro* cumulative release profile of sumatriptan succinate over six hour period from circle dissolving microneedle aided by iontophoresis; P1 microneedle (♦); P1 control (microneedle inverted on minipig tissue) (■); P1 microneedle + 100 µA/cm^2 (×); P1 microneedle + 300 µA/cm^2 (+); P1 microneedle + 500 µA/cm^2 (●); average values ± SD (n = 3).

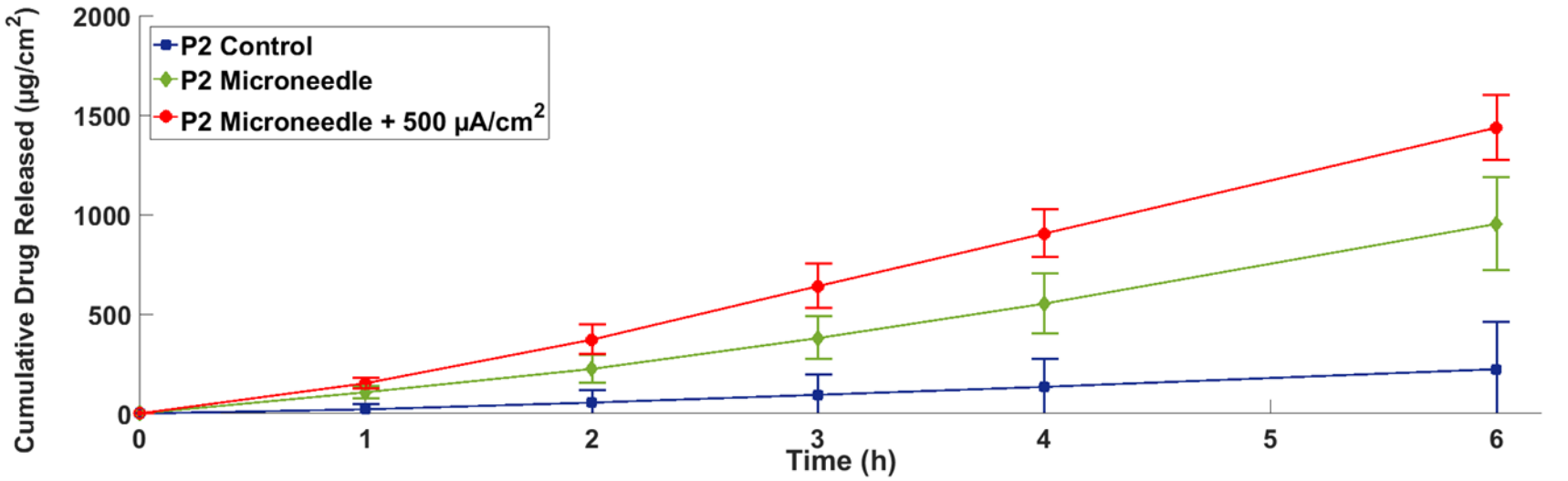

Figure 3.23 *In-vitro* cumulative release profile of sumatriptan succinate over six hour period from circle dissolving microneedle aided by iontophoresis; P2 microneedle (♦); P2 control (microneedle inverted on minipig tissue) (■); P2 microneedle + 500 µA/cm^2 (●); average values ± SD (n = 3).

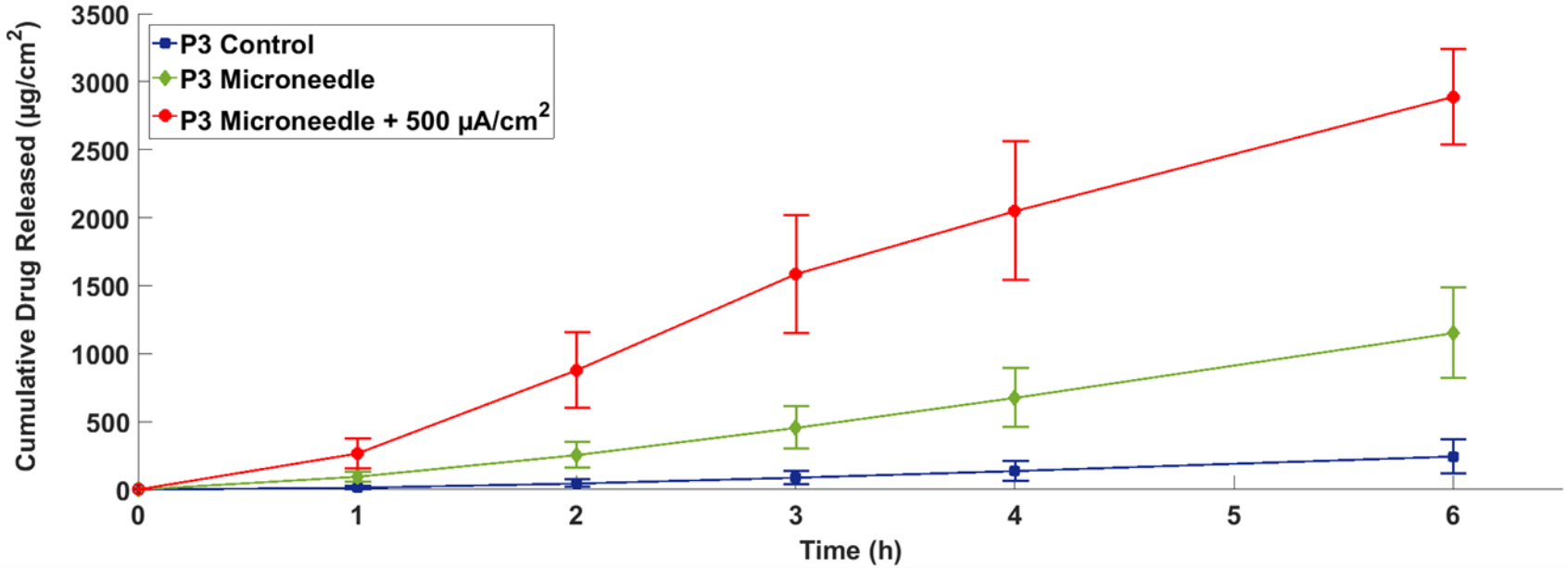

Figure 3.24 *In vitro* cumulative release profile of sumatriptan succinate over six hour period from circle dissolving microneedle aided by iontophoresis; P3 microneedle (♦); P3 control (microneedle inverted on minipig tissue) (■); P3 microneedle + 500 µA/cm^2 (●); average values ± SD (n = 3).

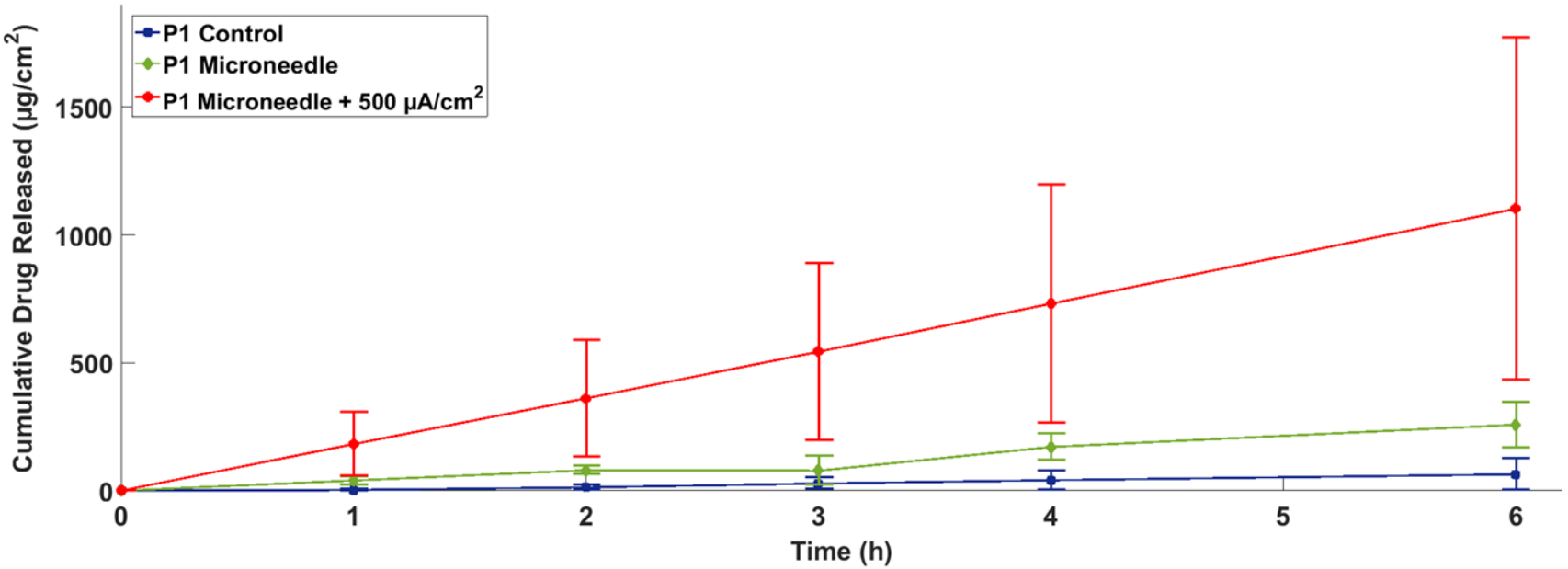

Figure 3.25 *In vitro* cumulative release profile of sumatriptan succinate over six hour period from square dissolving microneedle aided by iontophoresis; P1 square microneedle (♦); P1 square control (microneedle inverted on minipig tissue) (■); P1 square microneedle + 500 µA/cm^2 (●); average values ± SD (n = 3).

3.5 Transdermal Microneedle Devices for Drug Delivery of Sumatriptan Succinate With and Without Iontophoresis

The rate of sumatriptan succinate drug delivery to patients from the proposed microneedle device and iontophoretic microneedle device were determined using a one-compartment pharmacokinetic model. The one-compartment model was evaluated using microneedle *in vitro* flux data and clinical trial data for sumatriptan succinate 6-mg subcutaneous injection (Imitrex®) reported in the literature [73]. The following clinical study parameters and assumptions were used to develop the one-compartment model,

- Drug administered at a constant zero-order infusion rate, R
- Drug eliminated by first-order process
- Mean plasma concentration, Cmax = 72 ng/ml
- Volume of distribution, V_D = 170 L
- Drug elimination half-life, $t_{1/2}$ = 2 h

The mass balance for slow, constant infusion (zero-order rate) of drug substance and elimination (first-order rate) is given by Equation 3.1, with drug in the body, D_B; infusion rate, R; and elimination rate, k_{EL}.

$$\frac{dD_B}{dt} = R - k_{EL} D_B \tag{3.1}$$

The concentration of drug in the body is written in terms of the plasma drug concentration, C_B, and volume of distribution, V_D; (i.e., $D_B = C_B V_D$)

$$V_B \frac{dC_B}{dt} = R - k_{EL} C_B V_D \tag{3.2}$$

Applying the steady-state approximation, Equation 3.2 is reduced to

$$R = k_{EL} V_D C_B^* \tag{3.3}$$

Where C_B^* represents the steady-state drug plasma concentration (i.e., C_{max}). The elimination rate can be was determined from its relationship to the drug half-life per Equation 3.4

$$t_{1/2} = \frac{0.693}{k_{EL}} \tag{3.4}$$

Applying sumatriptan clinical data for the volume of distribution (V_D = 170 L) and half-life (2 h) reveals the microneedle device must delivery an infusion rate of 4.24 mg/h to maintain the target plasma levels (Cmax = 72 ng/ml).

3.5.1 Sumatriptan Dissolving Microneedle Device Design

The *in vitro* results for P1 formulated dissolving microneedles (Section 3.3) demonstrated a mean steady-state flux of 395 μg/cm^2 over a 7 h period and lag time of approximately 39 minutes. Hypothetically, a dissolving microarray patch with area of 10.7 cm^2 and 118.8 mg sumatriptan could provide therapeutic relief (i.e., 72 ng/ml) from migraines over a 7 hour period. This is a significant improvement when compared to previous studies for development of a sumatriptan transdermal patch. A traditional sumatriptan patch formulated with methyl cellulose polymer and Azone® enhancer would require a 15 hour lag time and 293 cm^2 patch area [24].

It is suggested that a smaller sumatriptan microarray patch is designed by reducing the PVP content in the system which was shown to increase the *in vitro* steady-state drug flux. The patch should be modified to include an adhesive backing layer over the system for adhering the patch to the skin. A separate applicator device will be used by the patient to insert the microarray device into the patients skin. Once inserted into the skin, the patch would require a thirty minute application period for the microneedles to dissolve into the skin.

3.5.2 Sumatriptan Dissolving Microneedle Iontophoretic Device Design

The *in vitro* results for P3 formulated microneedles, combined with iontophoresis, showed a steady-state drug flux of 490 $\mu g/cm^2$ over four hours with no lag time. Theoretically, an iontophoretic microneedle device with surface area 8.7 cm^2, electrical current of 500 $\mu A/cm^2$ and 47.3 mg sumatriptan would provide a therapeutic plasma concentration over a 4-hour period. This iontophoretic microneedle patch would be more efficient and require 1/3 of the API when compared to the P1 formulated microneedle patch (Section 3.5.1).

An iontophoretic microneedle device would require a cathode patch, anode patch over the microneedle, and power source. A low voltage positive (+) current would be applied to the anode patch affixed above the dissolving microneedle. The current would travel through the microneedle, into the skin to the cathode patch situated in adjacent position on the skin. The power source would be programmed to apply current over the 4 hour application period. The power source system including the anode and cathode patches could be designed as either a single-use or multiple use system. For a multiple-use system, a new microneedle system would be applied to patch prior to each use.

CHAPTER 4

MATHEMATICAL MODELLING FOR THE *IN VITRO* RELEASE OF SUMATRIPTAN SUCCINATE FROM DISSOLVING MICRONEEDLE SYSTEMS

4.1 Development of Mathematical Model for the *In vitro* Dissolution and Release of Sumatriptan From Dissolving Microneedle Arrays

A mathematical model was derived to simulate the *in vitro* dissolution and release of drug from dissolving, pyramid-shaped polyvinylpyrrolidone-based microneedle systems, as previously described [49]. Simulation studies will aid in the evaluation and prediction of critical microarray design properties (e.g., drug loading, needle height and needle pitch-width) on transdermal drug delivery through the skin. The developed framework was validated using *in vitro* data from polyvinylpyrrolidone-based dissolving microneedles containing encapsulated sumatriptan succinate API described in Section 3.3.

Previous modeling research on microneedle systems has focused primarily on the optimization of drug delivery from solid and hollow microneedle devices. In 2004, Davis et al. developed a model for predicting the insertion and fracture forces of hollow microneedle systems from specific geometric parameters (e.g, needle tip radius, wall thickness, and wall angle) [43]. Later, Al-Qallaf et al. (2008) successfully developed a mathematical framework for predicting the optimum design parameters (e.g., number of needles, needle radius, pitch-width, etc) for the transdermal delivery of macromolecules from solid and hollow microneedle systems [44]. These studies were followed by the derivation of several diffusion models for solid [74] and hollow microarray devices [75, 76]. However, these governing equations do not include dissolution of the microneedle and, therefore, cannot be used to assess the performance of soluble microneedle patches.

A mathematical framework was developed by Kim et al. (2015) to describe the dissolution and release of an encapsulated active ingredient from a single cone-shaped microarray into a control volume. A set of equations were derived from the Nernst-Brunner equation for the dissolution of the microneedle and drug concentration profiles in the skin. The model was applied to simulate the release of fentanyl citrate from a single dissolving sucrose microneedle. It was possible to determine the effects of the fentanyl mass fraction and pitch width on transdermal delivery [77]. This research builds on this previous contribution by deriving a set of governing equations for the delivery of the API from a dissolving, pyramid-shaped microneedle into a control volume. *In-silico* modeling studies will help to evaluate and predict the influence of critical design parameters (drug load, polymer concentration, pitch width and needle height) on the release profile.

The mechanistic model described in this study is developed to capture the dissolution process immediately after insertion of the array into skin. In this study, the micron-sized needles are assumed to penetrate the epidermis but not the blood capillaries and nerves in the dermis. The microneedle system is comprised of a biocompatible, water-soluble polymer matrix encapsulating water-soluble drug molecules. Once inside the skin, the microarray is 'wetted' by the interstitial fluid, which allows the needles to quickly dissolve to release the drug. The dissolved drug accumulate in the epidermis, diffuses through the dermal layers and are absorbed into the systemic circulation.

The model was constructed by considering a rectangular control-volume encompassing a single pyramid-shaped needle (Figure 4.1). This control-volume represented the skin layer and was designed with a height equal to the skin depth, δ_S; length on each side equal to the pitch-width, p_w; and rectangular volume, v. The pyramid-shaped

needle was fully submerged into the skin (i.e., rectangular control-volume) with initial volume, $v_{c,0}$; side length, L; and height, h. The mathematical model considered a number of assumptions, including:

- One-dimensional drug transport in the negative z-direction.
- Drug metabolism in the skin is not considered.
- Drug binding to viable skin tissues is not considered.
- Mass transport through sides of control-volume is not considered.
- Impact of needle properties on insertion into skin was not considered.
- Decrease in needle volume directly correlates to increase in available skin layer volume.
- Microneedles and skin layer tissues are isotropic and dissolution occurs evenly over surfaces of needle.
- The API concentration in the skin is uniform (i.e, rate of diffusion is rapid compared to rate of dissolution).

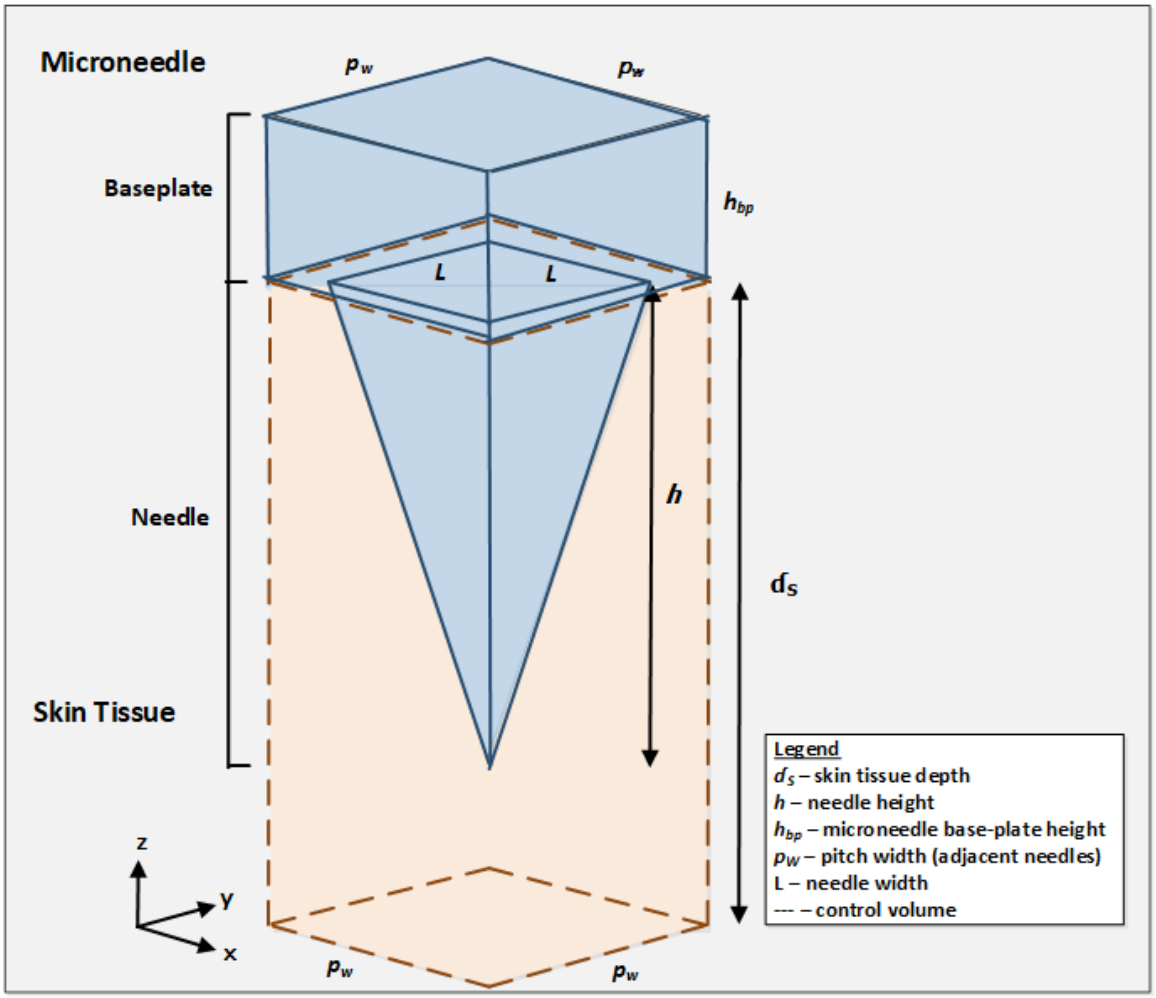

Figure 4.1 Drug release from dissolving pyramid-shaped microneedle with base-plate.

For the purpose of the model, the drug particles are transported in the negative z-direction towards the base of the rectangular volume (i.e., systemic circulation). The influence of various needles properties (i.e., needle height, pitch-width, base length) on microneedles ability to penetrate the stratum corneum and fully insert into the skin were not considered in this study. The model assumes individual needles fully insert into the skin for transdermal delivery of drug. *In vitro* experiments with blue dye (nitrazine yellow) demonstrated that circular microneedle arrays (N = 600) containing pyramid-shaped needles (h = 0.05cm, l = 0.03cm) properly insert into the skin (Section 3.2) [42].

The dimension of the control-volume was assumed to remain constant throughout the dissolution process. The needle volume, v_c, slowly decreases as it dissolves causing a similar increase in the volume of the skin layer, v. The microneedles and skin layer tissues are considered to be isotropic with the dissolution occurring evenly over the pyramid needle surfaces. This assumption is valid if the drug substance and polymer concentration are distributed homogenously throughout the pyramid needle. This leads to a constant half angle at the apex of the pyramid throughout the dissolution of the microneedle. The half angle is defined as the ratio of the pyramid needle height to the pyramid base length and is defined by Equation 4.1 and depicted in Figure 4.2b.

$$\tan\theta = \frac{L(t)}{2h(t)} = \frac{L_0}{2h_0} \tag{4.1}$$

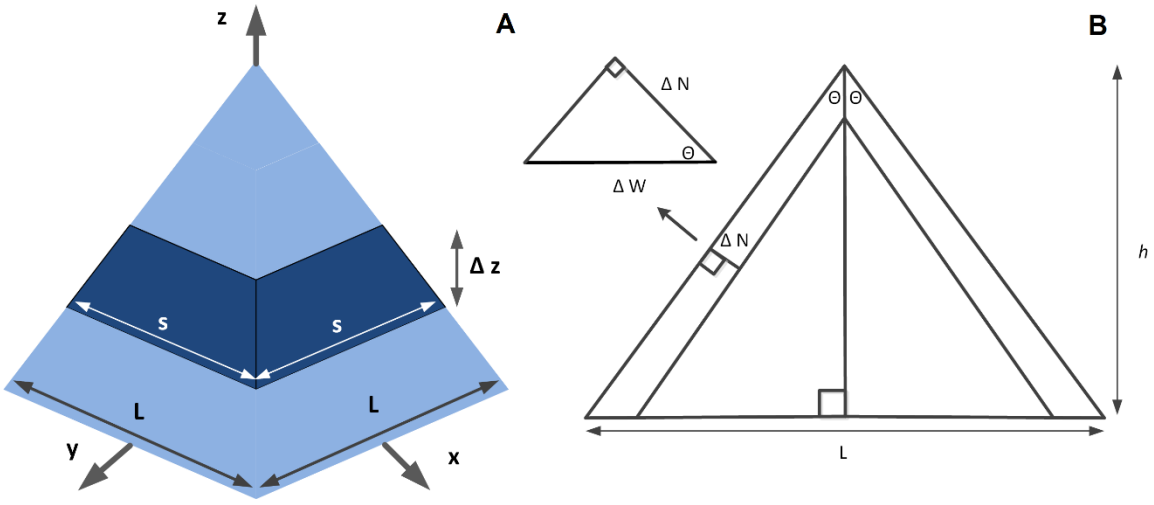

Figure 4.2 Schematic of pyramid-shaped needle; (A) cross-section view; (B) half angle view.

The concentration of active drug in the skin layer tissue was assumed to be uniform throughout the compartment. This is a realistic assumption because diffusion was faster

than the dissolution of the pyramid needles or the elimination of drug into systemic circulation.

The mathematical model for describing the dissolution of the microneedle is presented with the full derivations in Sections 4.1.1 and 4.1.2. The definition of the model parameters are provided in Table 4.1. The material balance for drug mass in the skin layer results in

$$\frac{dc(t)}{dt} = -\left(k_L c\right) + 4\left[\frac{k_D \tan\theta}{\rho\cos\theta}\right] h^2 \left[\frac{\beta\rho - c}{\nu_0 + \nu_{c,0} - \nu_c}\right]\left[c_S - \left(\frac{1-\beta}{\beta}\right)c(t)\right] \tag{4.2}$$

The height of the pyramid is defined as

$$\frac{dh(t)}{dt} = -\frac{k_D}{\rho\sin\theta}\left[c_S - \left[\frac{1-\beta}{\beta}\right]c(t)\right] \tag{4.3}$$

The initial conditions are

$$c(t=0) = 0 \tag{4.4}$$

and

$$h\,(t=0) = h_0 \tag{4.5}$$

The cumulative amount of drug released is

$$Q(t) = \beta\rho\nu_{C,0} - (\beta\rho\nu_C(\mathrm{t}) + \mathrm{c(t)}(\nu_0 + \nu_{C,0} - \nu_C(\mathrm{t}))) \tag{4.6}$$

Additional equations were derived to describe the long-term release of drug from dissolving microneedles containing a rectangular base-plate. The *in vitro* tests used to

validate the mathematical model were generated from dissolving microneedles containing a base-plate with uniform homogenous encapsulated PVP polymer and sumatriptan succinate drug. The base-plate equations were simplified with the following assumptions:

- The microneedle base-plate dissolves after the pyramid-shaped needles.
- The ratio of parallelepiped sides remain constant during the dissolution.

The following equations were derived to describe the dissolution of the base-plate following microneedle dissolution. The derivation of the equations is contained in Section 4.1.3 and the equation parameters are listed in Table 4.1. The drug concentration in the solid baseplate, c_{SD}, is described by

$$\frac{dc_{SD}}{dt} = -\frac{k_D \beta A_0 c_s}{d_s p_w^2}\left(\frac{d_s p_w^2 c_{SD}}{M_0}\right)^{\frac{2}{3}} \tag{4.7}$$

$$c_{SD}(0) = c_{SD,0} \tag{4.8}$$

The drug concentration in the skin layer, c(t), after base-plate begins to dissolve, is given by

$$\frac{dc}{dt} = -\frac{k_D \beta A_0 c_s}{d_s p_w^2}\left(\frac{d_s p_w^2 c_{SD}}{M_0}\right)^{\frac{2}{3}} - k_L c \tag{4.9}$$

$$c(0) = c_L \tag{4.10}$$

The cumulative amount of drug released is

$$Q(t) = (\beta\rho v_{C,0} + m_0) - d_s p_w^2 (c_{SD}(t) + c(t)) \tag{4.11}$$

Immediately after the microneedle dissolves, the solid base-plate concentration, c_{SD}, and skin layer concentration, c, are zero and $c(t_D)$, respectively. The cumulative percent drug released, M(t), is obtained by dividing Q(t) by $\beta\rho v_{C,0} + m_0$.

$$M(t) = 1 - \frac{d_s p_w^2 (c_{SD}(t) + c(t))}{(\beta\rho v_{C,0} + m_0)} \tag{4.12}$$

Table 4.1 Definition of Governing Equation Parameters

A	microneedle base-plate wet surface area (cm^2)	L	length microneedle base (cm)
β	mass fraction drug in microneedle (w/w)	M	Mass of drug in base-plate (g)
c	drug concentration in skin layer (g/cm^3)	N	thickness of dissolving pyramid outer layer (cm)
c_s	solubility matrix polymer in solvent (g/cm^3)	ρ	density of DMN (g/cm^3)
c_{SD}	Drug concentration in solid base-plate (g/cm^3)	p_w	pitch width (cm)
d_{bp}	depth of baseplate (cm)	θ	half angle at apex of needle (degree)
d_S	depth of skin layer (cm)	t	time (h)
γ	drug electromigration/convection parameter	t_D	microneedle dissolution time (h)
h	height of microneedle (cm)	v	volume of skin layer (cm^3)
k_D	dissolution rate constant (cm/hr)	v_c	volume of microneedle (cm^3)
k_L	elimination rate constant (hr^{-1})	subscript, $_0$	initial state

4.1.1 Derivation of Dissolution Governing Equation for Microneedle Height

The derivation of the governing equation for the height of the microneedle begins with defining the mass of an individual pyramid-shaped microneedle, with density, ρ; pyramid base length, L; needle height, h; half angle, θ; and volume, v_c.

$$\rho v_c(t) = \rho\left(\frac{1}{3}L^2(t)h(t)\right) \tag{4.13}$$

Substitute Equation 4.1 to define mass of microneedle in terms of microneedle height yields

$$\rho v_c(t) = \rho\left(\frac{4}{3}h^3(t)\tan^2\theta\right) \tag{4.14}$$

Taking the first derivative with respect to time results in

$$\frac{dv_c}{dt} = 4h^2(t)\tan^2\theta\frac{dh}{dt} \tag{4.15}$$

A cross-section of a pyramid needle is depicted by Figure 4.2a with height from z to z + Δz and side width, s. At zero time, the circumference of the pyramid needle is 4s with each side having width

$$s = \frac{L(l-h)}{h} \tag{4.16}$$

At time t + Δt, the outer layer pyramid dissolves by a thickness of Δd pictured in Figure 4.1b and is used to defined the reduction of the pyramid base width, ΔW.

$$\Delta W = \frac{\Delta N}{\cos\theta} \tag{4.17}$$

Thus, at time t + Δt the change in volume of the pyramid needle, due to dissolution, is

$$\Delta v_c = -\int_0^h (4s)\Delta W dz \tag{4.18}$$

Equation 4.18 is simplified with Equations 4.16 and 4.17 to yield

$$\Delta v_c = -4\int_0^h \left(\frac{L(h-z)}{h}\right)\left(\frac{\Delta N}{\cos\theta}\right)dz \tag{4.19}$$

Division of both sides of Equation 4.19 by Δt, taking the limit as Δt → 0, and integrating produces

$$\frac{dv_c}{dt} = -2hL\sec\theta\frac{dN}{dt} \tag{4.20}$$

In Equation 4.20, the last term is determined from the Nerst and Brunner equation [78]; with dissolution constant, k_D, solubility of PVP in the body fluid, c_S, and the mass fraction of drug in the microneedle, β.

$$\frac{dn}{dt} = \frac{k_D}{\rho}\left[c_S - \left[\frac{1-\beta}{\beta}\right]c\right] \tag{4.21}$$

The Equation 4.20 and Equation 4.21 resulted in

$$\frac{dv_c}{dt} = -2hL\sec\theta\left[\frac{k_D}{\rho}\left[c_S - \left[\frac{1-\beta}{\beta}\right]c\right]\right] \tag{4.22}$$

Finally, the right-hand side of Equations 4.15 and 4.22 yields the governing equation for the height of the pyramid needle over time and initial condition:

$$\frac{dh}{dt} = -\frac{k_D}{\rho \sin\theta}\left[c_S - \left[\frac{1-\beta}{\beta}\right]c\right] \tag{4.23}$$

$$h(0) = h_0 \tag{4.24}$$

4.1.2 Derivation of Dissolution Governing Equation for Skin Layer Drug Concentration

It is necessary to first determine the volume of the compartment (i.e., skin layer), v(t), at time t. The skin layer volume consists of the initial volume of the skin layer, v_0, and the volume gained as the microneedle dissolves in the tissue, $v_{c,0}$ - v_c (t). Here, $v_{c,0}$ represents the initial microneedle volume at zero time and v_c(t) is the microneedle volume at time t. Thus, the skin layer volume is

$$v(t) = v_0 + \left(v_{c,0} - v_c(t)\right) \tag{4.25}$$

A mass balance on the skin layer control volume demonstrates the accumulation of drug substance in the skin layer, $\frac{d(vc)}{dt}$, is the difference between the drug released from the dissolving microneedle, $-\left((k_L d_s)c_{z=d_s}\right)p_w{}^2$, and the drug exiting the skin layer into the bloodstream, $\beta\rho\left(-\frac{dv_c}{dt}\right)$.

$$\frac{d(vc)}{dt} = -\left((k_L d_s)c_{z=d_s}\right)p_w{}^2 + \beta\rho\left(-\frac{dv_c}{dt}\right) \tag{4.26}$$

The equations are simplified by applying the following chain rule (Equation 4.27)

$$\frac{d(vc)}{dt} = v\frac{dc}{dt} + c\frac{dv}{dt} \tag{4.27}$$

After combining Equations 4.27 and 4.26, the following equation is obtained:

$$v\frac{dc}{dt} = -(k_L c)d_s {p_w}^2 + (\beta\rho - c)\left(-\frac{dv_c}{dt}\right) \tag{4.28}$$

Finally, both sides of Equation 4.28 are divided by *v* to give

$$\frac{dc}{dt} = -\left(k_L c\right) + 4\left[\frac{k_D \tan\theta}{\rho\cos\theta}\right]h^2\left[\frac{\beta\rho - c}{v_0 + v_{c,0} - v_c}\right]\left[c_S - \left(\frac{1-\beta}{\beta}\right)c\right] \tag{4.29}$$

The initial condition is

$$c(0) = 0 \tag{4.30}$$

4.1.3 Derivation of the Dissolution Equation for Drug Release From the Microneedle Base-plate

The derivation of the governing equation for the base-plate of the microneedle begins with defining the mass of the parallelepiped (Figure 4.1); with mass of drug remaining in parallelepiped, M; mass transfer coefficient, k_D; parallelepiped 'wet' surface area, A; solubility of matrix polymer in solvent, C_S; and concentration of drug in liquid phase, c.

$$\frac{dM}{dt} = -k\beta A(C_S - C_{aq}) \tag{4.31}$$

The Equation 4.31 was simplified by assuming Caq << C_S for most *in vitro* situations to give

$$\frac{dM}{dt} = -k\beta AC_S \tag{4.32}$$

Since the density remains constant during dissolution, it can be shown that:

$$A = A_0\left(\frac{M}{M_0}\right)^{\frac{2}{3}} \tag{4.33}$$

Equation 4.32 is simplified to yield

$$\frac{dM}{dt} = -k\beta A_0 C_S\left(\frac{M}{M_0}\right)^{\frac{2}{3}} \tag{4.34}$$

with the initial condition

$$M(0) = M_0 \tag{4.35}$$

As a results, we have the following system:

$$\frac{dc_{SD}}{dt} = -\frac{k_D\ \beta\ A_0\ c_s}{d_s p_w^2}\left(\frac{d_s p_w^2 c_{SD}}{M_0}\right)^{\frac{2}{3}} \tag{4.36}$$

$$c_{SD}(0) = c_{SD,0} \tag{4.37}$$

$$\frac{dc}{dt} = -\frac{k_D\ \beta\ A_0\ c_s}{d_s p_w^2}\left(\frac{d_s p_w^2 c_{SD}}{M_0}\right)^{\frac{2}{3}} - k_L c \tag{4.38}$$

$$c(0) = c_L \tag{4.39}$$

4.2 *In vitro* Release Studies for Validation of Sumatriptan Microneedle Dissolution Mathematical Model

The dissolution mathematical model (Section 4.1) was analyzed using *in vitro* data from pyramid-shaped dissolving sumatriptan microneedles to estimate dissolution and elimination rate constants. The predicted drug release profile was validated against *in vitro* data for three separate sumatriptan microneedle formulations. Simulation experiments to evaluate key design parameters (drug load, polymer concentration, needle height and pitch width) for release of sumatriptan succinate from dissolving pyramid-shaped microneedles [49].

4.2.1 Comparison of Simulated and Experimental *In vitro* Minipig Results

The dissolution model for predicting drug release from dissolving pyramid-shaped microneedles was evaluated against *in vitro* data from dissolving microneedles containing the base-plate and formulated to release the sumatriptan succinate. Equation 4.12 was used to predict the drug release profiles of three different sumatriptan formulations (P1, P2, and P3) with different drug loading and polymer concentration (Table 2.1). The microneedle dimensions and formulation parameters were determined by experiments in the lab (Section 3.2) and are summarized in Table 3.1. Regression techniques, implemented in Mathematica®, were applied to the *in vitro* data for all formulations to derive estimates for the dissolution rate constants, k_D, and elimination rate constants, k_L. The standard weighted squared error between simulated values from Equation 4.12 and *in vitro* results was minimized with respect to k_L and k_D (Table 4.2). The predicted k_D and k_L values were used to generate theoretical release profile which compared well with the experimental results, see Figures 4.3 – 4.5.

Table 4.2 Estimated Sumatriptan Microneedle Formulation Parameters for Dissolution Model

Formulation	**t_{D1}^* (h)**	**k_D^* (cm/h)**	**k_L^* (h^{-1})**
Circle Arrays			
P1	1.28 ± 0.6	0.0143 ± 0.0074	0.0516 ± 0.0030
P2	0.51 ± 0.6	0.0388 ± 0.055	0.0569 ± 0.0052
P3	0.23 ± 0.2	0.0912 ± 0.088	0.0621 ± 0.0016

*value ± confidence interval

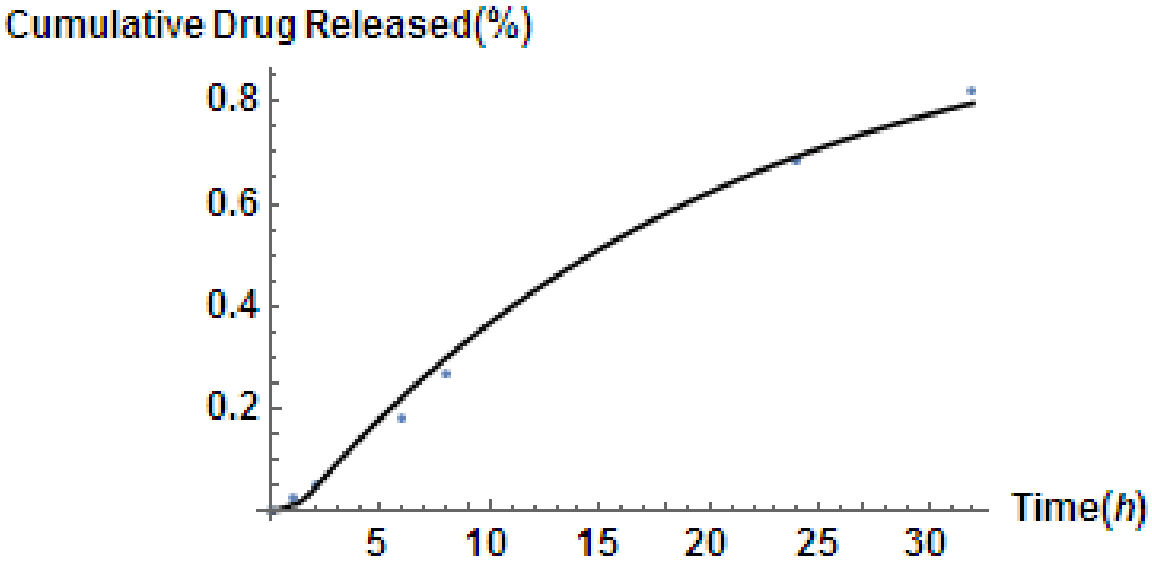

Figure 4.3 Plots comparing minipig *in vitro* cumulative percent release of P1 microneedles (solid dots) to predicted profiles (solid lines).

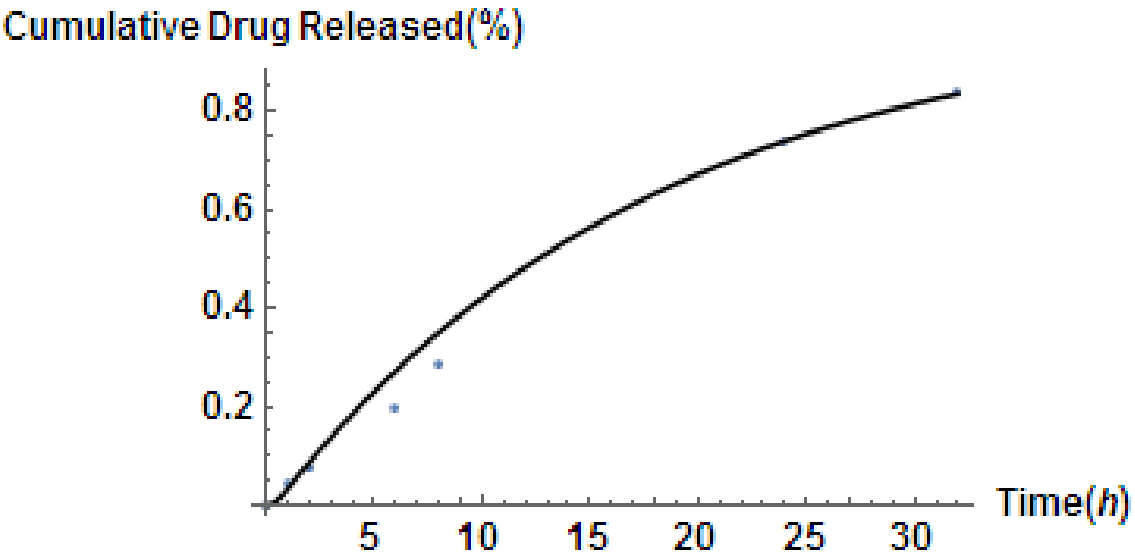

Figure 4.4 Plots comparing minipig *in vitro* cumulative percent release of P2 microneedles (solid dots) to predicted profiles (solid lines).

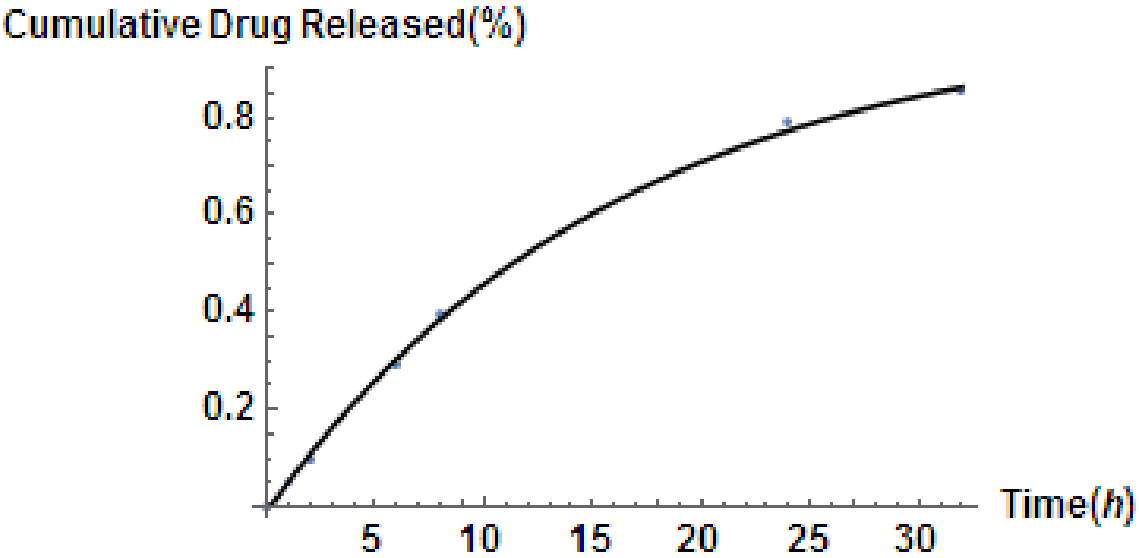

Figure 4.5 Plots comparing minipig *in vitro* cumulative percent release of P3 microneedles (solid dots) to predicted profiles (solid lines).

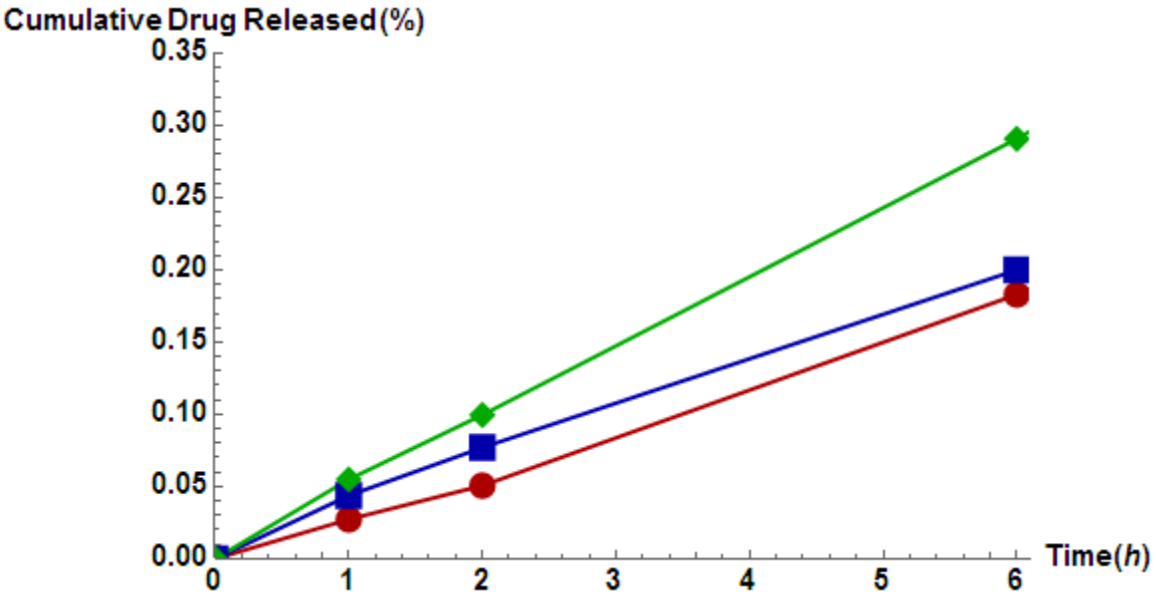

Figure 4.6 *In vitro* percent release sumatriptan succinate from dissolving microneedle after 6 hours from formulation P1 (●), P2 (■) and P3(♦); average values (n = 3).

Estimated dissolution times for microneedles from each formulation were generated using the model and predicted k_D and k_L values (Table 4.2). The dissolution time for the P1 formulation (13.8 min) was similar to dissolution times calculated observed experimentally in the lab (< 15 minutes). Tomographic imaging studies conducted in the lab showed P1 formulated dissolving microarrays with circle geometry dissolving in approximately 10 minutes (Section 3.2). Similar experimental results related to dissolution of PVP-based microneedles in porcine skin were reported by both Sullivan and Quin [79, 80]. The P1 and P2 formulations, on the other hand, demonstrated significantly higher dissolution times of 30.6 and 76.8 minutes, respectively. However, it should be noted that the confidence intervals were very high for all three formulations.

The estimated dissolution rate constant values correlated to experimental results with a similar trend of k_D [P1] < k_D [P2] < k_D [P3] as shown in Figure 4.6, where k_D [Pi] represents the Pi formulation value. A higher initial release is realized as the process is

governed by dissolution at early times. This behavior is predicted by Equation 4.9 for the accumulation of drug in the skin layer which indicates slow first-order clearance into the blood stream (first term on right-hand side) as compared to dissolution term (second term on right-hand side).

The relationships between the P1 – P3 microneedle formulation parameters (polymer conc., drug load and density) with the dissolution and elimination rates are not completely understood and require subsequent investigations. No trends were observed when comparing the drug load, β, to the k_D results. The density of the microneedle formulations increased in a similar manner to the k_D values: ρ [P1] < ρ [P2] < ρ [P3]. Further investigation is required to determine if drug release from microneedles can be altered by the density. A 10 % increase in PVP polymer matrix concentration from P3 to P2 related to a 42.5 % reduction in the k_D value. A similar increase in drug release with decreased polyvinylpyrrolidone concentration in dissolving microneedles was observed by Shah et al. [81]. On the other hand, the elimination rates remained constant with all three formulations, k_L [P1] < k_L [P2] < k_L [P3].

4.2.2 Simulation Studies

Simulation studies were conducted to determine optimal design parameter values for the sumatriptan succinate dissolving microneedle systems. The impact of changing the microneedle height, microneedle pitch-width or loading dose on drug delivery, was evaluated. The simulations were performed using the P1 microneedle formulation parameters.

The response to varying the initial microneedle height, h_0, was assessed by plotting skin layer concentration, $c(t)$, as a function of time for three h_0 values (Figure 4.7). The

initial height of the pyramid needles had a major effect on drug release as indicated by c_{max} values. For example, a 20% increase in height from 0.05 cm to 0.06 resulted in 69% increase in c_{max} values from 0.036 μg/ml to 0.061 μg/ml.

The influence of pitch width, p_w, on drug delivery was evaluated by plotting skin layer concentration, *c(t)*, as a function of height for three p_w values (Figure 4.8). The pitch width had a significant impact on skin layer concentration as a negligible increase in pitch width related to a considerable reduction in drug concentration. For example, a 50% increase in pitch width from 0.035 cm to 0.0525 cm resulted in a 44% decrease in drug concentration from 0.017 μg/ml to 0.0075 μg/ml.

The effect of drug loading, β, was measured by plotting skin layer concentration, *c(t)*, as a function of height for three β values (Figure 4.9). The sumatriptan concentration in the microneedles had a direct relationship with the drug layer concentration. Incremental variations in microneedle sumatriptan concentration led to proportional changes in drug layer concentration. For example, decreasing the sumatriptan content in microneedle three-fold from $\beta = 0.3$ to $\beta = 0.1$ produced a three-fold decrease in skin concentration from 0.017 μg/ml to 0.051 μg/ml.

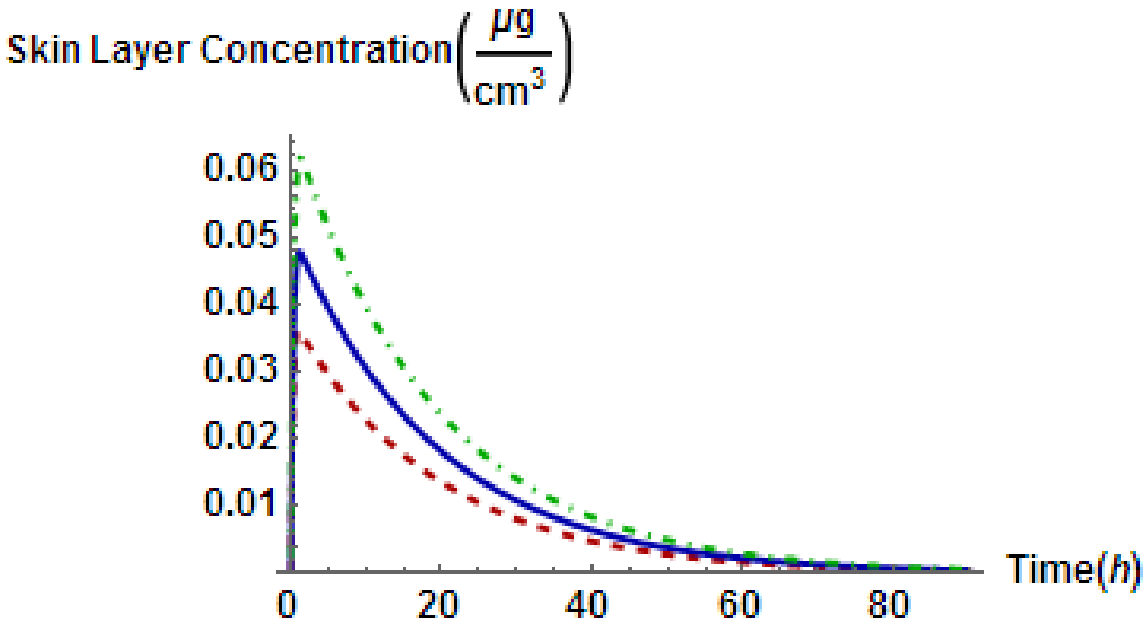

Figure 4.7 Modelling effect of needle height on sumatriptan succinate release using P1 formulation parameters; needle height, h [h = 0.06cm (– •), h = 0.1 (—), h = 0.1(--)].

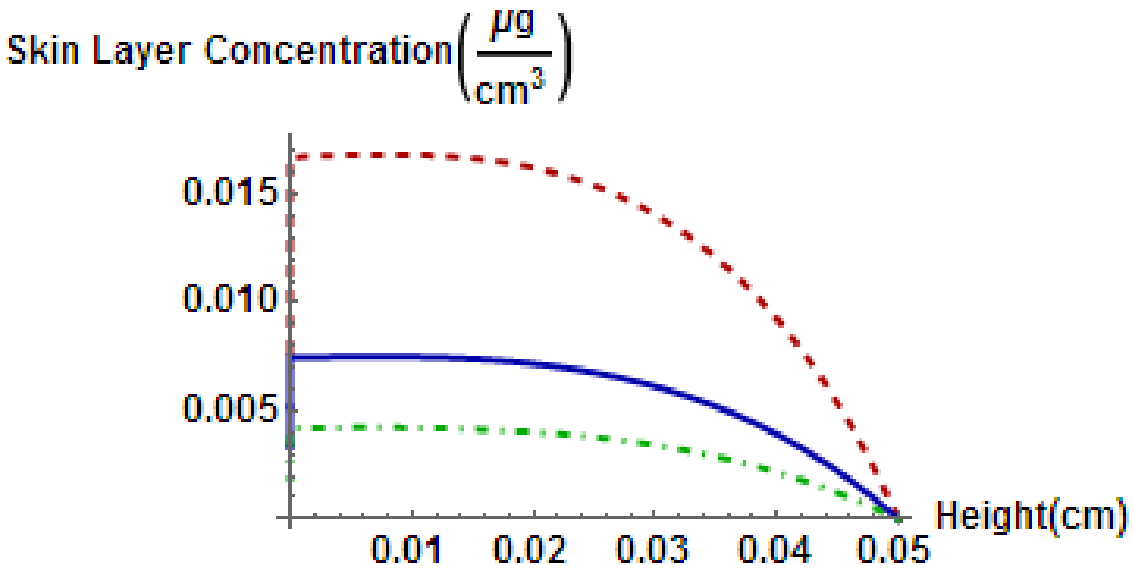

Figure 4.8 Modelling effects of pitch width on sumatriptan succinate release using P1 formulation parameters; pitch width, p_w, of microneedle [p_w = 0.035cm (--), p_w = 0.0525cm (—), p_w = 0.07cm (– •)].

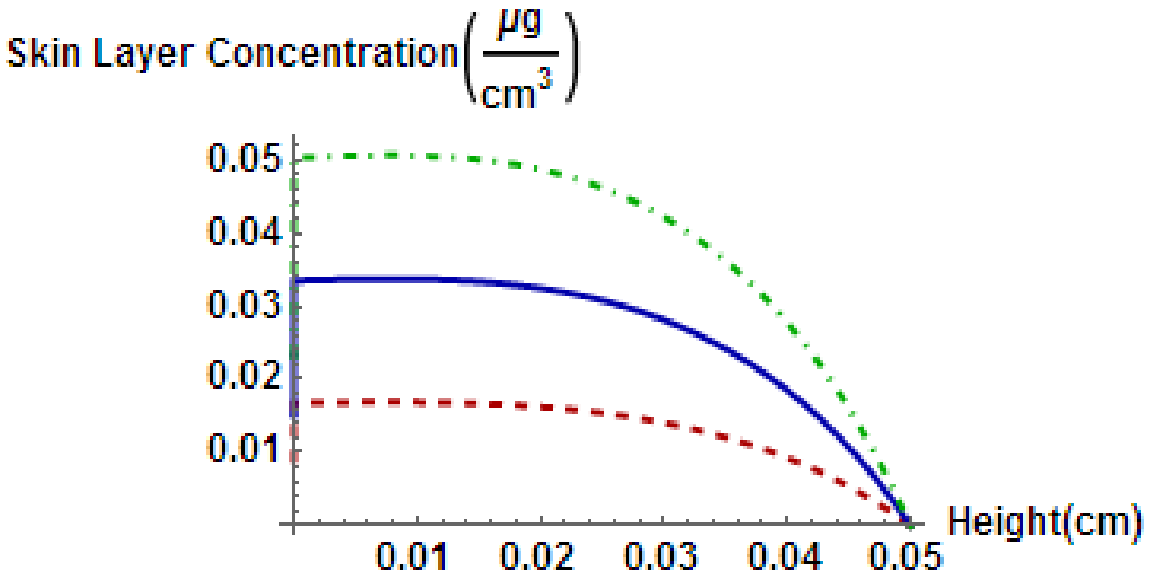

Figure 4.9 Modelling effects of drug loading on sumatriptan succinate release using P1 formulation parameters; mass fraction (β) sumatriptan succinate in microneedle [β = 0.1% (− •), β = 0.2% (—), β = 0.3% (--)].

4.3 Development of Mathematical Model for *In vitro* Dissolution, Diffusion and Release of Drug Substance From Dissolving Microneedle Array

In this section, a mathematical model, which includes the dissolution and diffusion, is introduced to predict drug release from a dissolving pyramid-shaped microneedle. The previous model, developed in Section 4.1 and described in [49], estimated the percentage of drug released from dissolving microneedles using equations for microneedle height (Equation 4.3) and skin layer concentration (Equation 4.2). Note that the simplified model assumed a constant homogenous drug concentration in the skin layer. In this study, a new model is developed by applying Fick's second law of diffusion and a material balance on the drug in the skin. This approach will be used to predict the drug concentration profile within the epidermis over time during and after dissolution of the microneedle.

The dissolution and diffusion equations were developed using a method similar to the homogenous model described in Section 4.1. The microneedle depicted in Figure 4.1 is used again to derive the equations. In this case, the assumptions made in generating the model are listed below:

- One-dimensional drug transport in the negative z-direction.
- Drug metabolism in the skin is not considered.
- Drug binding to viable skin tissues is not considered.
- Mass transport through sides of control-volume not considered.
- Impact of needle properties on insertion into skin was not considered.
- Decrease in needle volume directly correlates to increase in available skin layer volume.
- Microneedles and skin layer tissues are isotropic and dissolution occurs evenly over surfaces of needle.

A dissolution and diffusion model is described by the set of equations listed below and includes the governing equation for change in microneedle height and the change in skin layer drug concentration. A complete derivation of the governing equations for microneedle height and skin layer concentration are included in Sections 4.1.1 and 4.1.2, respectively. All parameter definitions are presented Table 4.1.

The material balance for drug mass in the skin layer is,

$$\frac{\partial c}{\partial t} = D\frac{\partial^2 c}{\partial z^2} + 4\left(\frac{k_D \tan\theta}{\rho\cos\theta}\right)h^2\left(\frac{\beta\rho - c}{v_0 + v_{c,0} - v_c}\right)\left(c_s - \left(\frac{1-\beta}{\beta}\right)c\right) \tag{4.40}$$

The height of the pyramid is defined as

$$\frac{dh(t)}{dt} = -\frac{k_D c_S}{\rho \sin\theta} \tag{4.41}$$

The initial conditions are

$$h(0) = h_0 \tag{4.42}$$

and

$$c(x,0) = 0 \tag{4.43}$$

It is assumed that the concentration at the boundary plane between the pyramid base and the baseplate remains unchanged while the microneedle dissolves,

$$\left.\frac{\partial c(z,t)}{\partial z}\right|_{z=0} = 0 \tag{4.44}$$

The drug concentration at the base of the control-volume (ie. blood stream) maintains sink conditions:

$$c(d_s,t) = 0 \tag{4.45}$$

Thus, diffusive flux, J(t), through the base of the control-volume (i.e., blood stream) is defined as

$$J(t) = -p_w^2 D \left.\frac{\partial c(z,t)}{\partial z}\right|_{z=d_s} \tag{4.46}$$

The cumulative amount of drug released $Q(t)$ is then determined from the diffusive flux, (J(t),

$$Q(t) = \int_0^t J(\tau) d\tau \tag{4.47}$$

The cumulative percent drug released, M(t), is obtained by dividing Q(t) by $\beta \rho v_{C,0} + m_0$.

$$M(t) = \frac{\int_0^t J(\tau) d\tau}{\left(\beta \rho v_{c,0} + m_0\right)} \tag{4.48}$$

In a second step, the dissolution and diffusion model equations were revised to describe the long-term release of drug from dissolving microneedles containing a rectangular base-plate. *In vitro* tests used to validate the model equations for release and diffusion of dissolving microneedles containing a rectangular base-plate with uniform homogenous encapsulated PVP polymer and sumatriptan succinate drug. The base-plate equations were developed with similar assumptions to the previous base-plate equations for the dissolution model (Equations 4.7 to 4.10):

- The microneedle base-plate dissolves after the pyramid-shaped microneedles.
- The ratios of parallelepiped sides remain constant during the dissolution.

In modeling the drug release from the microneedle and base-plate, the previous governing equations (Equations 4.40 - 4.45) are combined with the a new pyramid base boundary condition (Equation 4.49). Several conditions are applied to Equation 4.49 with

$t = \frac{h_0 \rho \sin(\theta)}{c_s k_d}$ describing the time it takes for microneedle to dissolve; $t = \frac{d_s p_w^2 c_{S0}}{k_d \beta A_0 c_s}$ defining the dissolution time of the base-plate alone.

$$p_w^2 D \left.\frac{\partial c(z,t)}{\partial z}\right|_{z=d_s} = \begin{cases} 0 & t < \frac{h_0 \rho \sin(\theta)}{c_s k_d} \\ -k_d \beta A_0 c_s & \frac{h_0 \rho \sin(\theta)}{c_s k_d} \le t < \frac{d_s p_w^2 c_{S0}}{k_d \omega A_0 c_s} + \frac{h_0 \rho \sin(\theta)}{c_s k_d} \\ 0 & t \ge \frac{d_s p_w^2 c_{S0}}{k_d \beta A_0 c_s} + \frac{h_0 \rho \sin(\theta)}{c_s k_d} \end{cases} \quad (4.49)$$

4.4 *In vitro* Release Studies for Validation of Sumatriptan Microneedle Dissolution and Diffusion Mathematical Model

Simulations, using the dissolution and diffusion mathematical model (Section 4.3) will be run to evaluate the effects of key design parameters (drug load, polymer concentration, needle height and pitch width) on the release of sumatriptan succinate from microneedles. Later, the model will be validated with *in vitro* data from pyramid-shaped sumatriptan microneedle devices containing a rectangular base-plate.

4.4.1 Simulation Experiments

The P1 formulated circle microneedle arrays were used as a base-case with dimensions and formulation parameters determined by laboratory experiments (Section 3.2) and summarized in Table 3.1. The dissolution rate (k_D = 0.0143 cm/h) for P1 formulation, determined through regression techniques in Section 4.2, was applied. The diffusion coefficient for sumatriptan succinate across Göttingen minipig skin (D) was approximated

from the steady-state diffusion equation and the lag-time method [82]. A value of D = 7.90 x 10^{-5} cm^2/h was determined.

Contour plots are shown in Figures 4.10 – 4.13 and demonstrate the influence of drug load, pitch width and needle height on the drug concentration within the epidermis after 4 hours. Changes in the load and pitch-width had a significant impact on drug diffusion. Reducing the drug load 20%, from β = 21.42% to β = 17.14%, led to a 50% decrease in sumatriptan concentration at base of skin compartment (Figure 4.11). Decreasing pitch-width 20% , from p_w = 0.035 cm to p_w = 0.028 cm, led to a 100% increase in drug content at the base of the control-volume (Figure 4.12). On the other hand, changes in the microneedle height had a less pronounced effect with a 20% decrease in height, *h*, from *h* = 0.05 cm to *h* = 0.04 cm, leading to a very negligible decrease in drug diffusion.

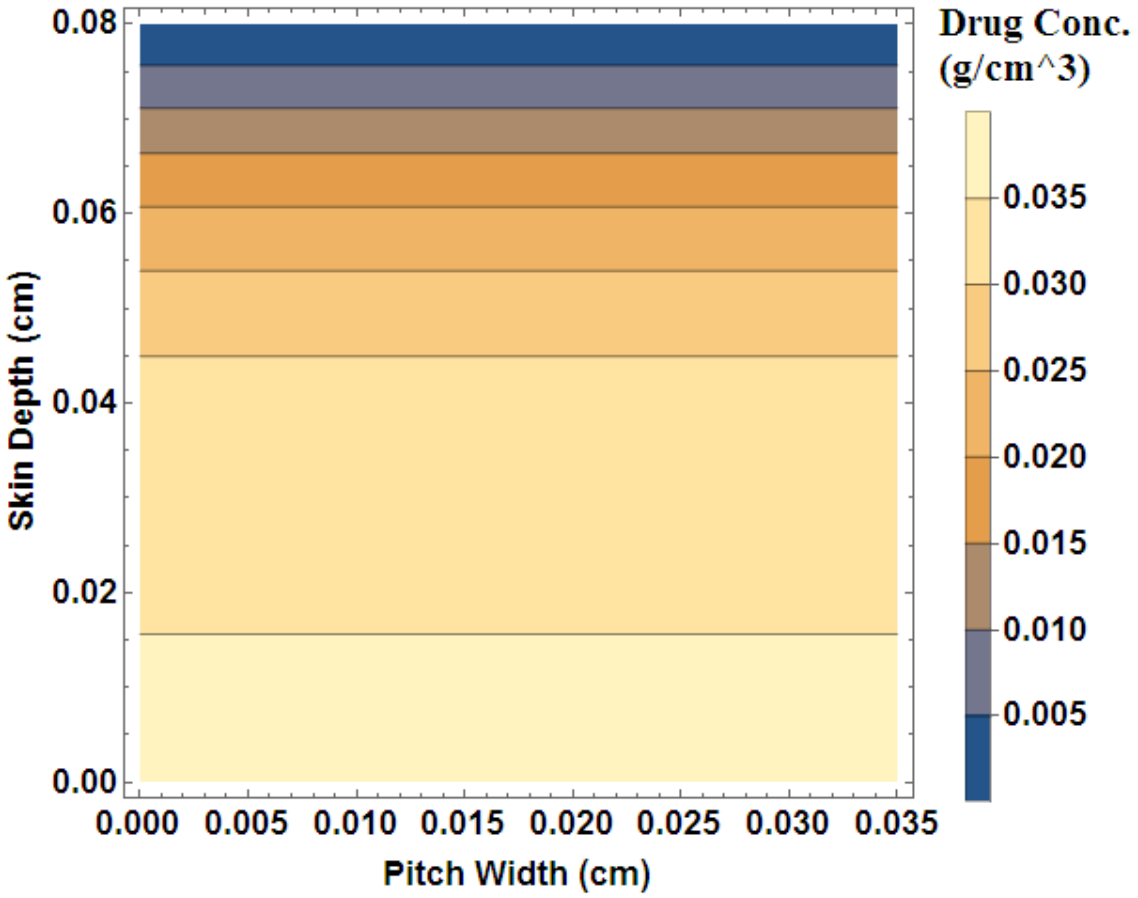

Figure 4.10 Contour plot of sumatriptan drug release from P1 microneedle after 4 hours [h = 0.05 cm, β = 21.42%, p_w = 0.035 cm].

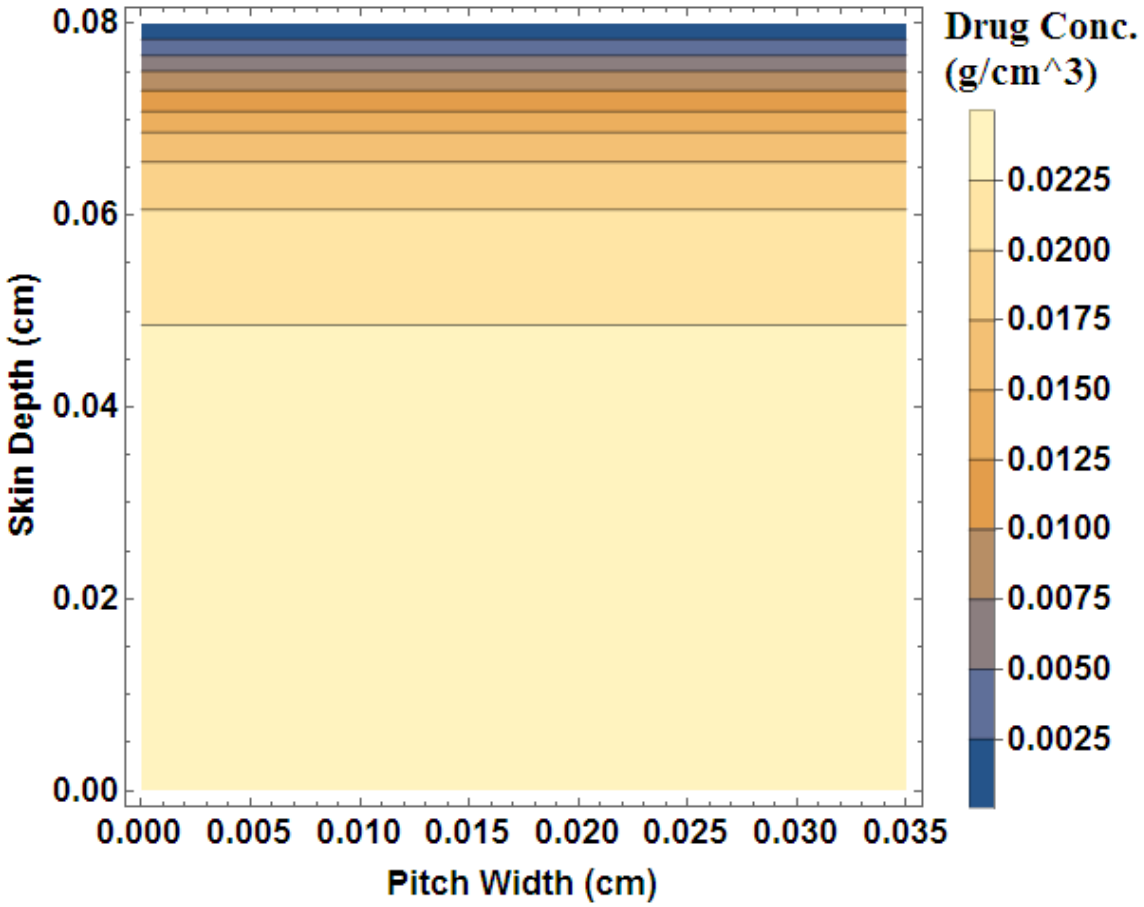

Figure 4.11 Contour plot of sumatriptan drug release from P1 microneedle after 4 hours with reduced mass fraction API [h = 0.05 cm, β = 17.14%, p_w = 0.035 cm].

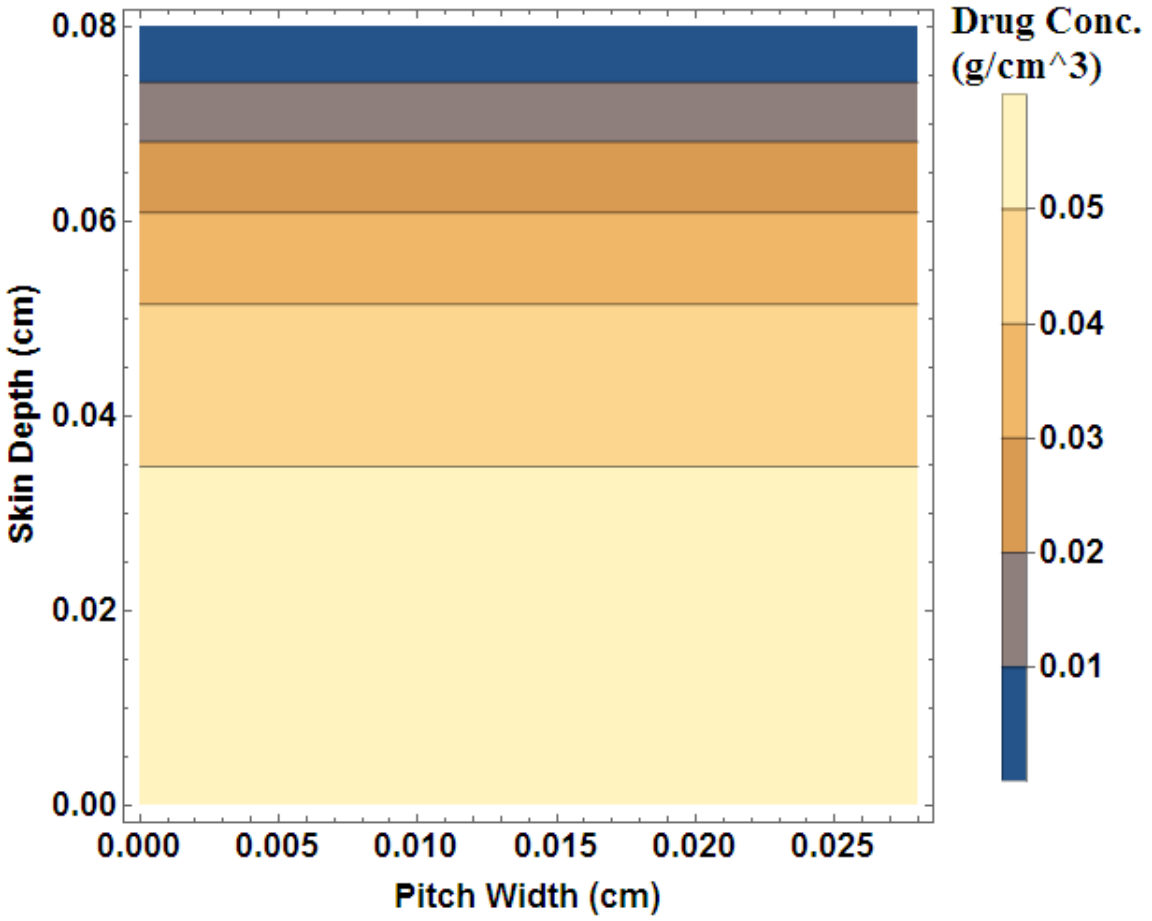

Figure 4.12 Contour plot of sumatriptan drug release from P1 microneedle after 4 hours with reduced pitch width [h = 0.05 cm, β = 21.42%, p_w = 0.028 cm].

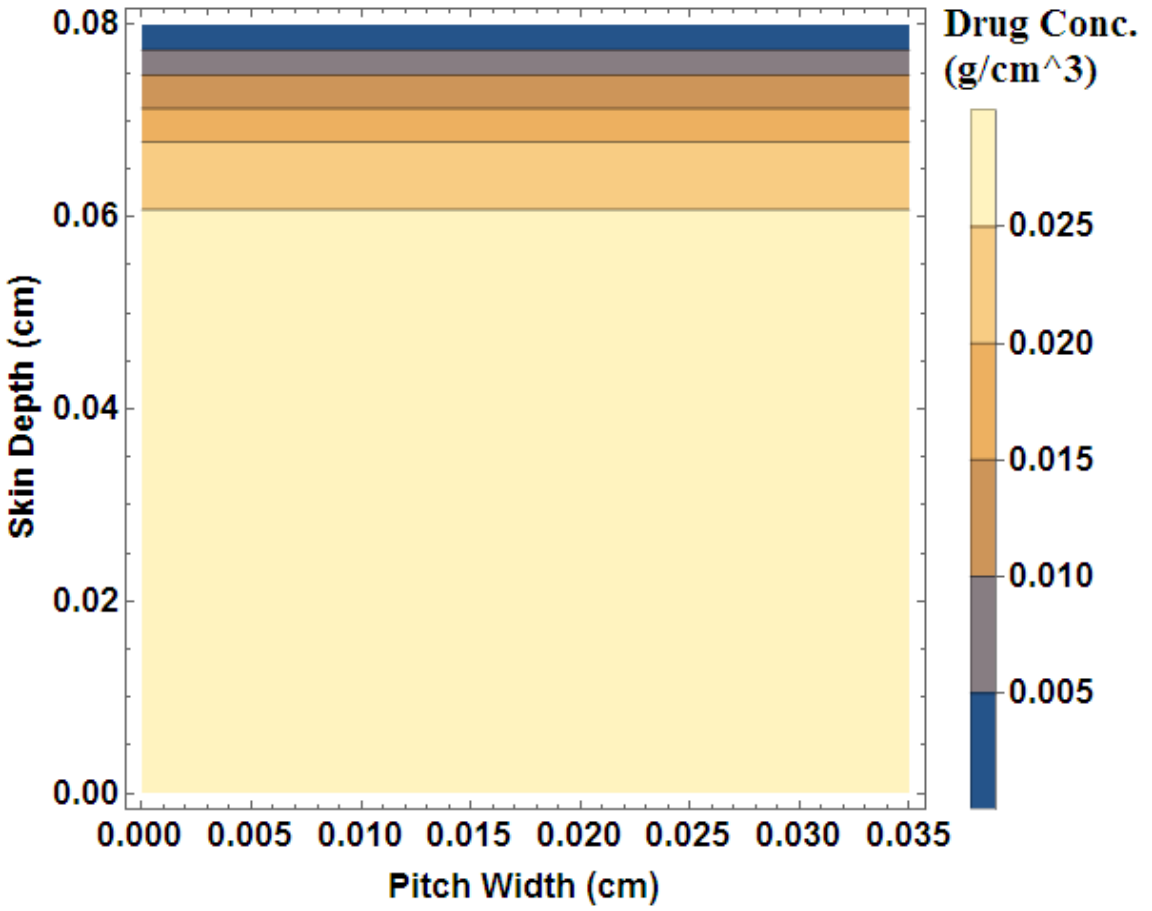

Figure 4.13 Contour plot of sumatriptan drug release from P1 microneedle after 4 hours with reduced microneedle height [h = 0.04 cm, β = 21.42%, p_w = 0.035 cm].

4.4.2 Comparison of Simulated and Experimental *In vitro* Minipig Results

A comparison was conducted to evaluate the dissolution and diffusion model estimated drug release profiles versus the *in vitro* data for the dissolving microarrays containing encapsulated sumatriptan in microneedles and a base-plate. Equations 4.48 and 4.49 were used to predict the drug release profiles of three different sumatriptan formulations (P1, P2, and P3) with different drug loading and polymer concentration (Table 2.1). Both the

microneedle dimensions and formulation properties were previously determined in lab experiments (Section 3.2) and are summarized in Table 3.1. *In vitro* data was augmented to include data from pull-points at 1, 2, 4, 6, 8, 24, 28 and 32 hours. Mathematica® software was used to apply regression techniques to the *in vitro* data for prediction of dissolution rate constant, k_D; and diffusion coefficient, D. The standard weighted squared error between simulated values from Equation 4.48 and *in vitro* results was minimized with respect to k_D and D (Table 4.3). The predicted k_D and D values were used to generate theoretical release profiles which compared extremely well with the experimental results (Figures 4.14 – 4.16). Additionally, contour plots showing the diffusion gradient in the skin layers after 4 hours are shown for each formulation (Figures 4.17 – 4.19).

The estimated diffusion coefficients for all three formulations showed the following trend, $D\,[P1] \approx D\,[P3] > D\,[P1]$ (Table 4.3), where D [Pi] represents the Pi formulation value. The 12 – 14% increase in D values for P1 and P2 indicates a possible inverse relationship between the diffusion coefficient and formulation drug content. On the other hand, dissolution rate constants for each of the formulations increased in the order of $k_D\,[P2] < k_D\,[P1] <<< k_D\,[P3]$. As expected, a similar trend was observed in relation to both the microneedle dissolution times and the base-plate dissolution times. The P3 formulated microneedles exhibited very rapid pyramid dissolution time (1.6 min) and base-plate dissolution (0.2 min) compared to P1 and P2 microneedles (> 37 min). This demonstrates that polymer content has a significant impact on dissolution with a 10% (w/w) reduction in PVP concentration between preparations P1 and P2 versus P3 yielding over 26,000% increase in k_D. The drug loading had a much less significant role with 10% (w/w) increase in sumatriptan between P2 and P1 only generating 38% increase in dissolution rate.

Table 4.3 Estimated Sumatriptan Microneedle Formulation Parameters for Dissolution and Diffusion Model

Formulation	t_{D1}^* (h)	t_{D2}^* (h)	k_D^* (cm/h)	D^* (10^{-4} cm^2/h)
Circle Arrays				
P1	0.625 ± 0.28	1.65 ± 0.024	0.0264 ± 0.012	1.57 ± 1.3
P2	0.904 ± 0.19	2.00 ± 0.0045	0.0192 ± 0.0040	1.75 ± 0.81
P3	0.0265 ± 0.22	0.0034 ± NA	7.01 ± NA	1.79 ± 0.88

*Microneedle dissolution time, t_{D1}; base-plate dissolution time, t_{D2}; dissolution rate constant, k_D; diffusion coefficient, D; value ± confidence interval (NA refers to standard deviation greater than 3 times the mean.

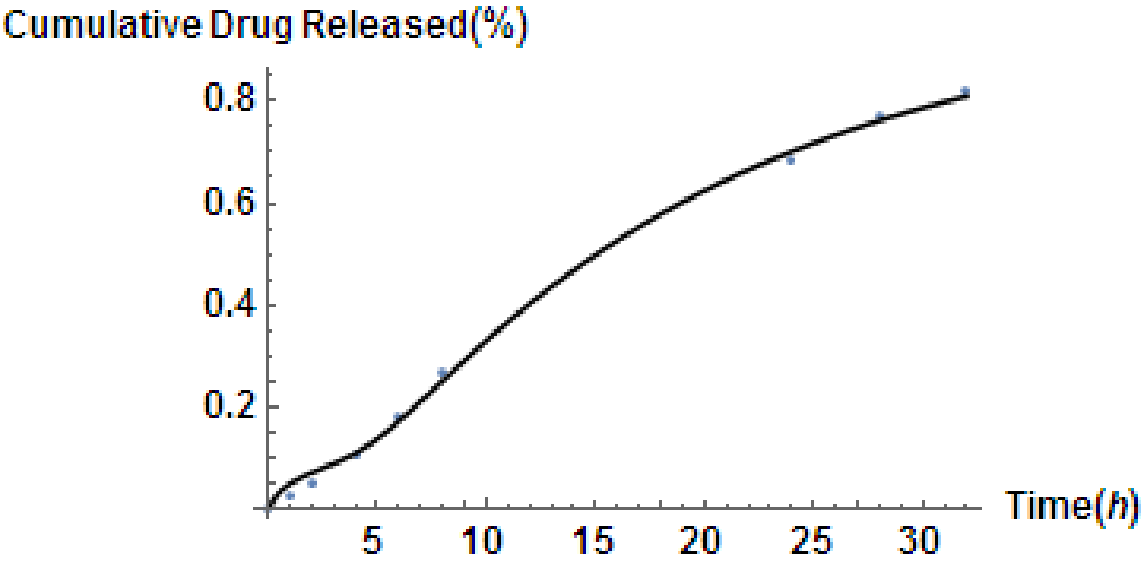

Figure 4.14 Plots comparing minipig *in vitro* cumulative percent release of P1 microneedles (solid dots) to predicted profiles (solid lines).

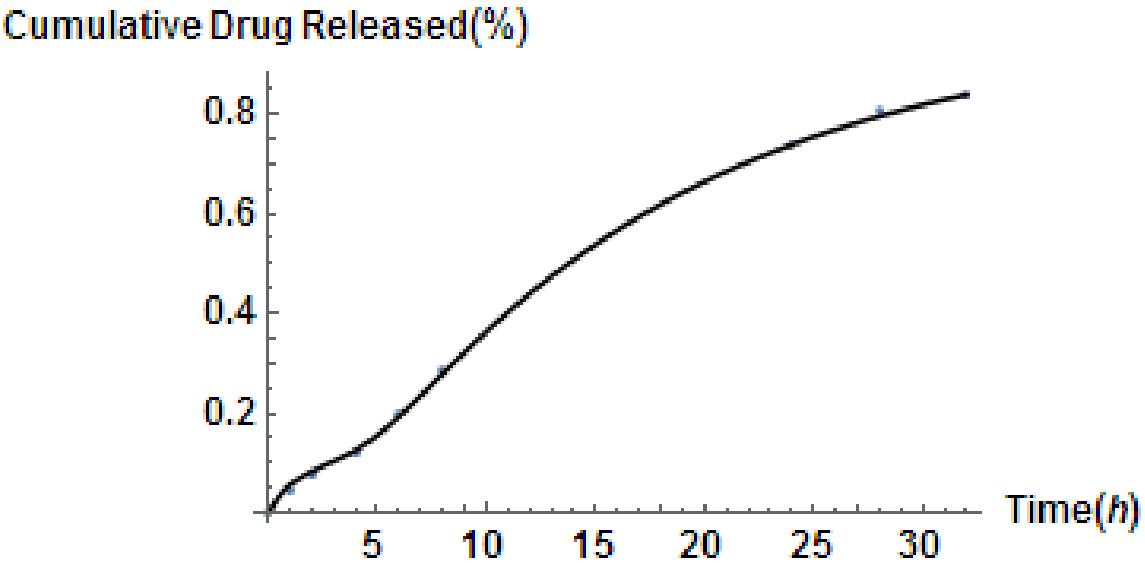

Figure 4.15 Plots comparing minipig *in vitro* cumulative percent release of P2 microneedles (solid dots) to predicted profiles (solid lines).

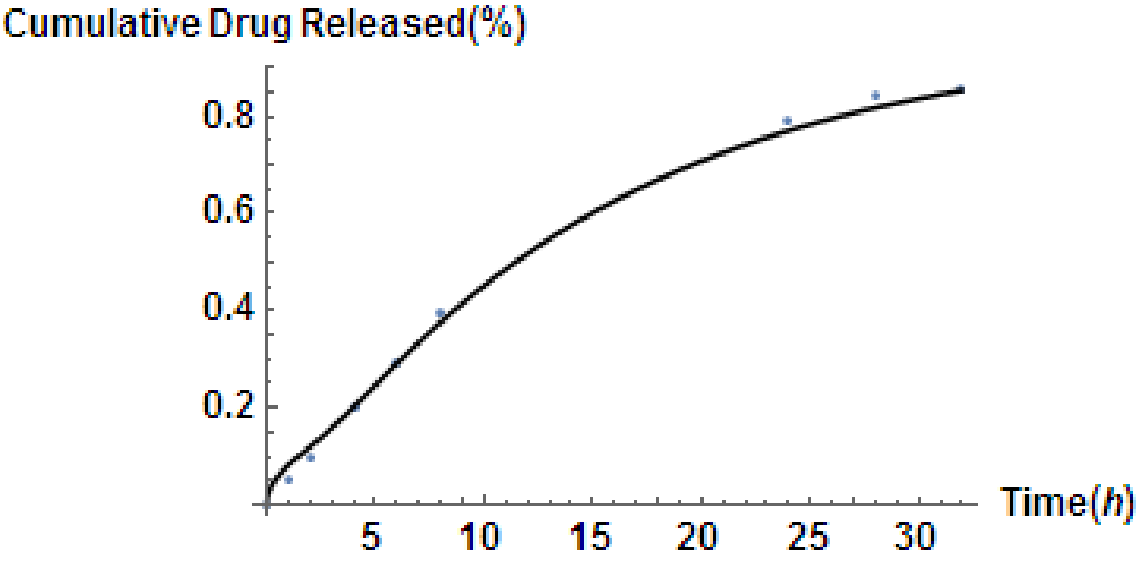

Figure 4.16 Plots comparing minipig *in vitro* cumulative percent release of P3 microneedles (solid dots) to predicted profiles (solid lines).

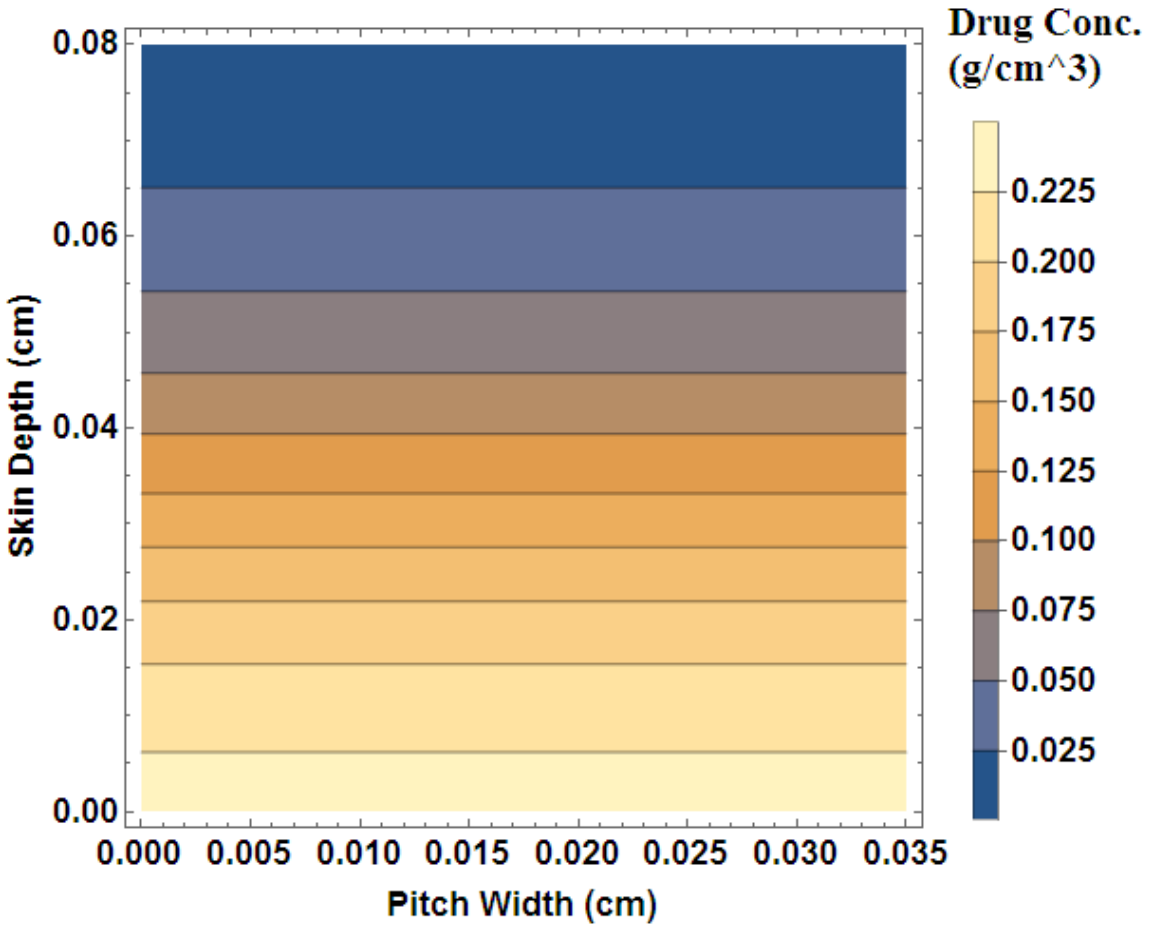

Figure 4.17 Contour plot of sumatriptan drug release from P1 microneedle after 4 hours.

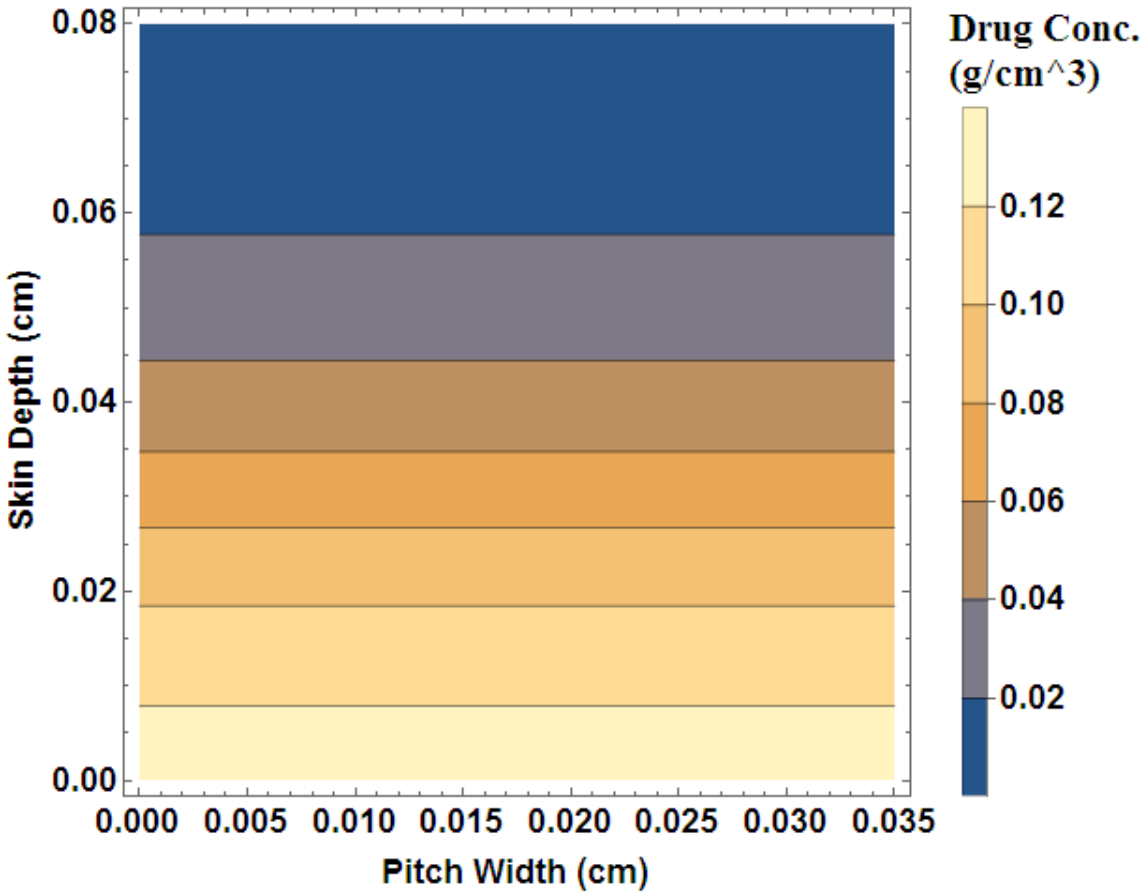

Figure 4.18 Contour plot of sumatriptan drug release from P2 microneedle after 4 hours.

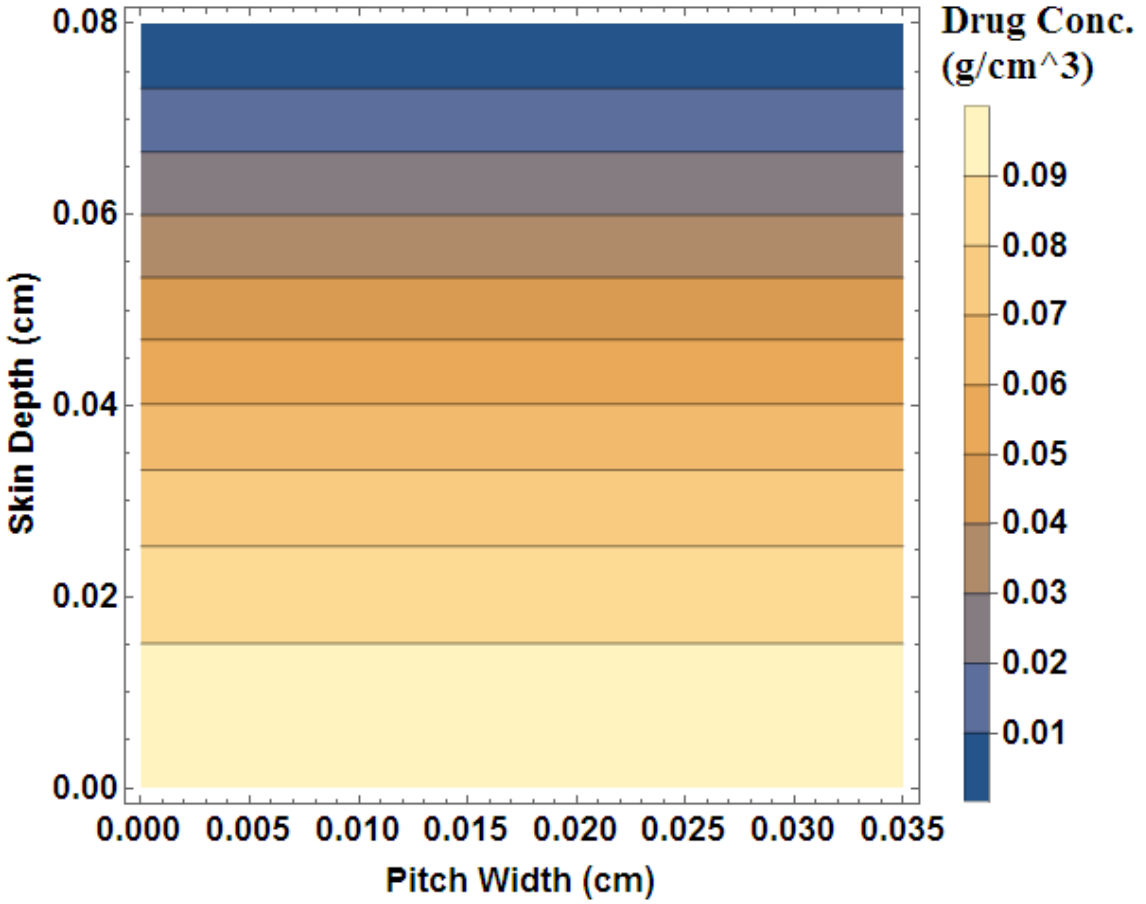

Figure 4.19 Contour plot of sumatriptan drug release from P3 microneedle after 4 hours.

4.5 Development of Mathematical Model for *In vitro* Dissolution, Diffusion, and Release of Sumatriptan From Dissolving Microneedle Array Aided by Iontophoresis

Here, a mathematical framework, incorporating dissolution, diffusion and electro-migration, is presented to estimate drug release from dissolving pyramid-shaped microarrays under a low-density electric current. For this study, a new electrophoretic transport model is derived by applying Ohm's law of electro-migration, Fick's second law of diffusion, and a mass balance on the drug in the skin. This method will allow for

researchers to predict how drug is transported during and after microneedle treatment combined with iontophoresis.

The equations for dissolution, diffusion and electrophoretic transport of ionic drug molecules were developed using the control-volume depicted in Figure 4.1. The model is based on the following assumptions, listed below:

- One-dimensional drug transport in the negative z-direction.
- Drug metabolism in the skin is not considered.
- Drug binding to viable skin tissues is not considered.
- Mass transport through sides of control-volume not considered.
- Impact of needle properties on insertion into skin was not considered.
- Decrease in needle volume directly correlates to increase in available skin layer volume.
- Microneedles and skin layer tissues are isotropic and dissolution occurs evenly over surfaces of needle.
- Electrical current is applied through an anode electrode placed above the microneedle array after insertion into the skin (Figure 1.3).

The developed equations are listed below and includes changes in the microneedle height and in the skin layer drug concentration. The detailed derivation provided in Sections 4.1.1 and 4.5.1. All of the equation parameters are listed in Table 4.1.

The material balance for drug mass in the skin layer is given by Equation 4.50; where γ is a dimensionless electromigration/convection parameter which represents the influence of the current applied to the microneedle and skin.

$$\frac{\partial c}{\partial t} = D\frac{\partial^2 c}{\partial z^2} - \frac{\gamma D}{\delta_S}\frac{\partial C}{\partial x} + 4\left(\frac{k_D \tan\theta}{\rho\cos\theta}\right)h^2\left(\frac{\beta\rho - c}{v_0 + v_{c,0} - v_c}\right)\left(c_s - \left(\frac{1-\beta}{\beta}\right)c\right) \qquad (4.50)$$

The height of the pyramid is defined as

$$\frac{dh(t)}{dt} = -\frac{k_d c_S}{\rho \sin\theta} \tag{4.51}$$

The initial conditions are

$$h(0) = h_0 \tag{4.52}$$

and

$$c(x,0) = 0 \tag{4.53}$$

The drug concentration at the base of the control-volume (ie. blood stream):

$$c(d_s,t) = 0 \tag{4.54}$$

Therefore, diffusive flux, J(t), through the base of the control-volume (i.e., blood stream) is defined as

$$J(t) = -p_w^2 D \left.\frac{\partial c(z,t)}{\partial z}\right|_{z=d_s} \tag{4.55}$$

The cumulative amount of drug released $Q(t)$ is then determined from the diffusive flux, (J(t),

$$Q(t) = \int_0^t J(\tau)\, d\tau \tag{4.56}$$

The cumulative percent drug released, M(t), is obtained by dividing Q(t) by $\beta\rho v_{C,0}$+m_0.

$$M(t) = \frac{\int_0^t J(\tau)\, d\tau}{\left(\beta\rho v_{c,0} + m_0\right)} \tag{4.57}$$

4.5.1 Derivation of Electrophoretic Transport Governing Equations for Skin Layer Concentration

The iontophoretic transport equation for ionic compounds through the skin is given by Equation 4.58 which defines the concentration of drug in the skin layer as the result of passive diffusion, electro-migration, and convection [83-85].

$$\frac{\partial c}{\partial t} = D\frac{\partial^2 c}{\partial z^2} - \frac{\nu D}{\delta_S}\frac{\partial c}{\partial x} - \upsilon\frac{\partial c}{\partial x} \tag{4.58}$$

Where υ is the convective flow velocity in the viable skin, and ν is an iontophoretic model parameter defined as $\nu = \frac{zFE}{RT}$; z is the ionized drug charge; F is the Faraday constant; E is the electric field; R is the ideal gas constant; and T is the temperature. Equation 4.58 is simplified by substituting the model parameter $\gamma = \frac{\nu D}{\delta_S} + \upsilon$, which accounts for electro-migration and convection processes. However, at relatively low fluid velocities the convection processes are negligible (i.e., $\gamma = \frac{\nu D}{\delta_S}$), yielding Equation 4.59,

$$\frac{\partial c}{\partial t} = D\frac{\partial^2 c}{\partial z^2} + \frac{\gamma D}{\delta_S}\frac{\partial c}{\partial x} \tag{4.59}$$

Therefore, drug accumulation in the control-volume, $\frac{d(vc)}{dt}$; is the result of passive diffusion $D\frac{\partial^2 c}{\partial z^2}$; the electro-migration of drug into the skin, $\frac{\upsilon D}{\delta_S}\frac{\partial c}{\partial x}$; and its elimination into the systemic circulation (Section 4.1.2), $4\left(\frac{k_D \tan\theta}{\rho\cos\theta}\right)h^2\left(\frac{\beta\rho - c}{v_0 + v_{c,0} - v_c}\right)\left(c_s - \left(\frac{1-\beta}{\beta}\right)c\right)$:

$$\frac{\partial c}{\partial t} = D\frac{\partial^2 c}{\partial z^2} - \frac{\gamma D}{\delta_S}\frac{\partial C}{\partial x} + 4\left(\frac{k_D \tan\theta}{\rho\cos\theta}\right)h^2\left(\frac{\beta\rho - c}{v_0 + v_{c,0} - v_c}\right)\left(c_s - \left(\frac{1-\beta}{\beta}\right)c\right) \qquad (4.60)$$

4.6 Simulation Studies to Evaluate Sumatriptan Microneedle Dissolution, Diffusion, and Electro-migration Mathematical Model

Computer simulations were conducted with the dissolution, diffusion, and electro-migration transport model (Section 4.5) to determine the effect of electrical current (i.e., parameter γ) on the release of sumatriptan succinate from dissolving pyramid-shaped microneedles. The study uses the P1 circle microarray system dimensions and formulation parameters that were determined previously in Section 3.2 and summarized in Table 3.1. *In vitro* minipig release data were used to determine the dissolution rate (k_D = 0.0143 cm/h) by applying regression techniques described in Section 4.2. Also, release values were used to estimate the diffusion coefficient (7.901 x 10^{-5} cm^2/h) from the steady-state diffusion equation for lag time, $t_{lag} = h^2/6D$ [82]. The electromigration/convection parameter, γ, was approximated to be 0.8 based on reference data for similar iontophoretic *in vitro* experiments applied to the drug amitriptyline HCL [84, 86].

Equation 4.66 was used to predict the *in vitro* drug release profiles of P1 formulated microarray patches under varied electrical current (Figure 4.19). The γ parameter correlates

to the influence of current on the drug transport with increased γ values related to increased current levels [84]. The study showed a favorable increase in percent sumatriptan released through the skin. A γ value of 1.6 related to an estimated 42% drug released after 8 hours, as compared to approximately 34% with no applied current.

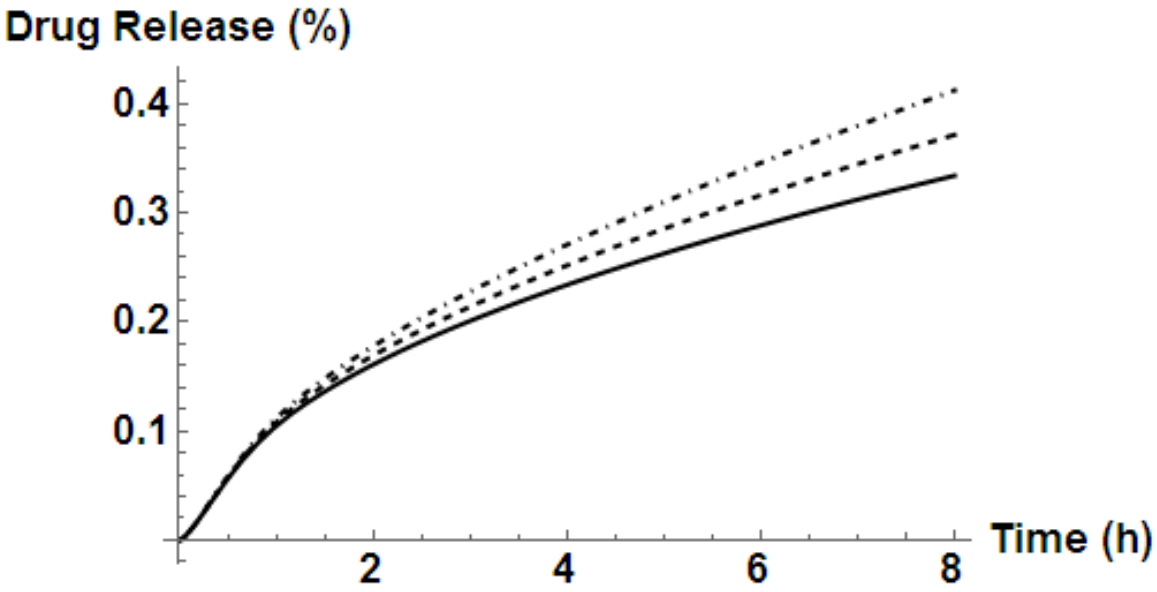

Figure 4.20 Predicted effect of the iontophoretic parameter, γ, on *in vitro* cumulative percent sumatriptan released from P1 microneedles over an 8 hour period; γ = 0 (solid); γ = 0.8 (dashed); and γ = 1.6 (dot-dashed).

CHAPTER 5

CONCLUSION

This research involves a dissolving polyvinylpyrrolidone-based microneedle device designed for the transdermal delivery of sumatriptan succinate for migraine relief. The product is a suitable alternative drug delivery method that is painless and with minimal unwanted side effects. The microneedle systems were fabricated from a 0.785-cm^2 circular array with 600 pyramid-shaped needles with consistent height (500 µm), width (300 µm), and pitch (350 µm). Three formulations (P1, P2, P3) were successfully prepared from 5 – 10% (w/w) sumatriptan succinate API, 20 – 30% (w/w) polyvinylpyrrolidone, polysorbate 80, glycerol and purified water. Tensile tests showed that the microarray strength was improved by increasing polyvinylpyrrolidone concentration or decreasing the sumatriptan load. *In vitro* experiments were carried out on female Göttingen minipig skins with and without iontophoresis (i.e., low electrical current). Microneedles from each formulation properly inserted into the minipig skin as observed with optical microscope and visual inspection with indicator solution (Nitrazine yellow dye). Transepidermal water loss (TEWL) studies performed pre-and post- microneedle treatment demonstrated a 4.9-fold reduction in the barrier function. This change was greater than the 4.6-fold decrease observed following removal of the stratum corneum by tape-stripping (15x). These TEWL results indicate the microarrays produce an array of low-resistance tunnels which facilitate transport of water through the stratum corneum. *In vitro* release studies showed a major decrease in the lag time and an increased steady-state flux compared to previously developed sumatriptan transdermal delivery systems. Additional iontophoretic *in vitro*

experiments were conducted on each of the three microneedle formulations using a small electrical current of 100 – 500 μA/cm^2. The electrical current significantly increased the flux of sumatriptan across the skin with only one third of the API required to deliver a similar therapeutic dose as that of a microneedle device alone.

The design of new dissolving microneedle systems will require additional experimental design work and *in vitro* studies to optimize the microneedle geometry and formulation parameters. Model-based design was selected in this contribution as an efficient approach to assist researchers in the design and optimization of microneedle systems for drug delivery of macromolecules.

Initially, a mathematical model was derived to predict sumatriptan succinate delivery from a pyramid-shaped microarray system. The model was applied to the three different sumatriptan microarray formulations to estimate the cumulative amount of drug released calculate the dissolution and elimination rate constants. It was concluded that increasing the drug load led to a rise in the maximum drug concentration in the skin; increasing the microneedle height resulted in a minor enhancement of drug layer concentration; and increasing the pitch width significantly reduced the sumatriptan content in the epidermis. Next, a second mathematical model was generated to describe the dissolution and diffusion of the medication through the dermal layers. The platform was used to predict diffusion profiles of the three sumatriptan formulations and estimate the diffusion coefficient and dissolution rate constants. Computer simulations determined that the polyvinylpyrrolidone concentration had a major impact on the microneedle dissolution. Reduction of the pitch width greatly increased diffusion through the skin. Finally, mathematical equations were derived to describe the dissolution and permeation of soluble microarrays and changes in

the dermal drug concentration following the application of a low-density electric current. Simulation studies showed that moderate improvement in the sumatriptan drug release could be achieved by increasing the current density.

REFERENCES

[1] L. Zhu, L. Lu, S. Wang, J. Wu, J. Shi, T. Yan, C. Xie, Q. Li, M. Hu, Z. Liu, Oral absorption basics: pathways and physicochemical and biological factors affecting absorption, in: Developing solid oral dosage forms, Elsevier, Amsterdam, 2017, pp. 297-329.

[2] B. Homayun, X. Lin, H.-J. Choi, Challenges and recent progress in oral drug delivery systems for biopharmaceuticals, Pharmaceutics, 11 (2019) 129.

[3] M. Goldberg, I. Gomez-Orellana, Challenges for the oral delivery of macromolecules, Nat Rev Drug Discov, 2 (2003) 289.

[4] S.K. Bardal, J.E. Waechter, D.S. Martin, Applied pharmacology, Elsevier Health Sciences, China, 2011.

[5] S.S. Jhee, T. Shiovitz, A.W. Crawford, N.R. Cutler, Pharmacokinetics and pharmacodynamics of the triptan antimigraine agents: a comparative review, Clin Pharmacokinet, 40 (2001) 189-205.

[6] M.A. Moskowitz, F.M. Cutrer, Sumatriptan: a receptor-targeted treatment for migraine, Annu Rev Med, 44 (1993) 145-154.

[7] M.M. Johnston, A.M. Rapoport, Triptans for the management of migraine, Drugs, 70 (2010) 1505-1518.

[8] R.B. Lipton, M.E. Bigal, M. Diamond, F. Freitag, M.L. Reed, W.F. Stewart, A.A. Group, Migraine prevalence, disease burden, and the need for preventive therapy, Neurology, 68 (2007) 343-349.

[9] Y.W. Woldeamanuel, R.P. Cowan, Migraine affects 1 in 10 people worldwide featuring recent rise: a systematic review and meta-analysis of community-based studies involving 6 million participants, J Neurol Sci, 372 (2017) 307-315.

[10] R. Burstein, R. Noseda, D. Borsook, Migraine: multiple processes, complex pathophysiology, J Neurosci, 35 (2015) 6619-6629.

[11] S.D. Silberstein, Migraine symptoms: Results of a survey of self-reported migraineurs, Headache, 35 (1995) 387-396.

[12] L. Kelman, D. Tanis, The relationship between migraine pain and other associated symptoms, Cephalalgia, 26 (2006) 548-553.

[13] P. Fowler, L. Lacey, M. Thomas, O. Keene, R. Tanner, N. Baber, The clinical pharmacology, pharmacokinetics and metabolism of sumatriptan, Eur Neurol, 31 (1991) 291-294.

[14] C. Duquesnoy, J. Mamet, D. Sumner, E. Fuseau, Comparative clinical pharmacokinetics of single doses of sumatriptan following subcutaneous, oral, rectal and intranasal administration, Eur J Pharm Sci, 6 (1998) 99-104.

[15] C.G. Dahlöf, J. Saiers, Sumatriptan injection and tablets in clinical practice: results of a survey of 707 migraineurs, Headache, 38 (1998) 756-763.

[16] M.R. Prausnitz, R. Langer, Transdermal drug delivery, Nat Biotechnol, 26 (2008) 1261-1268.

[17] R. Liuzzi, A. Carciati, S. Guido, S. Caserta, Transport efficiency in transdermal drug delivery: what is the role of fluid microstructure?, Colloids Surf B, 139 (2016) 294-305.

[18] M.N. Pastore, Y.N. Kalia, M. Horstmann, M.S. Roberts, Transdermal patches: history, development and pharmacology, Br J Pharmacol, 172 (2015) 2179-2209.

[19] S. Wiedersberg, R.H. Guy, Transdermal drug delivery: 30+ years of war and still fighting!, J Control Release, 190 (2014) 150-156.

[20] A. Williams, B. Barry, Penetration enhancers, Adv Drug Deliv Rev, 64 (2012) 128-137.

[21] M.R. Prausnitz, P.M. Elias, T.J. Franz, M. Schmuth, J.-C. Tsai, G.K. Menon, W.M. Holleran, K.R. Feingold, Skin barrier and transdermal drug delivery, Dermatology, 3 (2012) 2065-2073.

[22] A. Femenia-Font, C. Padula, F. Marra, C. Balaguer-Fernandez, V. Merino, A. Lopez-Castellano, S. Nicoli, P. Santi, Bioadhesive monolayer film for the in vitro transdermal delivery of sumatriptan, J Pharm Sci, 95 (2006) 1561-1569.

[23] C. Balaguer-Fernandez, C. Padula, A. Femenia-Font, V. Merino, P. Santi, A. Lopez-Castellano, Development and evaluation of occlusive systems employing polyvinyl alcohol for transdermal delivery of sumatriptan succinate, Drug Deliv, 17 (2010) 83-91.

[24] C. Balaguer-Fernandez, A. Femenia-Font, S. Del Rio-Sancho, V. Merino, A. Lopez-Castellano, Sumatriptan succinate transdermal delivery systems for the treatment of migraine, J Pharm Sci, 97 (2008) 2102-2109.

[25] K.L. Dechant, S.P. Clissold, Sumatriptan, Drugs, 43 (1992) 776-798.

[26] M.R. Prausnitz, Microneedles for transdermal drug delivery, Adv Drug Deliv Rev, 56 (2004) 581-587.

[27] M.R. Prausnitz, Engineering microneedle patches for vaccination and drug delivery to skin, Annu Rev Chem Biomol Eng, 8 (2017) 177-200.

[28] E. Larraneta, R. Lutton, A.D. Woolfson, L. Donnelly, Microneedle arrays as transdermal and intradermal drug delivery systems: materials science, manufacture and commercial development, Mater Sci Eng R Rep, 104 (2016) 1-32.

[29] B.N. Nalluri, S.S. Anusha, S.R. Bramhini, J. Amulya, A.S. Sultana, C.U. Teja, D.B. Das, In vitro skin permeation enhancement of sumatriptan by microneedle application, Curr Drug Deliv, 12 (2015) 761-769.

[30] Y.-C. Kim, J.-H. Park, M.R. Prausnitz, Microneedles for drug and vaccine delivery, Adv Drug Deliv Rev, 64 (2012) 1547-1568.

[31] J.W. Lee, S.O. Choi, E.I. Felner, M.R. Prausnitz, Dissolving microneedle patch for transdermal delivery of human growth hormone, Small, 7 (2011) 531-539.

[32] D. Wu, Y.S. Quan, F. Kamiyama, K. Kusamori, H. Katsumi, T. Sakane, A. Yamamoto, Improvement of transdermal delivery of sumatriptan succinate using a novel self-dissolving microneedle array fabricated from sodium hyaluronate in rats, Biol Pharm Bull, 38 (2015) 365-373.

[33] Y. Ito, S. Kashiwara, K. Fukushima, K. Takada, Two-layered dissolving microneedles for percutaneous delivery of sumatriptan in rats, Drug Dev Ind Pharm, 37 (2011) 1387-1393.

[34] D. Kellerman, J. Lickliter, J. Mardell, T. von Stein, Pharmacokinetics and tolerability of a new intracutaneous microneedle system of zolmitriptan (ZP-Zolmitriptan), HEADACHE, 56 (2016) 07030-05774.

[35] Y.N. Kalia, A. Naik, J. Garrison, R.H. Guy, Iontophoretic drug delivery, Adv Drug Deliv Rev, 56 (2004) 619-658.

[36] Y. Wang, R. Thakur, Q. Fan, B. Michniak, Transdermal iontophoresis: combination strategies to improve transdermal iontophoretic drug delivery, Eur J Pharm Biopharm, 60 (2005) 179-191.

[37] M. Roustit, S. Blaise, J.L. Cracowski, Trials and tribulations of skin iontophoresis in therapeutics, Br J Clin Pharmacol, 77 (2014) 63-71.

[38] R.F. Donnelly, T.R.R. Singh, D.I. Morrow, A.D. Woolfson, Microneedle-mediated transdermal and intradermal drug delivery, John Wiley & Sons, Chichester, West Sussex, UK, 2012.

[39] T. Waghule, G. Singhvi, S.K. Dubey, M.M. Pandey, G. Gupta, M. Singh, K. Dua, Microneedles: a smart approach and increasing potential for transdermal drug delivery system, Biomed Pharmacother, 109 (2019) 1249-1258.

[40] S. Münch, J. Wohlrab, R. Neubert, Dermal and transdermal delivery of pharmaceutically relevant macromolecules, Eur J Pharm Biopharm, 119 (2017) 235-242.

[41] D.-J. Lim, J.B. Vines, H. Park, S.-H. Lee, Microneedles: a versatile strategy for transdermal delivery of biological molecules, Int J Biol Macromol, 110 (2018) 30-38.

[42] P. Ronnander, L. Simon, H. Spilgies, A. Koch, S. Scherr, Dissolving polyvinylpyrrolidone-based microneedle systems for in-vitro delivery of sumatriptan succinate, Eur J Pharm Sci, 114 (2018) 84-92.

[43] S.P. Davis, B.J. Landis, Z.H. Adams, M.G. Allen, M.R. Prausnitz, Insertion of microneedles into skin: measurement and prediction of insertion force and needle fracture force, J Biomech, 37 (2004) 1155-1163.

[44] B. Al-Qallaf, D.B. Das, Optimization of square microneedle arrays for increasing drug permeability in skin, Chemical Engineering Science, 63 (2008) 2523-2535.

[45] A. Davidson, B. Al-Qallaf, D.B. Das, Transdermal drug delivery by coated microneedles: Geometry effects on effective skin thickness and drug permeability, Chem Eng Res Des, 86 (2008) 1196-1206.

[46] K.S. Kim, K. Ita, L. Simon, Modelling of dissolving microneedles for transdermal drug delivery: theoretical and experimental aspects, Eur J Pharm Sci, 68 (2015) 137-143.

[47] A. Ripolin, J. Quinn, E. Larraneta, E.M. Vicente-Perez, J. Barry, R.F. Donnelly, Successful application of large microneedle patches by human volunteers, Int J Pharm, 521 (2017) 92-101.

[48] P. González-Vázquez, E. Larrañeta, M.T. McCrudden, C. Jarrahian, A. Rein-Weston, M. Quintanar-Solares, D. Zehrung, H. McCarthy, A.J. Courtenay, R.F. Donnelly, Transdermal delivery of gentamicin using dissolving microneedle arrays for potential treatment of neonatal sepsis, J Control Release, 265 (2017) 30-40.

[49] P. Ronnander, L. Simon, H. Spilgies, A. Koch, Modelling the in-vitro dissolution and release of sumatriptan succinate from polyvinylpyrrolidone-based microneedles, Eur J Pharm Sci, 125 (2018) 54-63.

[50] M.R. Marques, R. Loebenberg, M. Almukainzi, Simulated biological fluids with possible application in dissolution testing, Dissolut Technol, 18 (2011) 15-28.

[51] M.H. Qvist, U. Hoeck, B. Kreilgaard, F. Madsen, S. Frokjaer, Evaluation of Gottingen minipig skin for transdermal in vitro permeation studies, Eur J Pharm Sci, 11 (2000) 59-68.

[52] H. Todo, Transdermal permeation of drugs in various animal species, Pharmaceutics, 9 (2017) 33.

[53] J.G. Fujimoto, C. Pitris, S.A. Boppart, M.E. Brezinski, Optical coherence tomography: an emerging technology for biomedical imaging and optical biopsy, Neoplasia, 2 (2000) 9-25.

[54] Y.A. Gomaa, D.I. Morrow, M.J. Garland, R.F. Donnelly, L.K. El-Khordagui, V.M. Meidan, Effects of microneedle length, density, insertion time and multiple applications on human skin barrier function: assessments by transepidermal water loss, Toxicol In Vitro, 24 (2010) 1971-1978.

[55] Y. Werner, M. Lindberg, Transepidermal water loss in dry and clinically normal skin in patients with atopic dermatitis, Acta Derm Venereol, 65 (1985) 102-105.

[56] E. Elmahjoubi, Y. Frum, G.M. Eccleston, S.C. Wilkinson, V.M. Meidan, Transepidermal water loss for probing full-thickness skin barrier function: correlation with tritiated water flux, sensitivity to punctures and diverse surfactant exposures, Toxicol In Vitro, 23 (2009) 1429-1435.

[57] C. Surber, F.P. Schwarb, E.W. Smith, Tape-stripping technique, J Toxicol Cutan Ocul Toxicol, 20 (2001) 461-474.

[58] A. Femenia-Font, C. Balaguer-Fernandez, V. Merino, A. Lopez-Castellano, Iontophoretic transdermal delivery of sumatriptan: effect of current density and ionic strength, J Pharm Sci, 94 (2005) 2183-2186.

[59] V. Dhote, P. Bhatnagar, P. MISHRA, S. MAHAJAN, D. MISHRA, Iontophoresis: a potential emergence of a transdermal drug delivery system, Sci Pharm, 80 (2011) 1-28.

[60] N. Dixit, V. Bali, S. Baboota, A. Ahuja, J. Ali, Iontophoresis-an approach for controlled drug delivery: a review, Curr Drug Deliv, 4 (2007) 1-10.

[61] W. Schwarz, PVP: a critical review of the kinetics and toxicology of polyvinylpyrrolidone (povidone), CRC Press, Chelsea, MI, 1990.

[62] R. Awasthi, S. Manchanda, P. Das, V. Velu, H. Malipeddi, K. Pabreja, T.D. Pinto, G. Gupta, K. Dua, Poly (vinylpyrrolidone), in: Engineering of Biomaterials for Drug Delivery Systems, Elsevier, Duxford, UK, 2018, pp. 255-272.

[63] S. Vollbracht, A.M. Rapoport, New treatments for headache, Neurol Sci, 35 (2014) 89-97.

[64] C.M. Perry, A. Markham, Sumatriptan, Drugs, 55 (1998) 889-922.

[65] A. Femenía-Font, C. Balaguer-Fernández, V. Merino, A. López-Castellano, Iontophoretic transdermal delivery of sumatriptan: effect of current density and ionic strength, J Pharm Sci, 94 (2005) 2183-2186.

[66] M.W. Pierce, Transdermal delivery of sumatriptan for the treatment of acute migraine, Neurotherapeutics, 7 (2010) 159-163.

[67] U.F.a.D. Administration, Guidance for industry, sterile drug products produced by aseptic processing—current good manufacturing practice, Silver Spring, (2004).

[68] W. Drexler, U. Morgner, F. Kärtner, C. Pitris, S.A. Boppart, X. Li, E. Ippen, J. Fujimoto, In vivo ultrahigh-resolution optical coherence tomography, Opt Lett, 24 (1999) 1221-1223.

[69] D. Huang, E.A. Swanson, C.P. Lin, J.S. Schuman, W.G. Stinson, W. Chang, M.R. Hee, T. Flotte, K. Gregory, C.A. Puliafito, Optical coherence tomography, Science, 254 (1991) 1178-1181.

[70] E. Berardesca, G. Borroni, Instrumental evaluation of cutaneous hydration, Clin Dermatol, 13 (1995) 323-327.

[71] A.M. Barbero, H.F. Frasch, Pig and guinea pig skin as surrogates for human in vitro penetration studies: a quantitative review, Toxicol In Vitro, 23 (2009) 1-13.

[72] M. Pierce, C. O'Neill, E. Felker, T. Sebree, Sumatriptan iontophoretic transdermal system: history, study results, and use in clinical practice, Headache, 53 (2013) 34-42.

[73] G.L. Plosker, D. McTavish, Sumatriptan. A reappraisal of its pharmacology and therapeutic efficacy in the acute treatment of migraine and cluster headache, Drugs, 47 (1994) 622-651.

[74] O. Olatunji, D.B. Das, V. Nassehi, Modelling transdermal drug delivery using microneedles: Effect of geometry on drug transport behaviour, J Pharm Sci, 101 (2012) 164-175.

[75] R. Zhang, P. Zhang, C. Dalton, G.A. Jullien, Modeling of drug delivery into tissues with a microneedle array using mixture theory, Biomech Model Mechanobiol, 9 (2010) 77-86.

[76] I. Mansoor, J. Lai, S. Ranamukhaarachchi, V. Schmitt, D. Lambert, J. Dutz, U.O. Häfeli, B. Stoeber, A microneedle-based method for the characterization of diffusion in skin tissue using doxorubicin as a model drug, Biomed Microdevices, 17 (2015) 61.

[77] K.S. Kim, K. Ita, L. Simon, Modelling of dissolving microneedles for transdermal drug delivery: theoretical and experimental aspects, Eur J Pharm Sci, 68 (2015) 137-143.

[78] A. Dokoumetzidis, P. Macheras, A century of dissolution research: from noyes and whitney to the biopharmaceutics classification system, Int J Pharm, 321 (2006) 1-11.

[79] S.P. Sullivan, D.G. Koutsonanos, M. Del Pilar Martin, J.W. Lee, V. Zarnitsyn, S.O. Choi, N. Murthy, R.W. Compans, I. Skountzou, M.R. Prausnitz, Dissolving polymer microneedle patches for influenza vaccination, Nat Med, 16 (2010) 915-920.

[80] H.L. Quinn, L. Bonham, C.M. Hughes, R.F. Donnelly, Design of a dissolving microneedle platform for transdermal delivery of a fixed-dose combination of cardiovascular drugs, J Pharm Sci, 104 (2015) 3490-3500.

[81] V. Shah, B.K. Choudhury, Fabrication, Physicochemical Characterization, and Performance Evaluation of Biodegradable Polymeric Microneedle Patch System for Enhanced Transcutaneous Flux of High Molecular Weight Therapeutics, AAPS PharmSciTech, 18 (2017) 2936-2948.

[82] S. Mitragotri, Y.G. Anissimov, A.L. Bunge, H.F. Frasch, R.H. Guy, J. Hadgraft, G.B. Kasting, M.E. Lane, M.S. Roberts, Mathematical models of skin permeability: an overview, Int J Pharm, 418 (2011) 115-129.

[83] K. Tojo, Mathematical models of transdermal and topical drug delivery, Biocom Systems, Fukuoka, (2005) 26-27.

[84] L. Simon, A.N. Weltner, Y. Wang, B. Michniak, A parametric study of iontophoretic transdermal drug-delivery systems, J Membrane Sci, 278 (2006) 124-132.

[85] R. Wei, L. Simon, L. Hu, B. Michniak-Kohn, Effects of iontophoresis and chemical enhancers on the transport of lidocaine and nicotine across the oral mucosa, Pharm Res, 29 (2012) 961-971.

[86] Y. Wang, Transdermal delivery of tricyclic antidepressants using iontophoresis, chemical enhancers and superporous hydrogels, Rutgers The State University of New Jersey, New Brunswick, NJ, 2004.